CORRESPONDENCE: sjohnson@usgs.gov

GOLD
OPEN ACCESS

THE GEOLOGICAL SOCIETY
OF AMERICA®

Shelf evolution along a transpressive transform margin, Santa Barbara Channel, California

Samuel Y. Johnson[1], Stephen R. Hartwell[1], Christopher C. Sorlien[2], Peter Dartnell[1], and Andrew C. Ritchie[1]
[1]U.S. Geological Survey, Pacific Coastal and Marine Science Center, 2885 Mission St., Santa Cruz, California 95060, USA
[2]Earth Research Institute, University of California, 6832 Ellison Hall, Santa Barbara, California 93106, USA

ABSTRACT

High-resolution bathymetric and seismic reflection data provide new insights for understanding the post–Last Glacial Maximum (LGM, ca. 21 ka) evolution of the ~120-km-long Santa Barbara shelf, located within a transpressive segment of the transform continental margin of western North America. The goal is to determine how rising sea level, sediment supply, and tectonics combine to control shelf geomorphology and history. Morphologic, stratigraphic, and structural data highlight regional variability and support division of the shelf into three domains. (1) The eastern Santa Barbara shelf is south of and in the hanging wall of the blind south-dipping Oak Ridge fault. The broad gently dipping shelf has a convex-upward shape resulting from thick post-LGM sediment (mean = 24.7 m) derived from the Santa Clara River. (2) The ~5–8-km-wide Ventura Basin obliquely crosses the shelf and forms an asymmetric trough with thick post-LGM sediment fill (mean = 30.4 m) derived from the Santa Clara and Ventura Rivers. The basin is between and in the footwalls of the Oak Ridge fault to the south and the blind north-dipping Pitas Point fault to the north. (3) The central and western Santa Barbara shelf is located north of and in the hanging wall of the North Channel–Pitas Point fault system. The concave-up shape of the shelf results from folding, marine erosion, and the relative lack of post-LGM sediment cover (mean = 3.8 m). Sediment is derived from small steep coastal watersheds and largely stored in the Gaviota bar and other nearshore mouth bars. Three distinct upper slope morphologies result from a mix of progradation and submarine landsliding.

Ages and rates of deformation are derived from a local sea-level-rise model that incorporates an inferred LGM shoreline angle and the LGM wave-cut platform. Post-LGM slip rates on the offshore Oak Ridge fault are a minimum of 0.7 ± 0.1 mm/yr. Slip rates on the Pitas Point fault system are a minimum of 2.3 ± 0.3 mm/yr near Pitas Point, and decrease to the west across the Santa Barbara Channel. Documentation of fault lengths, slip rates, and rupture modes, as well as potential zones of submarine landsliding, provide essential information for enhanced regional earthquake and tsunami hazard assessment.

■ INTRODUCTION

Continental shelves develop and evolve primarily in response to tectonics, sediment supply, and eustatic fluctuations (e.g., Pratson et al., 2007). In passive and convergent continental margins, tectonics typically exert a regional control through processes such as thermal subsidence or growth of accretionary prisms. In contrast, the role of tectonics in transform continental margins can be both more local and complex, resulting from deformation on crustal faults that may have variable locations, trends, and geometries relative to plate motions and geologic framework. Few investigations have explicitly explored shelf evolution in such heterogeneous settings.

Here we investigate a transpressional, 120-km-long section of continental shelf in the Santa Barbara Channel, within the distributed Pacific–North America transform plate boundary in California. The Santa Barbara shelf (Figs. 1 and 2) extends for ~120 km from Point Conception to the Hueneme submarine canyon, ranges significantly in both width (5–19 km), gradient (0.2°–0.8°), and sediment cover, and is cut and deformed by active faults considered capable of generating large earthquakes and tsunamis. The goal of this paper is to document latest Quaternary shelf evolution and geomorphology in this dynamic region in order to both enhance understanding of shelf evolution and to inform regional geologic hazard assessment.

Recent high-resolution geophysical data collected for the California Seafloor Mapping Program (CSMP; Johnson et al., 2017a) provide the foundation for this study. Each of eight U.S. Geological Survey (USGS) CSMP publications (Johnson et al., 2012, 2013a, 2013b, 2013c, 2014, 2015a, 2017a, 2017b) include 10 or more thematic map sheets and a digital data catalog. These publications focus on data presentation, and are intended to inform a host of coastal management needs. This report significantly expands the minimalist and local (1:24,000 map scale) geologic analysis in the CSMP publications with a regional integrated focus on latest Pleistocene to Holocene shelf morphology and evolution. Mapping results are herein summarized in sections on seismic stratigraphy, sediment distribution and thickness, active faults and folds, and shelf and upper slope morphology. These results provide the basis for a discussion of local sea-level history and deformation rates,

Figure 1. Regional map showing part of southern California, important faults, and location of northern Santa Barbara Channel in the west-trending Western Transverse Ranges (WTR) geologic province. Abbreviations: BB—Big Bend region, San Andreas fault (SAF); CB—Catalina basin; CI—Catalina Island; CIP—Channel Islands platform; CT—Channel Islands thrust; DF—Dume fault; EF—Elsinore fault; Go—Goleta; HC—Hueneme Canyon; HF—Hosgri fault; MCF—Malibu Coast fault; MD—Mojave Desert; NIF—Newport-Inglewood fault; NPF—North Channel–Pitas Point fault system; O—Oxnard; ORF—Oak Ridge fault; P—Palos Verdes; PA—Point Arguello; PC—Point Conception; PVF—Palos Verdes fault; SB—Santa Barbara; SBB—Santa Barbara Basin; SC—Santa Cruz Island; SCB—Santa Cruz basin; SGF—San Gabriel fault; SMF—Santa Monica fault; SMM—Santa Monica Mountains; SN—San Nicolas Island; SPB—San Pedro basin; SR—Santa Rosa Island; SYF—Santa Ynez fault; V—Ventura; VB—Ventura Basin. Fault locations are from Chaytor et al. (2008), Fisher et al. (2009a, 2009b), Jennings and Bryant (2010), and the U.S. Geological Survey (2015).
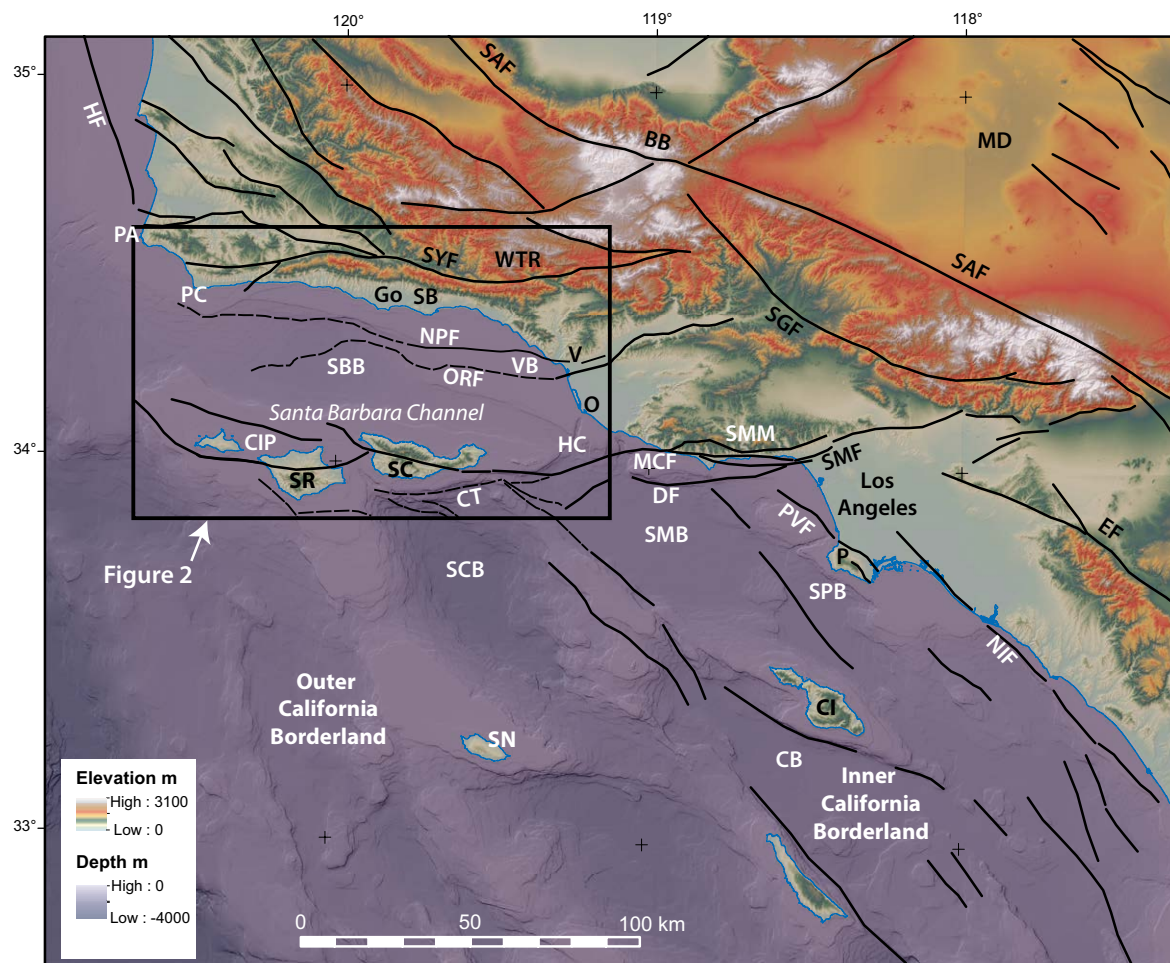
synthesis of post-Last Glacial Maximum (LGM) shelf and upper slope evolution, and a final section outlining significance for assessment of earthquake and tsunami hazards.

■ REGIONAL GEOLOGY AND TECTONICS

The Santa Barbara Channel region is part of the west-striking Western Transverse Ranges province (Figs. 1 and 2), a coherent crustal block within the distributed Pacific–North America transform plate margin. The San Andreas fault, the primary structure within the plate boundary, has a slip rate and trend to

the north in central California of ~30–36 mm/yr and 319° (Sieh and Jahns, 1984; Argus and Gordon, 2001; McCaffrey, 2005; Titus et al., 2011). Notably, the Big Bend region of the San Andreas fault (fault trend of 281°) aligns with the Western Transverse Ranges and is just 65 km north of Ventura (Fig. 1). The combination of Neogene transform motion and block rotation (Kamerling and Luyendyk, 1979, 1985; Luyendyk et al., 1980; Hornafius et al., 1986; Nicholson et al., 1994) is responsible for the anomalous east-west structural trend of the Santa Barbara Channel region relative to the dominant northwest trend of most structures and bathymetric features in the offshore Southern California Borderland to the south and the central California continental margin to the north (Fig. 1).
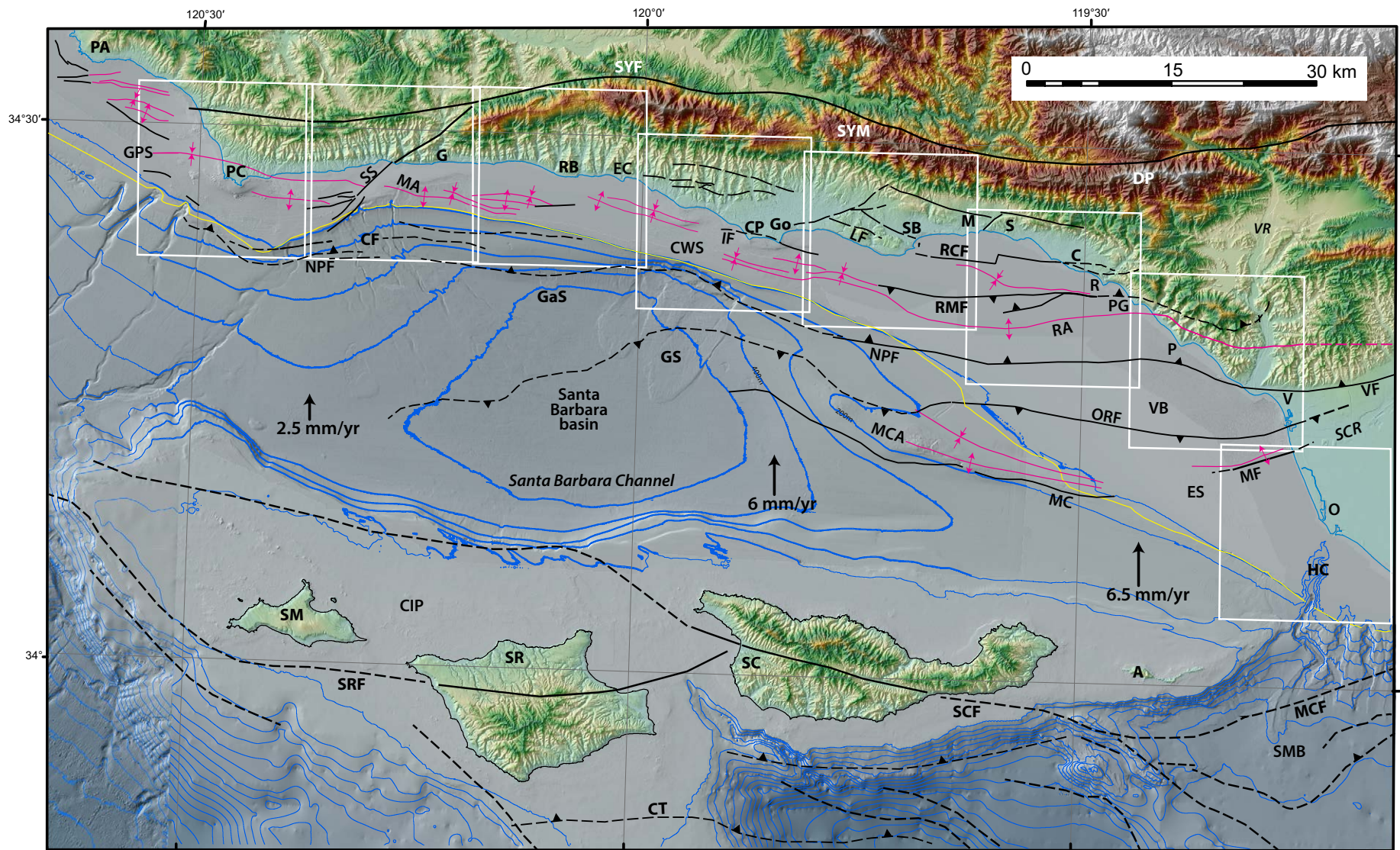
Figure 2. Map of Santa Barbara Channel region (box in Fig. 1) showing the more continuous faults and folds on and near the Santa Barbara shelf, which is between the mainland shoreline and the shelf break (yellow line). Locations of the blind North Channel–Pitas Point fault (NPF) and Oak Ridge thrust fault (ORF) systems are vertical projections from the fault tips based on U.S. Geological Survey seismic reflection profiles on the shelf (e.g., Figs. 4 and 7) industry seismic reflection data at greater water depths (Sorlien and Nicholson, 2015). White boxes show outlines of map and digital data sets developed for the California Seafloor Mapping Program (CSMP; Johnson et al., 2012, 2013a, 2013b, 2013c, 2014, 2015a, 2017b, 2017c). Fault locations are from CSMP and from Sorlien et al. (2006), Chaytor et al. (2008), Minor et al. (2009), Schindler (2010), and the U.S. Geological Survey (2015). Black arrows show modeled north-south shortening rates based on global positioning system data (Marshall et al., 2013). Abbreviations: A—Anacapa Island; C—Carpinteria; CIP—Channel Islands platform; CF—Conception fan; CP—Coal Oil Point; CT—Channel Islands thrust; CWS—central and western Santa Barbara shelf; DP—Divide Peak; EC—El Capitan; ES—eastern Santa Barbara shelf; G—Gaviota; GaS—Gaviota slide; Go—Goleta; GPS—Government Point syncline; GS—Goleta slide; HC—Hueneme canyon; IF—Isla Vista fault; LF—Lavigia fault; M—Montecito; MA—Molino anticline; MF—Montalvo fault; MC—Mid-Channel fault; MCA—Mid-Channel anticline; MCF—Malibu Coast fault; O—Oxnard; P—Pitas Point; PA—Point Arguello; PC—Point Conception; PG—Punta Gorda; R—Rincon Point; RA—Rincon–Ventura Avenue–South Ellwood anticline; RB—Refugio Beach; RCF—Rincon Creek fault; RMF—Red Mountain fault; S—Summerland; SB—Santa Barbara; SC—Santa Cruz Island; SCF—Santa Cruz Island fault; SCR—Santa Clara River; SR—Santa Rosa Island; SM—San Miguel Island; SMB—Santa Monica basin; SRF—Santa Rosa Island fault; SS—south branch of Santa Ynez fault; SYF—Santa Ynez fault; SYM—Santa Ynez Mountains; V—Ventura; VB—Ventura Basin; VF—Ventura fault; VR—Ventura River.

The Santa Barbara shelf and coastal zone and the Santa Ynez Mountains extend west from the Santa Clara River valley to Point Conception (Figs. 1 and 2). Modeling of geodetic data by Marshall et al. (2013) indicates that this region is now undergoing ~2.5 mm/yr (in the west) to 6.5 mm/yr (in the east) of north-south contraction (Fig. 2). Although different models exist for the geometry of the faults that accommodate this shortening (e.g., Shaw and Suppe, 1994; Huftile and Yeats, 1995; Sorlien et al., 2000; Redin et al., 2005; Plesch et al., 2007; Sorlien and Nicholson, 2015), there is consensus that the main fault systems are west-striking blind thrust or reverse faults.

The north-dipping North Channel–Pitas Point fault system (which herein includes the Ventura fault) extends westward across the shelf and slope from Pitas Point to Point Conception (Figs. 1 and 2; Heck, 1998; Sorlien and Nicholson, 2015). Folded and faulted strata along the fault and in its hanging wall are as young as Holocene. Estimated coastal uplift rates based on marine terraces range from ~0.15 mm/yr to as much as 5–8 mm/yr (Lajoie et al., 1982, 1991; Muhs et al., 1992; Rockwell et al., 1992, 2016; Trecker et al., 1998; Duvall et al., 2004; Gurrola et al., 2014), the variability reflecting both location and conflicting interpretations. Uplift of the Santa Ynez Mountains has occurred within the past 5 m.y. (Atwater, 1998).

The Oxnard coastal plain, hosting the Santa Clara River, is south of the North Channel–Pitas Point fault system (Figs. 1 and 2). The topographic depression at the river mouth extends westward offshore across the shelf as the Ventura Basin and farther west as the northern part of the Santa Barbara Basin. The south-dipping, west-striking Oak Ridge fault lacks bathymetric expression but extends for ~60 km across the eastern Santa Barbara Channel and forms the southern margin of the Ventura Basin.

The Santa Barbara shelf is entirely in the Santa Barbara littoral cell, which extends from Point Arguello on the northwest to Hueneme Canyon on the southeast (Fig. 2; Hapke et al., 2006). Littoral drift is to the east-southeast (Barnard et al., 2009), and sediment trapped in Hueneme Canyon at the end of the cell is transported to the deep-water Santa Monica Basin (Figs. 1 and 2; Normark et al., 2009).

■ DATA ACQUISITION

High-resolution bathymetry and backscatter data have been collected for the entire Santa Barbara mainland shelf, extending from Hueneme Canyon to Point Conception (Fig. 2). The data within state waters (shoreline to 5.6 km offshore) are available in USGS CSMP publications (Johnson et al., 2017a) as well as through the data library of the California State University at Monterey Bay Seafloor Mapping Lab (2016) and National Oceanic and Atmospheric Administration National Centers for Environmental Information (2014). Near-seamless offshore coverage of the Santa Barbara nearshore, shelf, slope, and basin (Fig. 2) results from combining state waters data with those collected farther offshore by the Monterey Bay Aquarium Research Institute (2002) and Dartnell et al. (2012).

In 2007, 2008, and 2014, the USGS collected ~1000 km of mostly single-channel high-resolution seismic reflection data between Hueneme Can-

yon and Point Arguello (Fig. 3; Sliter et al., 2008; Johnson et al., 2016). These data, acquired using the SIG 2Mille minisparker (https://www.marine-seismic-equipments.net/) and the EdgeTech 512 chirp (https://www.edgetech.com/products/sub-bottom-profiling/), can resolve geologic features a few tens of centimeters to meters thick down to subbottom depths of as much as 300 m under optimal geologic conditions. Our work also incorporates USGS seismic reflection data collected in 1973 (Vedder, 1975), 1980 and 1981 (Burdick and Richmond, 1982), and 2002 (Normark et al., 2003). The quality of data from all surveys is variable, locally poor due to structural complexity (e.g., steep bedding-plane dips), and the common presence of gas (Hovland and Judd, 1988; Fader, 1997).

Although the focus of this study is shallow geology, we also examined deeper conventional seismic reflection data collected for petroleum exploration in the 1970s and 1980s (Triezenberg et al., 2016) to provide a larger lower resolution structural context. Many of these profiles are included in Fisher et al. (2009b), Johnson et al. (2012, 2013a, 2013b, 2013c, 2014, 2015a, 2017b, 2017c), Sorlien and Nicholson (2015), and elsewhere. These industry profiles generally have their northern endpoints several kilometers from the shoreline and do not provide comprehensive coverage of the shelf.

■ RESULTS

Seismic Stratigraphy of the Santa Barbara Shelf

We developed a simple seismic-stratigraphic model for the Santa Barbara shelf comprising three units (as labeled in Fig. 4).

1. Global sea level was ~119–124 m lower during the latest Pleistocene (~21 k.y. ago) LGM (Stanford et al., 2011). During the LGM, the Santa Barbara shelf was an emergent alluvial plain. Post-LGM sea-level rise led to progressive landward migration of the wave-cut platform and shoreline. Post-LGM sediments (H) overlie this transgressive surface of erosion and are typically characterized by flat, parallel, low- to moderate-amplitude, moderate- to high-frequency, moderately continuous reflections (terminology from Mitchum et al., 1977).

2. Pre-LGM Quaternary sediments (Q) underlie post-LGM sediments in much of the eastern Santa Barbara shelf (Figs. 2 and 4C). Pre-LGM and post-LGM stratigraphic units are characterized by relatively similar seismic facies because deltaic deposition associated with the Santa Clara and Ventura Rivers was apparently continuous from the LGM lowstand through the post-LGM period of sea-level rise (Dahlen et al., 1990; Dahlen, 1992). In this area, the contact between Q and overlying H was mapped using a combination of factors: recognizing subtle differences in seismic facies characteristics (e.g., an upward decrease in reflection amplitude) between lowstand deltaic deposits and transgressive marine deposits; tracing stratigraphic horizons southeastward from angular unconformities mapped to the northwest; and mapping and tracing horizons from the base of buried channels inferred to have formed during the LGM lowstand (following Dahlen, 1992).
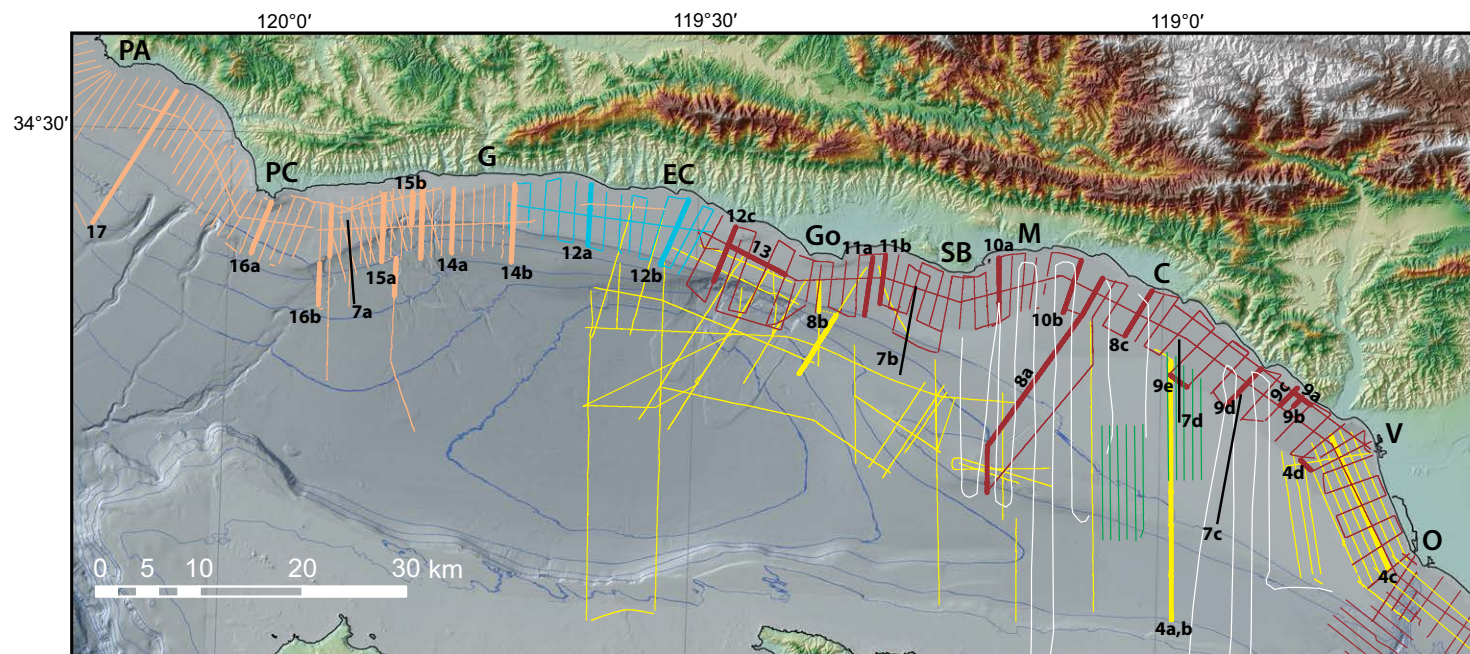
Figure 3. Map of northern Santa Barbara shelf area (see Figs. 1 and 2) showing locations of seismic reflection profiles used in this investigation; bolder lines show profiles included in this report as figures (black labels). Orange tracklines are from U.S. Geological Survey (USGS) cruise 2014–632-SC; blue tracklines are from USGS cruise S-7–08-SC; brown tracklines are from USGS cruise Z-3–07-SC; yellow tracklines are from USGS cruise A-1–02-SC; white tracklines are from 1973 USGS cruise (Vedder, 1975); green tracklines are from 1980 to 1981 USGS data sets (Burdick and Richmond, 1982); black lines are from USGS National Archive of Marine Seismic Surveys database (Triezenberg et al., 2016). Abbreviations as in Figure 2.

3. Neogene to upper Quaternary marine sedimentary rocks (QTu) generally underlie post-LGM (H) sediments in the central and western Santa Barbara shelf (Figs. 2 and 4), where the base of the post-LGM depositional unit is typically a nearly flat angular unconformity. The QTu units include the Miocene Rincon Shale and Monterey Formation, the Miocene–Pliocene Sisquoc Formation, the Pliocene Repetto and Pico Formations, and the Pleistocene Casitas and Santa Barbara Formations. On seismic reflection profiles, these strata yield parallel, continuous low-amplitude, high-frequency reflections and are commonly folded, in many places too steeply to be imaged.

Sediment on the Santa Barbara Shelf

Sediment Supply

The Santa Clara and Ventura Rivers (Fig. 2) currently provide the largest modern sediment supply to the Santa Barbara shelf. The Santa Clara River, the largest coastal watershed (4220 km^2) in southern California, now has an estimated annual sediment flux of 2.2×10^6 m^3 (Warrick and Farnsworth, 2009).

The Ventura River watershed (585 km^2) currently yields ~189,000 m^3 of sediment annually, an amount reduced by upstream dams. Sediment supply in the western part of the littoral cell (between Point Arguello and the Ventura River) is largely from the Gaviota Creek and Rincon Creek watersheds (52 km^2 and 38 km^2, respectively), and many small (typically <15 km^2) transverse coastal watersheds, which collectively supply an estimated annual 448,000 m^3 of sediment (Warrick and Farnsworth, 2009; Warrick and Mertes, 2009). Although sediment supply to the Santa Barbara shelf has almost certainly fluctuated over the past 21 k.y. in response to a range of factors (e.g., climate changes, landscape evolution, land-use changes), the modern estimates provide the only quantitative proxy for post-LGM sediment supply.

Sediment Distribution and Thickness

In Johnson et al. (2012, 2013a, 2013b, 2013c, 2014, 2015a, 2017b, 2017c), high-resolution seismic reflection data were used to map the transgressive surface of erosion and post-LGM sediment thickness at the 1:50,000 scale between Hueneme Canyon and Point Conception (Fig. 5; calculated at 1600 m/s)
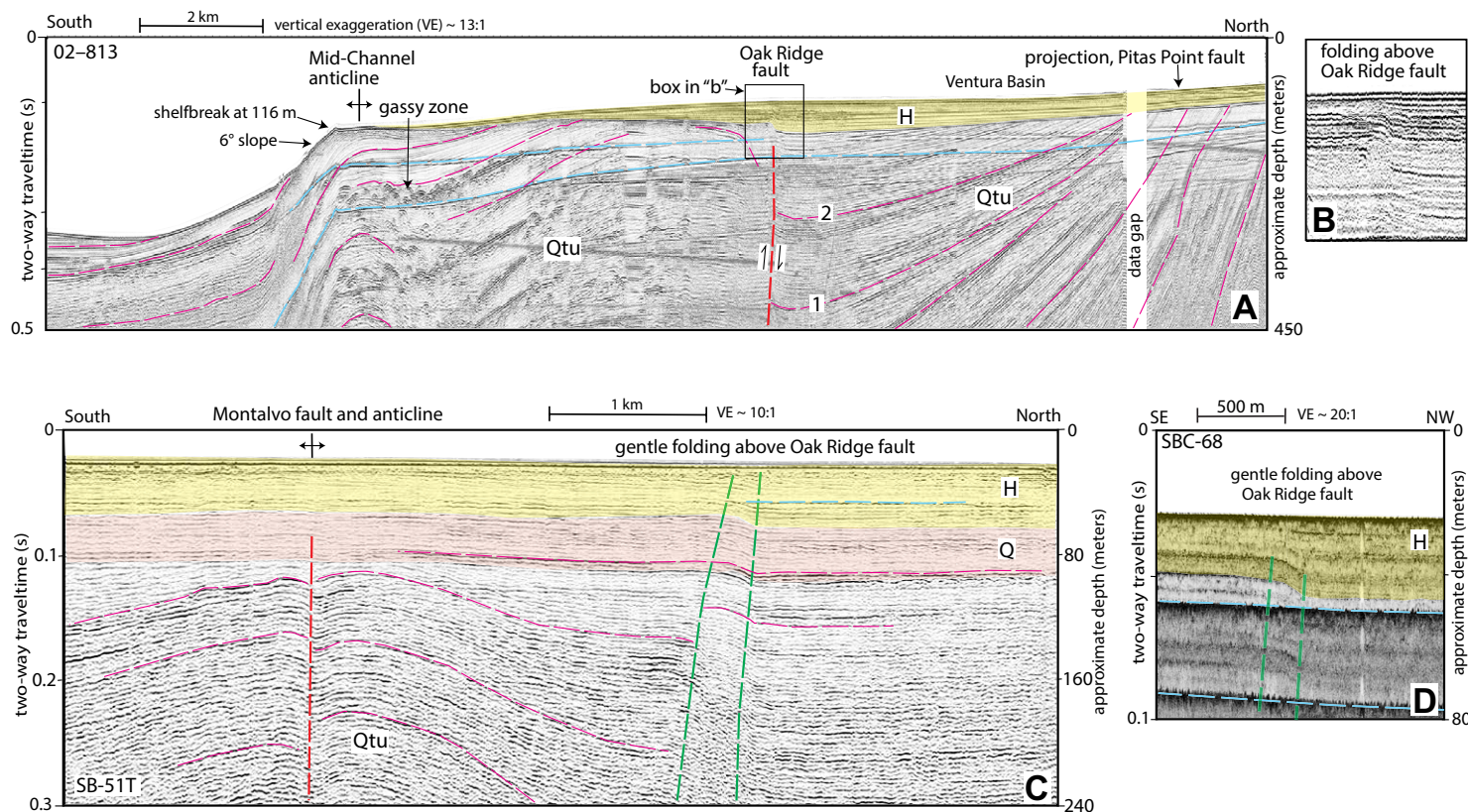
Figure 4. (A, B) U.S. Geological Survey seismic reflection minisparker profile 02–813 from the Santa Barbara shelf. (C) Minisparker profile SB-51T. (D) Chirp profile SBC-68. Locations are shown in Figure 3. Yellow shading shows latest Pleistocene to Holocene (post–Last Glacial Maximum, LGM) deposits (H); orange shading shows inferred upper Quaternary deltaic deposits (Q); QTu is deformed, older upper Quaternary strata. Red dashed lines show faults; green lines in C and D show axes of shallow folds that formed above blind Oak Ridge fault; thin magenta lines (including 1 and 2 in A) highlight continuous reflections and are intended to highlight dips; blue dashed line shows seafloor multiple. VE—vertical exaggeration.

using gridding methods described in Wong et al. (2012). Sediment thickness maps developed for parts of this area have previously been presented at scales ranging from ~1:235,000 to 1:1,000,000 (e.g., Dahlen et al., 1990; Dahlen, 1992; Slater et al., 2002; Draut et al., 2009; Sommerfield et al., 2009). This earlier work does not incorporate the CSMP (2016) high-resolution bathymetry and most of the comprehensive seismic reflection data used in this study (Fig. 3).

The maps in Figure 5 show that post-LGM shelf sediment thickness ranges from 0 to 57 m. Seafloor outcrops are assigned thicknesses of 0–0.1 m. There are widespread areas of smooth, relatively flat, sediment-covered seafloor where QTu bedrock extends to the near surface, into a zone that is difficult to map because of reverberations of the seafloor reflection. Although the bed-

rock-sediment interface can't be effectively mapped in this zone, we show it as having thin sediment cover (between 0.1 and 2.5 m thick), and group this zone with bedrock in Figure 6.

Sediment thickness data indicate a total post-LGM sediment volume on the shelf (10 m water depth to shelf break) between Hueneme Canyon and Point Conception of 17.6 km^3; the volume is increased to 18.1 km^3 when the area to the west in Figure 5 between Point Conception and Point Arguello is added (Table 1). This revises previous estimates of 22.1 km^3 and 21.2 km^3 for an area that extends from Point Conception to Point Mugu, ~6 km farther east than the area shown in Figure 5 (Slater et al., 2002; Sommerfield et al., 2009). Tables 1 and 2 present sediment thickness and volume data for several discrete areas on the Santa Barbara shelf, discussed herein.
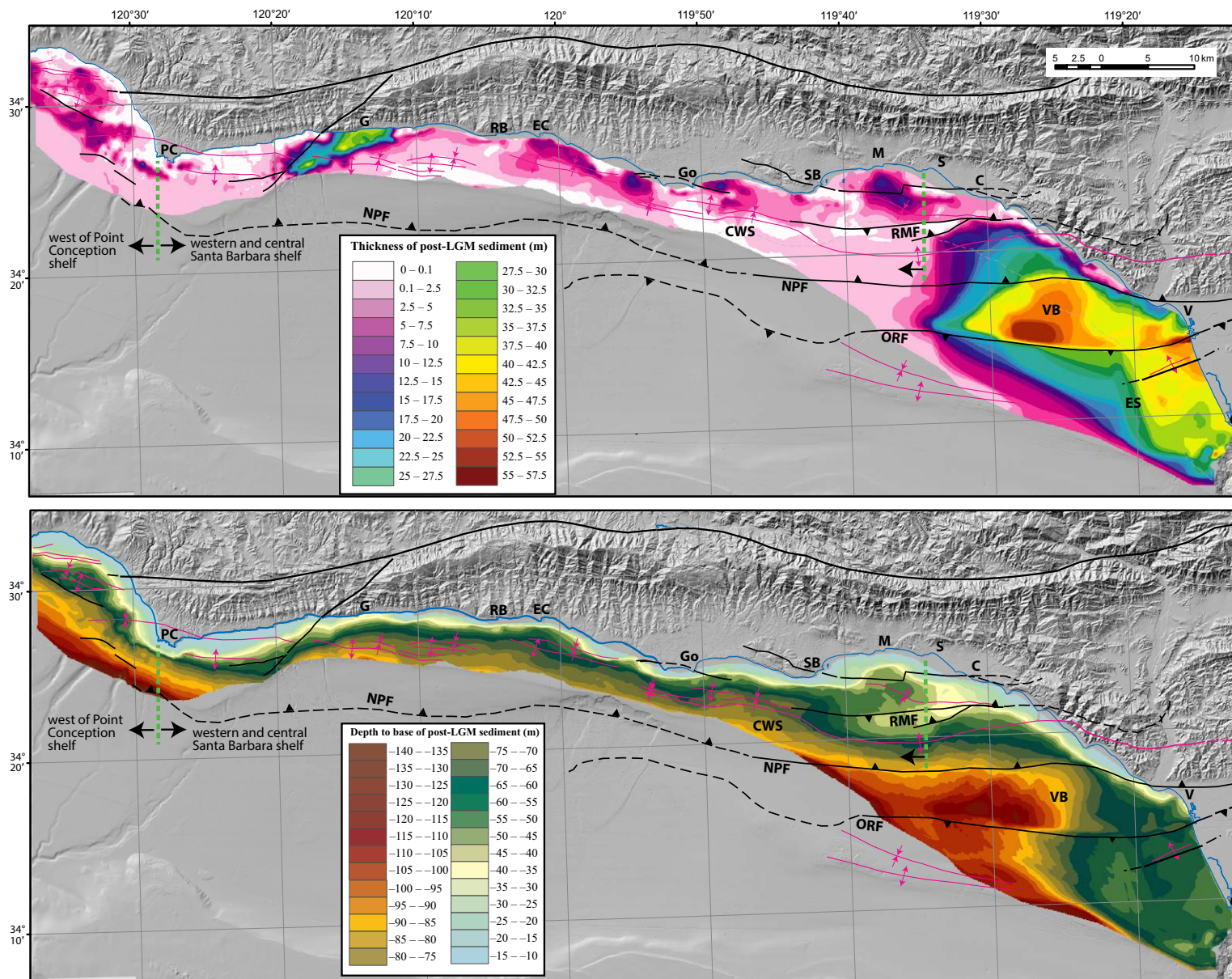
Figure 5. Maps of post–Last Glacial Maximum (LGM) shelf sediment thickness and depth (below sea level) to the base of the post-LGM sediment layer. Dashed green lines show boundaries of central and western Santa Barbara shelf used in compiling Tables 1 and 2. Faults and folds are simplified from Figure 2. Abbreviations: C—Carpinteria; CWS—central and western Santa Barbara shelf; EC—El Capitan; ES—eastern Santa Barbara shelf; G—Gaviota; Go—Goleta; M—Montecito; O—Oxnard; ORF—Oak Ridge fault; PC—Point Conception; NPF—North Channel–Pitas Point fault system; RB—Refugio Beach; RMF—Red Mountain fault; S—Summerland; SB—Santa Barbara; V—Ventura, VB—Ventura Basin.
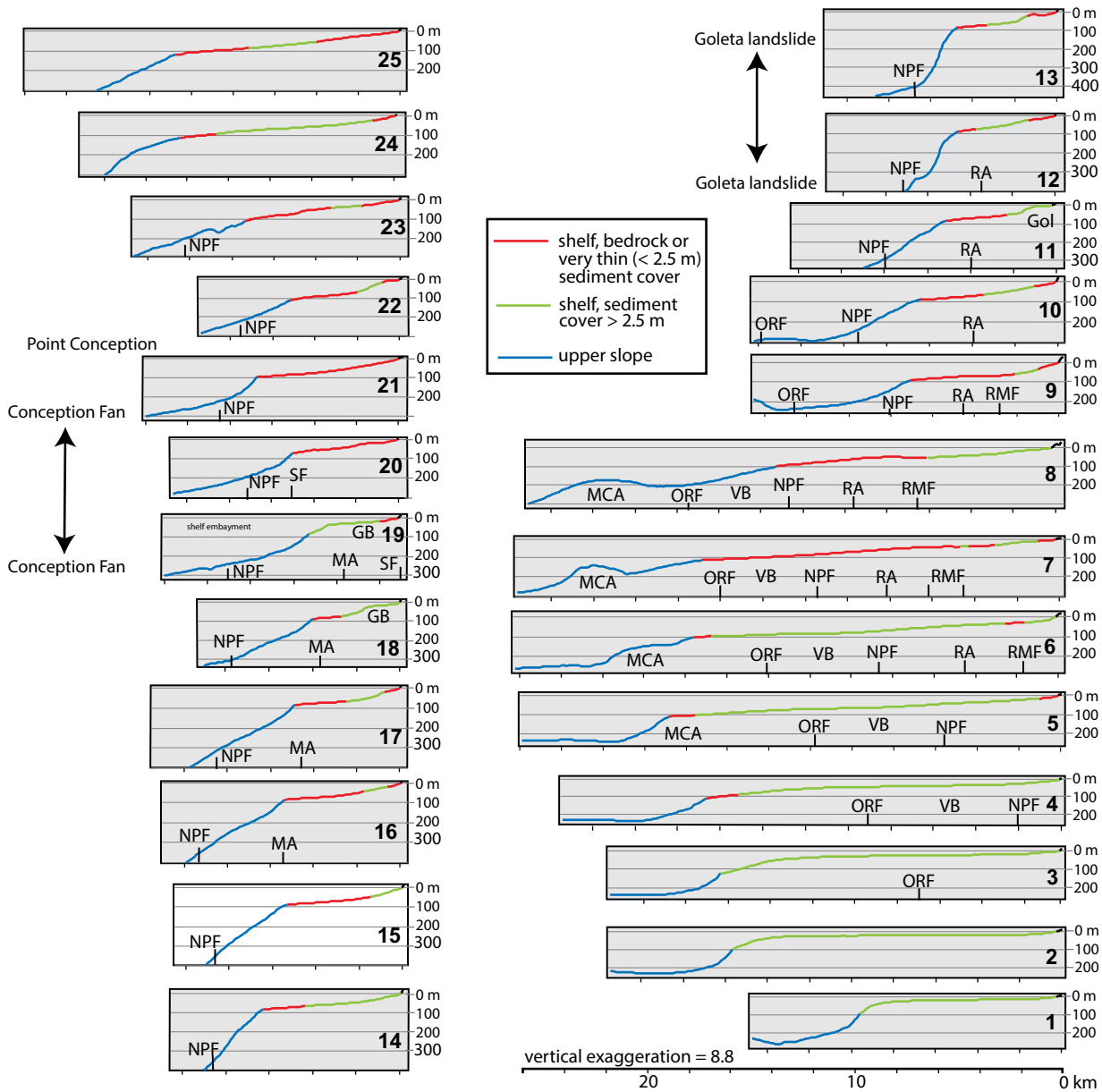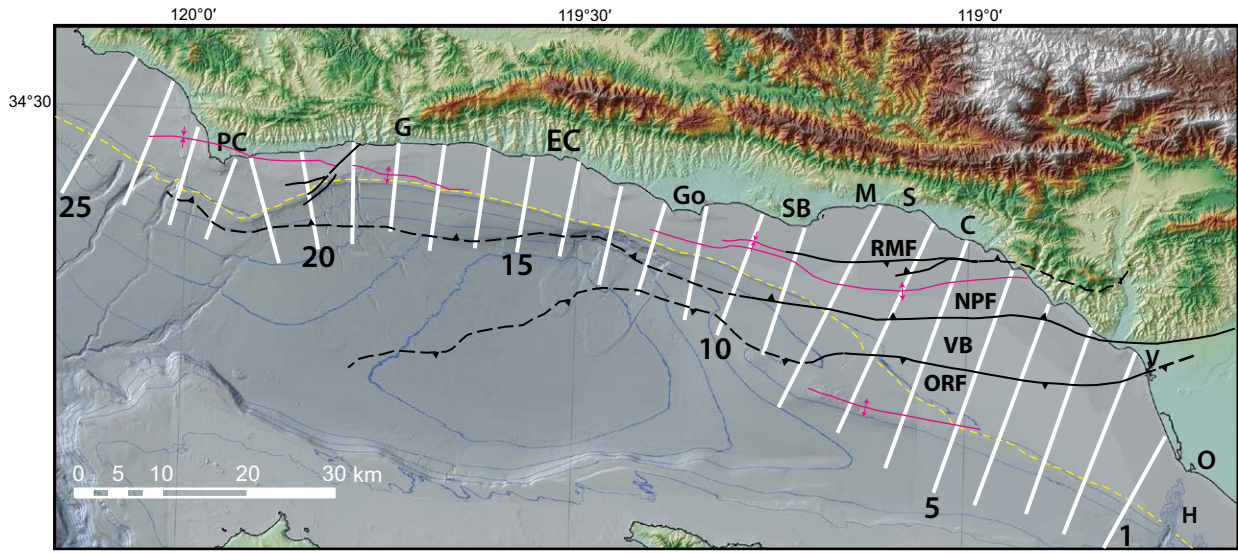
Figure 6. Bathymetry profiles crossing the shelf and upper slope. Vertical black lines show where tips of North Channel–Pitas Point fault (NPF) and Oak Ridge fault (ORF) underlie the bathymetric profile, and where Mid-Channel anticline (MCA), Red Mountain fault (RMF), Rincon anticline (RA), Molino anticline (MA), and south strand of Santa Ynez fault (SF) intersect the profiles. Other abbreviations: C—Carpinteria; EC—El Capitan; G—Gaviota; GB—Gaviota bar, Go—Goleta; Gol—Goleta bar; H—Hueneme Canyon; M—Montecito; O—Oxnard; PC—Point Conception; SB—Santa Barbara; V—Ventura, VB—Ventura Basin.

TABLE 1. AREA, SEDIMENT THICKNESS, AND SEDIMENT VOLUME DATA FOR THE ENTIRE SANTA BARBARA SHELF

Regional sediment thickness zones	Area (km^2)	Mean sediment thickness (m)	Sediment volume (× 10^6 m^3)
Entire shelf, Hueneme Canyon to west Point Conception	1288.2	14.1	18,128.8
South of Oak Ridge fault	302.8	24.7	7484.9
Ventura Basin	209.3	30.4	6353.4
North of Pitas Point fault, east of 119°34′	123.5	14.8	1828.9
Between 119°34′ and Point Conception	508.3	3.8	1946.8
West of Point Conception	144.2	3.6	514.8

Active Structures Mapped on the Santa Barbara Shelf and Upper Slope

Figure 2, simplified from the onshore-offshore geologic maps in Johnson et al. (2012, 2013a, 2013b, 2013c, 2014, 2015a, 2017b, 2017c), shows active faults and folds on the shelf and upper slope. On the shallow seismic reflection data active faults are identified based on the abrupt truncation or warping of post-LGM reflections, and/or juxtaposition of reflection panels with different seismic parameters such as reflection presence, amplitude, frequency, geometry, continuity, and vertical sequence. Identification of warped post-LGM strata indicates active folding. It is noteworthy that several important faults, includ-

ing the Pitas Point fault and the Oak Ridge fault, are blind thrusts with fault tips commonly below the depth of our shallow seismic profiles. Deformation associated with such blind faults can produce fault-related folding in post-LGM strata just a few meters below the seafloor. Evidence of such folding is preserved only once deformed beds are buried below the influence of erosional shelf processes. The focus of this work on shallow high-resolution data notably contrasts with numerous other regional studies that focus on deeper structure based on petroleum-industry seismic reflection data (e.g., Fig. 7) and borehole analysis (e.g., Shaw and Suppe, 1994; Tennyson and Kropp, 1998; Sorlien et al., 2000; Redin et al., 2005; Fisher et al., 2009b; Sorlien and Nicholson, 2015).

TABLE 2. AREA AND SEDIMENT THICKNESS AND VOLUME DATA FOR THE CENTRAL AND WESTERN SANTA BARBARA SHELF AND THE ZONE WEST OF POINT CONCEPTION

Regional sediment thickness zones	Area (km^2)	Mean sediment thickness (m)	Sediment volume (× 10^6 m^3)
Entire central and western Santa Barbara shelf	508.3	3.8	1946.8
10–20 m water depth	49.8	8.6	426.8
20–30 m water depth	32.0	8.5	272.1
30–40 m water depth	37.7	9.6	360.1
40–50 m water depth	72.2	3.8	273.3
50–60 m water depth	72.7	3.1	228.1
60–70 m water depth	100.9	2.7	270.2
70–80 m water depth	102.8	0.9	88.9
80–90 m water depth	31.0	0.7	21.2
>90 m water depth	9.3	0.7	6.3
Gaviota Bar (sediment thickness >5 m)	42	19.5	817
Entire west of Point Conception shelf	144.2	3.6	512.5
10–20 m water depth	5.9	1.6	9.4
20–30 m water depth	17.3	2.1	35.7
30–40 m water depth	7.9	3.5	27.5
40–50 m water depth	14.0	5.0	70.4
50–60 m water depth	15.9	3.9	62.6
60–70 m water depth	12.8	7.4	95.3
70–80 m water depth	18.9	6.6	125.5
80–90 m water depth	15.9	1.8	27.9
>90 m water depth	35.8	1.6	58.2

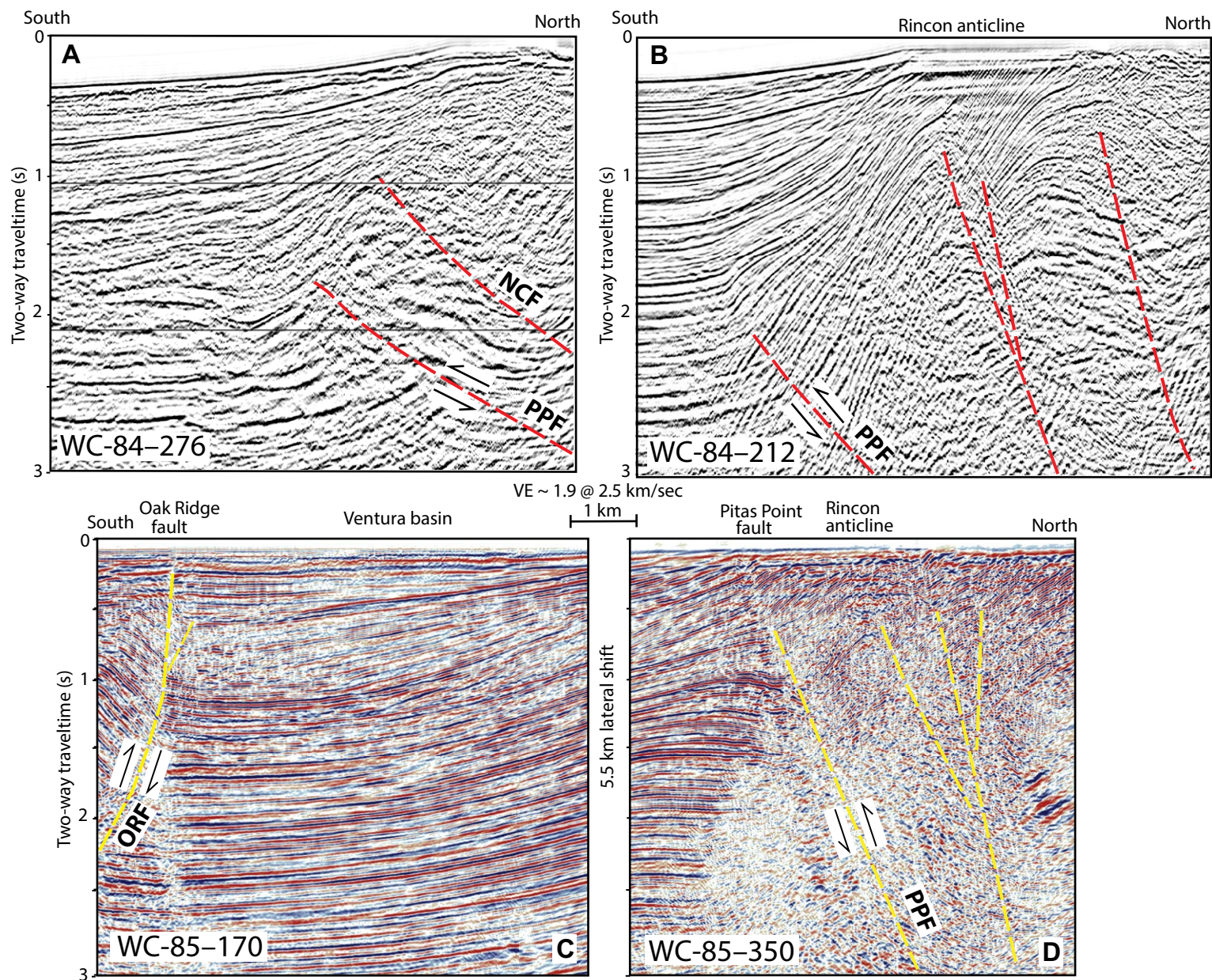*Note:* See also text Figure 5.

Figure 7. Industry seismic reflection profiles showing deeper structure of the Santa Barbara shelf and slope. Locations are shown in Figure 3. VE—vertical exaggeration. (A) Western. Interpretation of WC 84–276 is from Sorlien and Nicholson (2015). NCF—North Channel fault; PPF—Pitas Point fault. (B) Central. Modified version of WC-84–212 is in Johnson et al. (2013a). (C, D) Eastern. Modified versions of WC-85–170 and WC-85–130 are in Johnson et al. (2013b, 2013c). ORF—Oak Ridge fault.

Johnson et al. | Shelf evolution, Santa Barbara Channel

Mid-Channel Anticline

Keller et al. (2007, their figure 10) described the Mid-Channel anticline (Fig. 2) as an actively growing, south-verging hanging-wall anticline above a blind, north-dipping backthrust (Mid-Channel fault) in the hanging wall of the south-dipping Oak Ridge fault (see following). Maps (e.g., Fig. 2), bathymetric profiles (Fig. 6), and seismic reflection profiles (Figs. 4A and 8A) show the anticline as a ridge that extends eastward from the eastern Santa Barbara Basin, impinging obliquely on the shelf break and upper slope. Hopkins (2006) and Keller et al. (2007) suggested that the anticline is propagating to the west and noted that thinning and erosion of late Pleistocene (ca. 110 ka) strata over the anticline axis and on its flanks (e.g., Fig. 8A) provide evidence of recent activity. To the east, our analysis of both shallow and deep seismic reflection data indicates that this fold dies out to the east within a few kilometers of the shelf break.

Montalvo Fault

The Montalvo fault extends ~7 km west across the Santa Barbara shelf from the Santa Clara River valley, northeast of the Mid-Channel anticline (Yeats, 1983). This steep fault cuts the Montalvo anticline (Figs. 2 and 4C), and is ~2.5 km south of and in the hanging wall of the Oak Ridge fault. Figure 4C reveals minor offset and warping of inferred Pleistocene strata (unit QTu), while the overlying late Pleistocene (unit Q) and post-LGM (unit H) sections do not appear to be deformed. However, other nearby profiles that cross the Montalvo fault reveal from 0 to 7 m of offset on the inferred base-LGM surface as well as relatively shallow (within 12 m of the seafloor) fault offsets in the post-LGM section (Fisher et al., 2005b, their figure 2; Johnson et al., 2012, their figure 2 on sheet 8). The local, variable character of shallow-fault–related deformation is consistent with Fisher et al. (2005b), who inferred that this structure has mainly left-lateral slip. Deformation rates cannot be determined from these data, but would be difficult to derive from two-dimensional seismic reflection data if the sense of slip is mainly lateral. The fault has no obvious control on post-LGM sediment thickness (Fig. 5).

Oak Ridge Fault

The Oak Ridge fault extends obliquely across the shelf for ~33 km and at least another 60 km west of the shelf (as a system of related faults) into the Santa Barbara Basin (e.g., Greene et al., 1978; Sorlien et al., 2000; Fisher et al., 2005b). Structural cross sections based on offshore deep seismic reflection data (e.g., Fig. 7C) show the fault as a blind, south-dipping thrust or reverse fault (dip of 40°–80°) (e.g., Redin et al., 2005) overlain by a north-dipping fore-limb (locally the north limb of the Montalvo anticline).

In the shallow subsurface, the shelf seismic reflection profiles crossing the Oak Ridge fault (Fig. 4) reveal shallow (within 5–10 m of the seafloor) asymmetric folding in post-LGM strata with the fault tip locally imaged (Fig. 4A) at a depth of <200 m (also noted by Dahlen, 1992). On the Figure 4 profiles, the width of the shallow (above the transgressive surface of erosion) fold limb ranges from ~140 to 220 m, forelimb dips range from 2.5° to 7° and steepen with depth, and the amount of relief on folded reflections decreases landward from ~10.5 to 6.7 m. West of the shelf beneath the slope, inferred late Pleistocene strata are involved in broad folding of the forelimb above the projected Oak Ridge fault tip (Fig. 8B).

Ventura Basin

The Ventura Basin is a structural trough bounded to the south by the Oak Ridge fault and to the north by the North Channel–Pitas Point fault system (Figs. 2 and 5). Seismic profiles reveal significant north-south asymmetry, with the greatest thickness of post-LGM sediment (57 m) adjacent to the Oak Ridge fault (Fig. 5). This asymmetry also involves older, deeper strata. For example, the thickness of the stratigraphic interval between reflections 1 and 2 (within Qtu) in Figure 4A changes (north to south) from 30 to 138 m over a distance of 5 km, and industry seismic data also show that deeper basin fill thickens to the south (Figs. 7C, 7D).

North Channel–Pitas Point Fault System

The Pitas Point fault system extends across the Santa Barbara Channel for ~110 km from the city of Ventura to Point Conception (Fig. 2; e.g., Sorlien et al., 2000; Redin et al., 2005; Sorlien and Nicholson, 2015). Structural cross sections in the offshore interpret the Pitas Point fault as a blind, north-dipping thrust or reverse fault with dips ranging from 40° to 80° (Fig. 7; Tennyson and Kropp, 1998; Redin et al., 2005; Sorlien and Nicholson, 2015). West of Coal Oil Point (Fig. 2), regional cross sections and deeper seismic profiles (Fig. 7A) show that the fault system (as defined herein) includes the North Channel fault, a second major north-dipping structure above the Pitas Point fault.

As with the Oak Ridge fault, seismic reflection profiles (Fig. 9) show a narrow zone of fault-related folding (but not fault rupture) above the Pitas Point fault tip in the post-LGM stratigraphic unit just a few meters below the seafloor on the inner shelf. Three inner shelf (10–15 m water depths) profiles (Figs. 9A–9C) reveal limb widths in post-LGM strata of ~90 m and forelimb dips (true dips) of ~18°–26°, and the amount of relief on folded post-LGM reflections ranges from 21 to 25 m. Several high-resolution profiles show that this monoclinal folding changes markedly from east to west. Approximately 5 km west of the inner shelf profiles, limb width, forelimb true dip, and vertical relief on folded reflections change to ~55 m, 14°, and 12 m, respectively (Fig. 9D); another 5 km farther west, these parameters are 55 m, 4°, and 2 m (Fig. 9E).
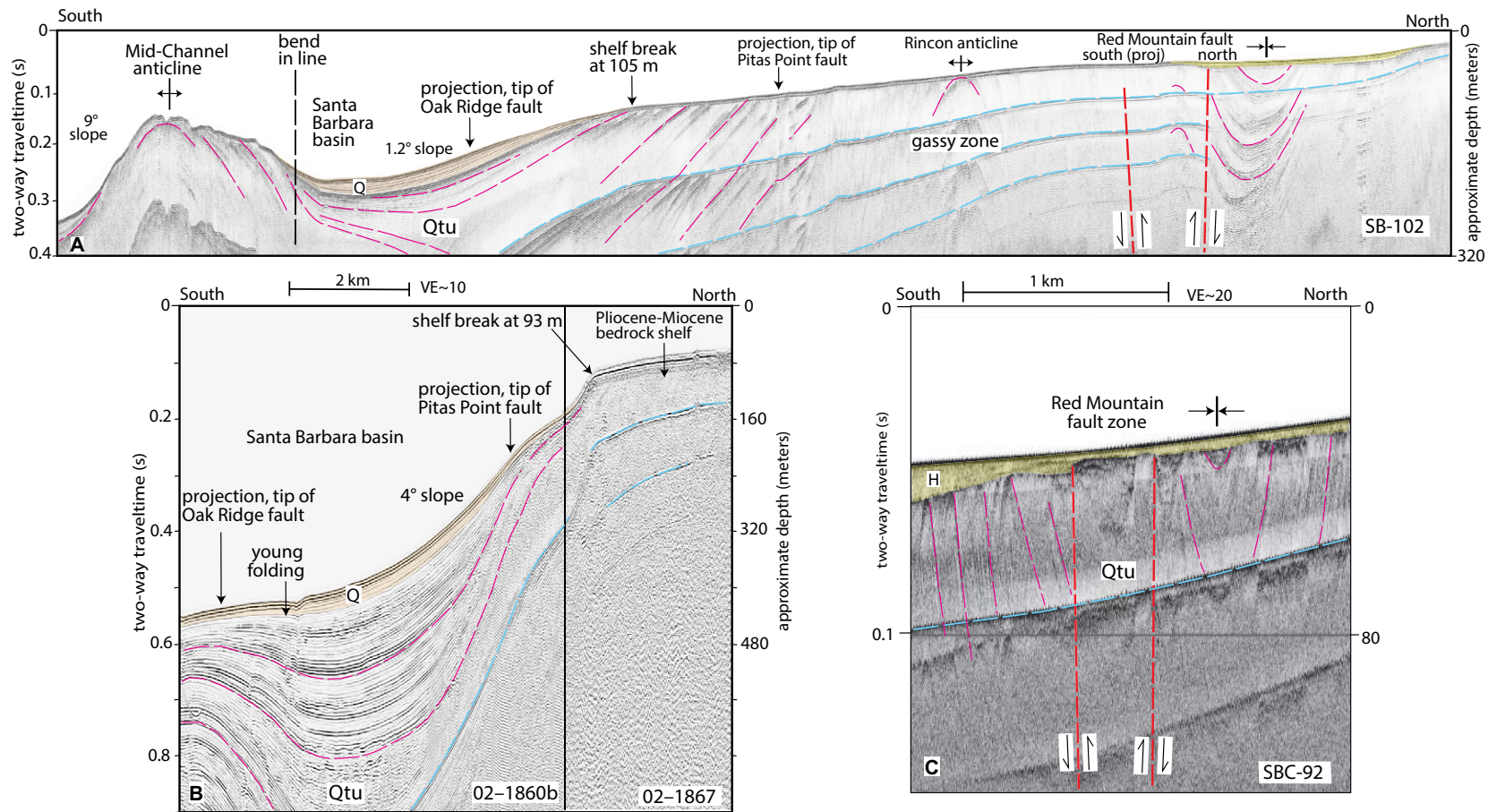
Figure 8. U.S. Geological Survey seismic reflection minisparker profiles. Locations are shown in Figure 3. VE—vertical exaggeration. Yellow shading shows latest Pleistocene to Holocene (H) deposits; orange shading shows inferred upper Quaternary (Q) deposits; QTu is older deformed Quaternary and Neogene strata. Red dashed lines show faults; thin magenta lines highlight prominent reflections and are intended to highlight dips; blue dashed line shows seafloor multiple. (A) Profile SB-102. (B) Profile 02–1860b-1867. Profile 02–1860b was also shown in Fisher et al. (2005b). (C) Chirp profile SBC-92.

This significant change in shallow structure is inferred to result from a westward increase in the depth of the fault tip. On land to the east, the Pitas Point fault is considered the Ventura fault (Sarna-Wojcicki et al., 1976; Yerkes et al., 1987; Hubbard et al., 2014). Hubbard et al. (2014) showed the tip of the Ventura fault on land at a depth of 200–250 m (below the depths shown in the seismic profiles of Fig. 9), providing an informed estimate for the inner shelf region. Farther west, south of Carpinteria, the fault tip is at a depth of ~500 m (Fig. 7D). West of Carpinteria, seismic profiles (Figs. 7A, 7B; Sorlien and Nicholson, 2015) and regional cross sections (Redin et al., 2005) show the depth of the fault tip ranging from 1 to 2 km.

Rincon Anticline

The Rincon anticline (Fig. 2) is located ~3.6–4.5 km north of the small fold at the tip of the Pitas Point fault, in the fault hanging wall. The axis of the anticline can be traced continuously across the shelf for 45 km from its eastern landfall 800 m south of Punta Gorda to a few kilometers west of Coal Oil Point, where it abruptly stops (Johnson et al., 2013b, 2013c; Conrad et al., 2014), a location coincident with the 25° change in the strike of the underlying Pitas Point fault (Sorlien and Nicholson, 2015). On land to the east, the structure is known as the Ventura Avenue anticline (e.g., Rockwell et al., 1988); in the offshore, the fold
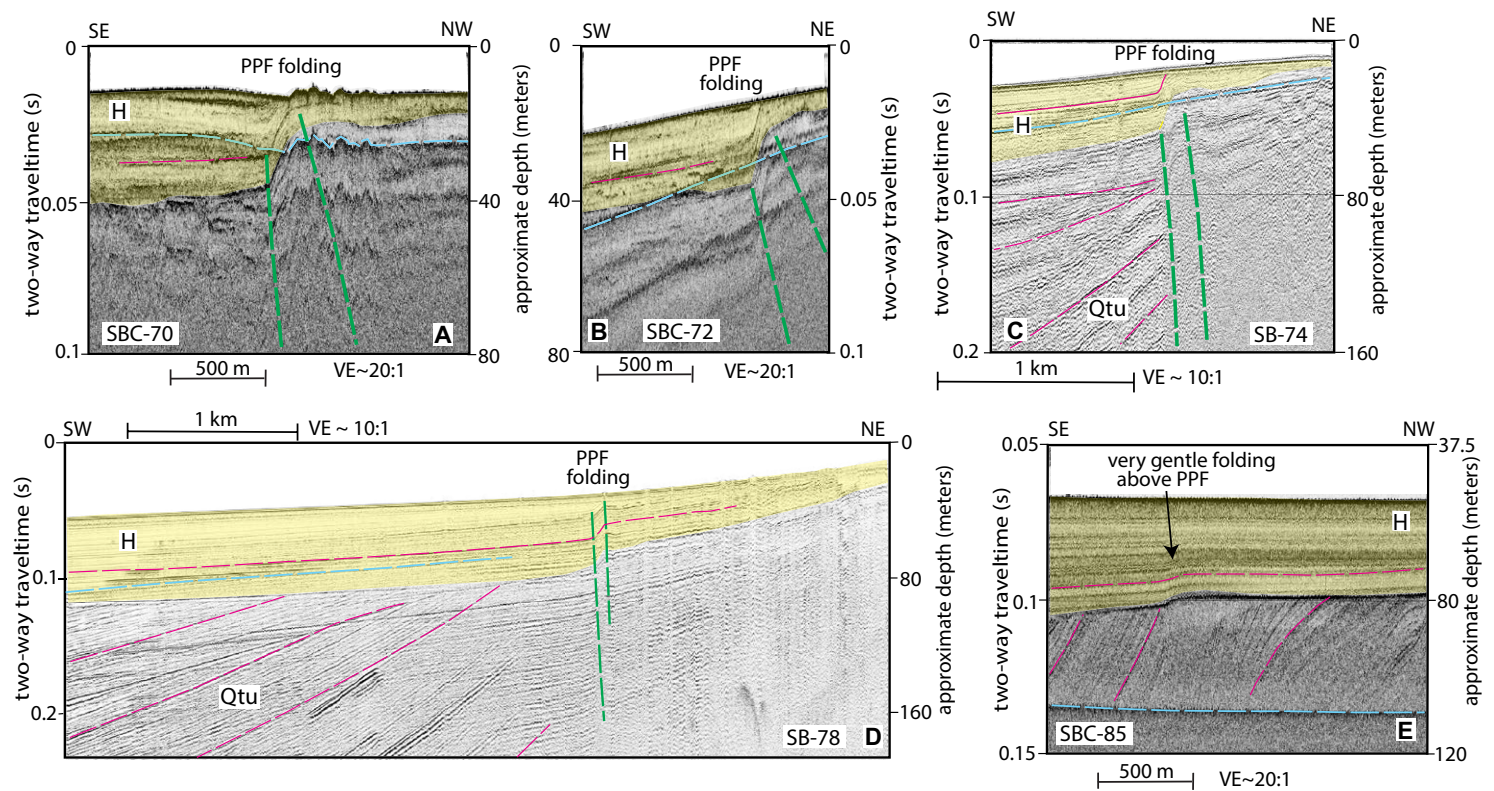
Figure 9. U.S. Geological Survey seismic reflection minisparker profiles. Locations are shown in Figure 3. VE—vertical exaggeration. (A) Chirp profile SBC-70. (B) Chirp profile SBC-72. (C) Profile SB 74. (D) Profile SB-78. (E) Chirp profile SBC-85. Yellow shading shows latest Pleistocene to Holocene (post–Last Glacial Maximum) deposits (H). QTu in C and D southwest of fold is upper Quaternary strata. PPF is Pitas Point fault. Green lines show axes of shallow folds that formed above blind Pitas Point fault; thin magenta lines highlight prominent reflections and are intended to highlight dips; blue dashed line shows seafloor multiple.

is also referred to as the Dos Cuadras anticline east of Santa Barbara, and the South Ellwood anticline west of Santa Barbara.

Rockwell et al. (1988) described late Quaternary uplift of the on-land Ventura Avenue anticline. On the inner shelf, shore-parallel profiles image base-of-LGM seismic reflections that rise 20–25 m between the tip of the Pitas Point fault and the anticline axis, and we attribute this rise to post-LGM anticlinal growth.

Red Mountain Fault

The Red Mountain fault is north of the Rincon anticline, and has been interpreted as a significant reverse or thrust system that merges at depth with the North Channel–Pitas Point fault system (e.g., Redin et al., 2005; Plesch et al., 2007). This fault extends west from on land into the offshore ~1 km north of

Punta Gorda (Fig. 2). Redin et al. (2005, their cross sections 32 and 33) documented more than 6 km of stratigraphic offset of early Pliocene strata on land, but this decreases rapidly to ~400 m offshore on the inner to mid-shelf south of Carpinteria. The Red Mountain fault bifurcates ~6 km west of Punta Gorda into a steep north-dipping south strand and a steep south-dipping north strand, forming the boundaries of a Neogene bedrock uplift (Figs. 2, 8A, and 8C; Johnson et al., 2013b). The south strand dies out in the shallow subsurface south of Montecito (Fig. 2), but may continue farther west as a blind fault. The north strand extends west to Santa Barbara where it offsets the axis of a tight syncline (Fig. 10A). West of Santa Barbara, this syncline (where it is also known as the South Ellwood syncline) broadens and its axis is no longer faulted in the shallow subsurface (Figs. 2 and 11). The combined fault-syncline can be traced in the offshore for 40 km.
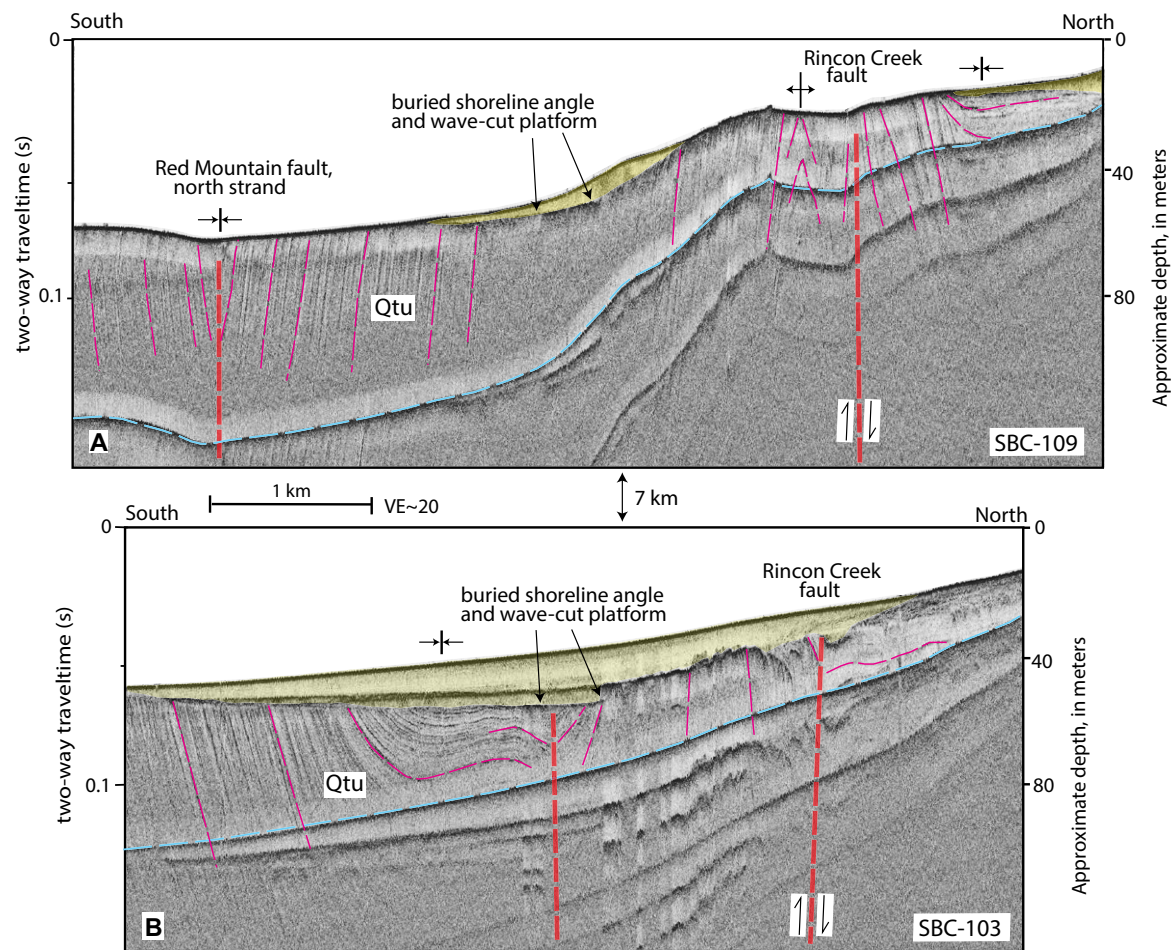
Figure 10. U.S. Geological Survey seismic reflection chirp profiles. (A) SBC-109. (B) SBC-103. Locations are shown in Figure 3. VE—vertical exaggeration. Yellow shading shows latest Pleistocene to Holocene (post–Last Glacial Maximum) deposits; QTu is deformed Quaternary and Neogene strata. Red dashed lines show faults; thin magenta lines highlight prominent reflections and are intended to highlight dips; blue dashed line shows seafloor multiple. Buried wave-cut platforms and shoreline angles are inferred to result from pulses of relative sea-level stability during the post-LGM transgression (e.g., Green et al., 2014).

Rincon Creek Fault

The west-striking steep Rincon Creek fault (Figs. 2 and 10) extends across the inner shelf between Carpinteria to within a few kilometers of Santa Barbara. This structure has been interpreted as a south-dipping reverse fault in the hanging wall of the Red Mountain fault (Jackson and Yeats, 1982; Redin et al., 2005), and forms the northern boundary of a west-trending bedrock uplift of complexly deformed Miocene Monterey Formation (Johnson et al., 2013c). South of Summerland, the trace of the Rincon Creek fault appears to be offset ~1000 m by a north-striking transfer zone or tear fault (Fig. 2). Farther west, the fault may extend on land at Santa Barbara as the Lavigia fault,

which similarly forms a local boundary between the Monterey Formation on the south and Quaternary strata (the Santa Barbara Formation) on the north (Minor et al., 2009). Thus, the segmented fault may have a total length of 20 km or more.

There is no evidence in our offshore data set for post-LGM activity on the Rincon Creek fault. The fault has no apparent influence on post-LGM sediment distribution and thickness, and is crossed by a post-LGM sediment trough south of Montecito (Figs. 5A and 12) that might be a broad lowstand paleo-channel system. Simms et al. (2016a) suggested that a combination of synclinal folding and downdropping on the Rincon Creek fault is responsible for active subsidence (~1.2 mm/yr) in the Carpinteria slough.
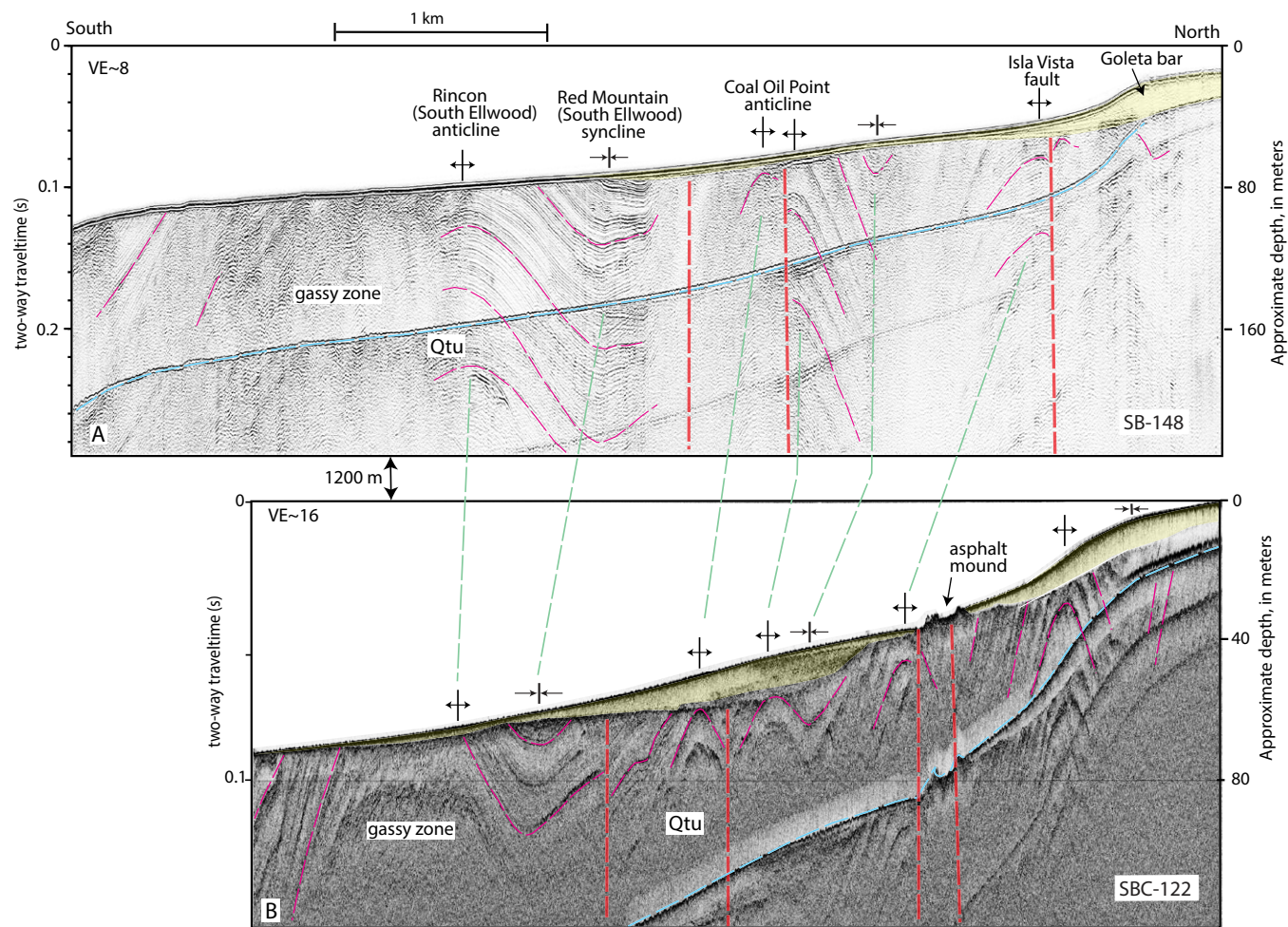
Figure 11. (A) U.S. Geological Survey seismic reflection minisparker profile SB-148. (B) Chirp profile SBC-122. Locations are shown in Figure 3. VE—vertical exaggeration. Yellow shading shows latest Pleistocene to Holocene (post–Last Glacial Maximum) deposits; QTu is deformed Quaternary strata in southern part of profile; Pliocene to Miocene strata are in northern part of profile. Red dashed lines show faults; thin magenta lines highlight prominent reflections and are intended to highlight dips; green dashed lines correlate folds between the two profiles; blue dashed line shows seafloor multiple.

Isla Vista Fault

The steep Isla Vista fault, mapped onshore by Minor et al. (2009), extends into the offshore both east of Goleta Point (Fig. 11A) and west of Coal Oil Point, and has a minimum mapped length (onshore and offshore) of ~10 km (Fig. 2). The eastern offshore part of this fault dies out 5 km east of Goleta Point in a zone of tight folding.

West of Coal Oil Point Structural Discontinuity

There is a significant discontinuity in shelf geologic structure ~4–5 km west of Coal Oil Point (Conrad et al., 2014, 2015). Just east of this discontinuity between Santa Barbara and Goleta, 2 shallow seismic reflection profiles spaced 1200 m apart cross 7 shallow fold axes and 3 fault zones over a cross-strike distance of 3.2 km (Fig. 11). Based on industry seismic reflection data,

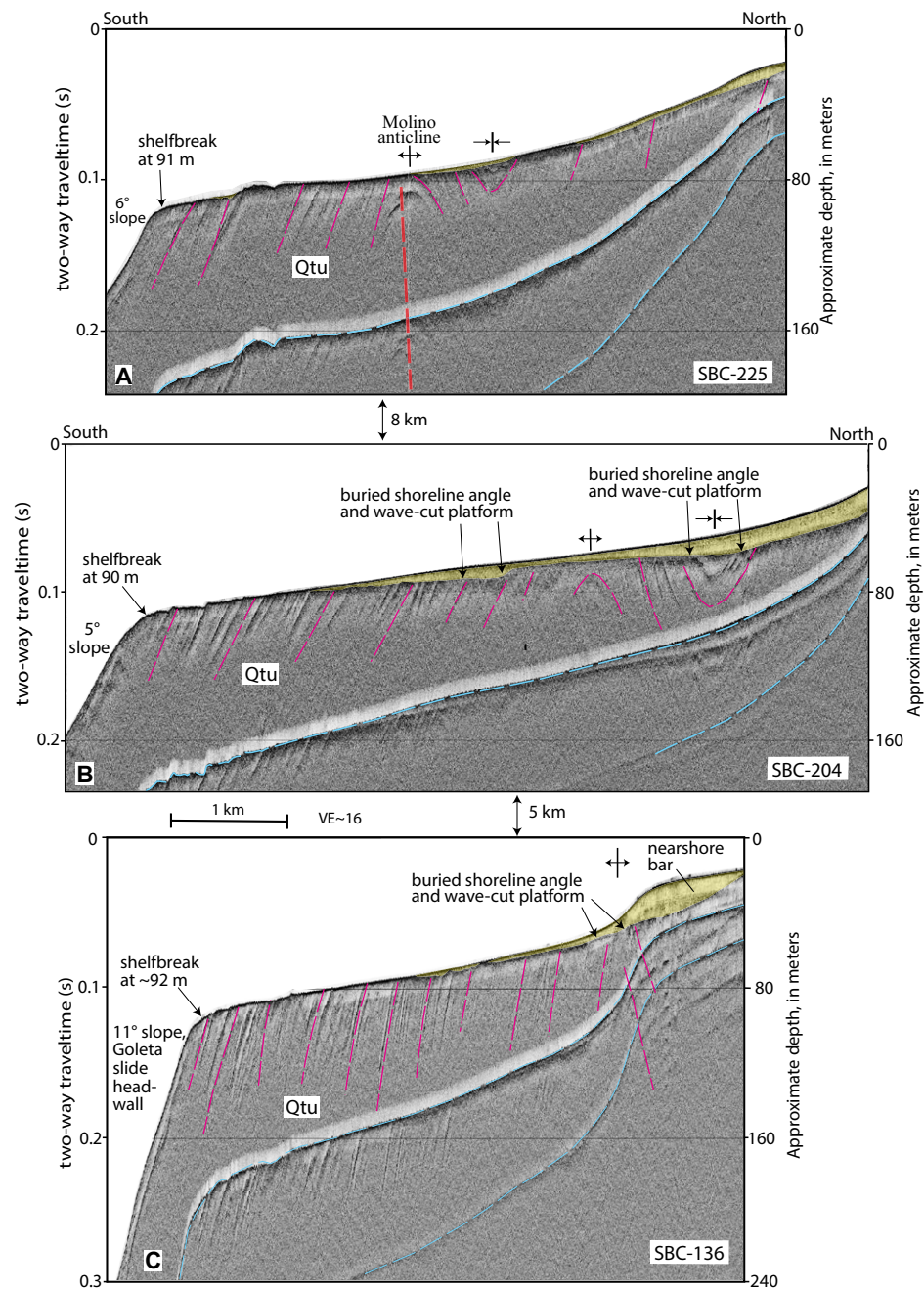Johnson et al. | Shelf evolution, Santa Barbara Channel

Figure 12. U.S. Geological Survey seismic reflection chirp profiles. (A) SBC-225. (B) SBC-204. (C) SBC-136. Locations are shown in Figure 3. VE—vertical exaggeration. Yellow shading shows latest Pleistocene to Holocene (post–Last Glacial Maximum, LGM) deposits; QTu is Miocene–Quaternary strata. Red dashed line shows fault; thin magenta lines highlight prominent reflections and are intended to highlight dips; blue dashed line shows seafloor multiple. Buried wave-cut platforms and shoreline angles are inferred to result from pulses of relative sea-level stability during the post-LGM transgression.

Leifer et al. (2010) showed similar but deeper structural complexity in the same area. This complexity is attributed to a dense network of thrusts and backthrusts that ultimately root in the North Channel–Pitas Point fault system. West of the discontinuity, seismic profiles show that most of the shelf is underlain by uniformly south-dipping bedrock (Fig. 12C), and that the axis of the southernmost shelf anticline has moved ~1700 m to the north (Fig. 2). The Rincon–South Ellwood anticline, continuous across the shelf for 45 km, disappears (or is displaced to the north), as do the other faults and folds imaged in Figure 11.

The discontinuity could be associated with a shallow, oblique, or across-strike tear fault. A shore-parallel, seismic reflection tie line profile across the mid-shelf (Fig. 13) images a zone of deformed strata coinciding with the discontinuity; however, the profile is difficult to interpret because its azimuth is subparallel to the strike of bedding planes.

A segment boundary in the North Channel–Pitas Point fault system proposed in Sorlien and Nicholson (2015) coincides with this structural discontinuity, and the two features may be related; they described a 25° east to west change (from 295° to 270°; Fig. 2) in the strike of the Pitas Point fault ~6–7 km west of Coal Oil Point based on subsurface mapping from three-dimensional seismic reflection data. The cross sections of Redin et al. (2005, their sections 35 and 36) also show significantly different deep structural geometries beneath the shelf on opposite flanks of this discontinuity. Segment boundaries have been suggested for similar bends in thrust systems of the eastern Ventura Basin (Yeats et al., 1997) and the California Coast Range (Stein and Ekström, 1992).

Faults and Folds West of Structural Discontinuity

West of the structural discontinuity noted here, the North Channel–Pitas Point fault system continues west beneath the slope for ~45 km to Point Conception. Well-constrained cross sections (Redin et al., 2005; their sections 40 and 41) indicate that the fault system ends a few kilometers west of Point Conception, in a transitional region between the contractional western Transverse Range province and the Hosgri strike-slip fault system to the north (Sorlien

et al., 1999). The shelf in this region is obliquely cut by the south branch of the Santa Ynez fault (see following).

Excluding the Gaviota bar and several other inner shelf bars (see following), the seafloor between Coal Oil Point and Point Conception largely consists of folded bedrock with local thin sediment cover (Fig. 5A). Closely spaced seismic reflection profiles reveal that the shallow folds display variable geometry, length, amplitude, continuity, and wavelength (Figs. 12–16). The most continuous folds are the 17-km-long, west-trending Molino anticline east of the south Santa Ynez fault (Figs. 12A and 14), and the 22-km-long Government Point syncline west of the Santa Ynez fault (Fig. 2; Fischer, 1998). The shelf notably broadens and flattens west of Point Conception (Figs. 16 and 17).

South Branch of Santa Ynez Fault

The steep southwest-striking south branch of the Santa Ynez fault as mapped by Dibblee (1950, 1981a, 1981b) is unique among regional structures in that it obliquely crosses the east-west structural grain of the Santa Barbara shelf and Santa Ynez Mountains. The fault was difficult to map in the offshore because the pre-LGM section on the shelf includes massive reflection-free zones, probably associated with gas or steep dips, and the adjacent slope is mainly underlain by massive to chaotic seismic facies of the Conception fan (Fig. 15). Compared to previous offshore mapping (Fischer, 1998), we show the fault as a steep zone (as wide as 1000 m) of parallel strands with a straighter trend (~224°). We infer that the fault formed the northwest margin of the Gaviota bar (see following), a relationship that suggests southeast-side down vertical offset, opposite to the sense of offset suggested by Rockwell et al. (1992) based on on-land marine terraces, and by topography in the Santa Ynez Mountains to the northeast (Fig. 2; Duvall et al., 2004). The fault zone cannot be traced across the slope into deeper water and appears to disperse into a diffuse zone of several shorter, more west-trending, faults on the outer shelf (Fig. 2). This fan-like pattern of faults is characteristic of terminating, transpressional, strike-slip faults (Christie-Blick and Biddle, 1985; Mann, 2007).
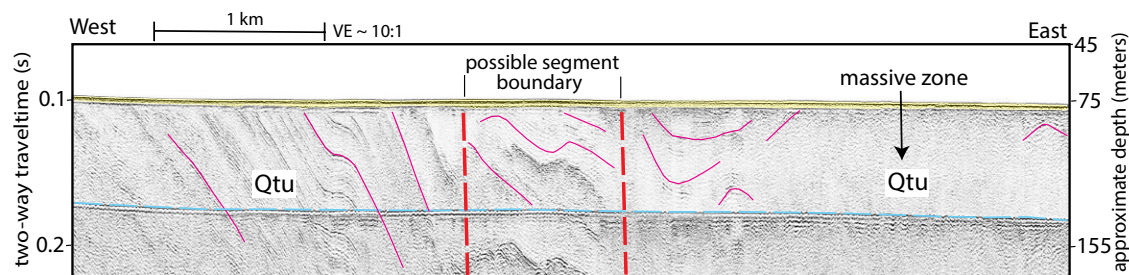

Figure 13. U.S. Geological Survey minisparker seismic reflection profile GS-141T Location shown in Figure 3. VE—vertical exaggeration. Yellow shading shows latest Pleistocene to Holocene (post–Last Glacial Maximum) deposits. QTu is deformed lower Quaternary and Neogene strata. Red dashed lines show faults; thin magenta lines highlight prominent reflections.

Figure 14. U.S. Geological Survey minisparker seismic reflection profiles. (A) GS-73. (B) GS-53. Locations are shown in Figure 3. VE—vertical exaggeration. Yellow shading shows latest Pleistocene to Holocene (post–Last Glacial Maximum) deposits; orange shading shows small shelf break deltas and correlative upper slope strata; QTu is deformed older Quaternary and Neogene strata. Red dashed lines shows faults; thin magenta lines highlight prominent reflections and are intended to highlight dips; blue dashed line shows seafloor multiple.
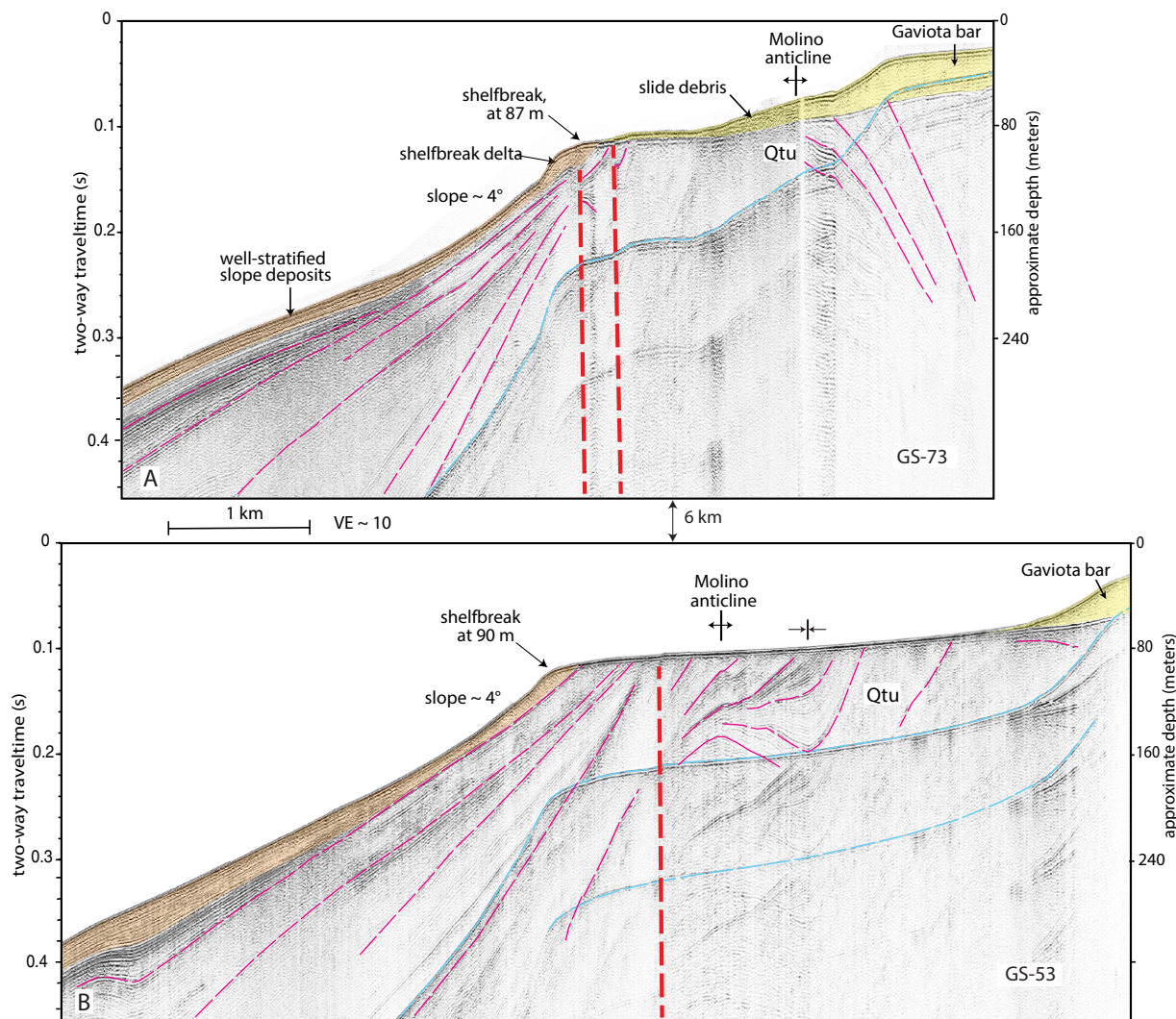
Morphology of the Shelf and Upper Slope

The morphology of the Santa Barbara shelf and upper slope is variable and complex. For our analysis, we combined bathymetry and sediment distribution data (Fig. 5) in a set of 25 shoreline to upper slope transects (Fig. 6). Transect lines were drawn to cross the shelf break every 5 km of longitude and are oriented approximately normal to the shelf break.

The location of the shelf break was mapped on the basis of slope and curvature maps and local, precise delineation of slope change on seismic reflection profiles (Fig. 3). Bathymetric transects also show locations of more important active faults and folds, and are color coded, showing (1) red: shelf with exposed bedrock or very thin (<2.5 m) sediment cover (see following); (2) green: shelf with thicker sediment cover; and (3) blue: upper slope.

Figure 15. U.S. Geological Survey minisparker seismic reflection profiles. (A) Combined GS-64R and GS-126A. SYF—Santa Ynez fault. (B) GS-70 with northern, shallow part of GS-69R. Locations are shown in Figure 3. VE—vertical exaggeration. Yellow shading shows latest Pleistocene to Holocene (post–Last Glacial Maximum) deposits; blue shading shows mixed massive, hummocky, and stratified slope deposits. QTu is older Quaternary and Neogene strata. Red dashed lines shows faults; thin magenta lines highlight prominent reflections and are intended to highlight dips; blue dashed line shows seafloor multiple.
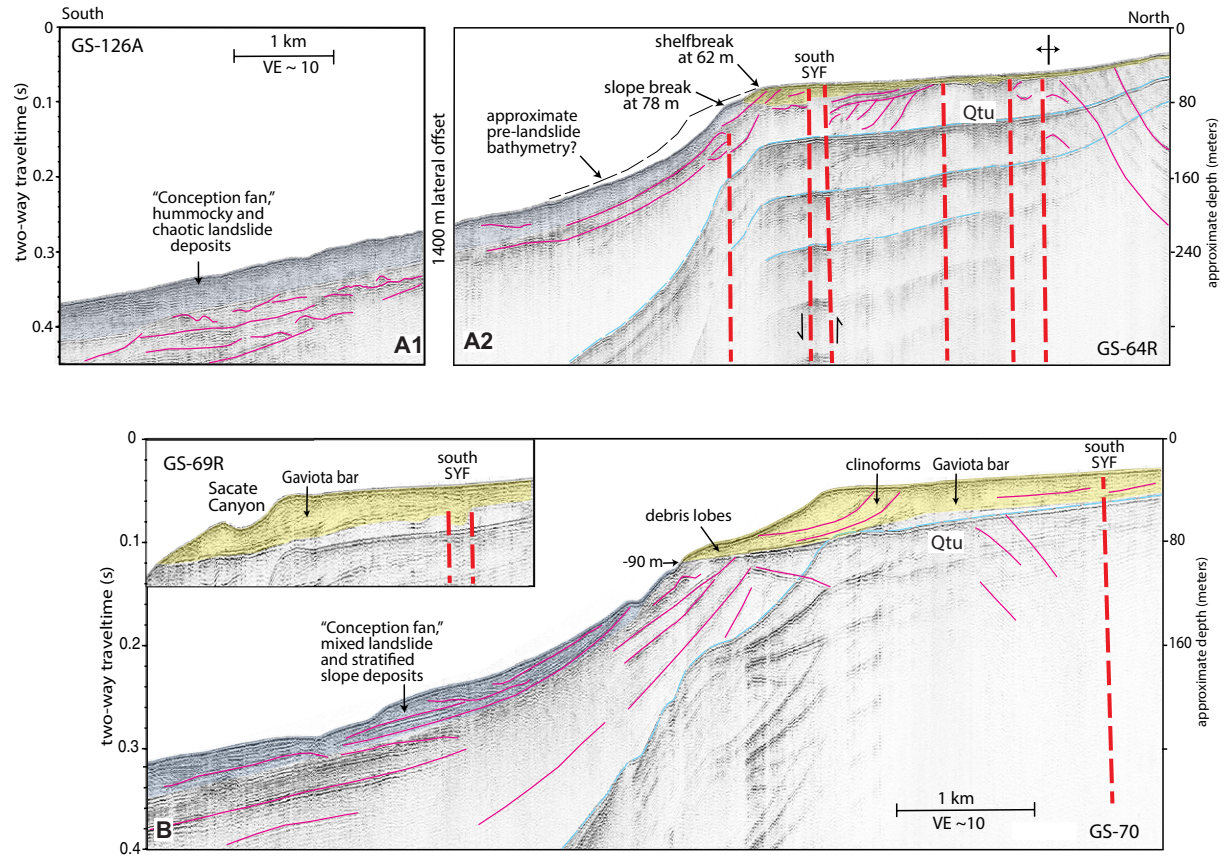
Offshore Oxnard to Carpinteria (Transects 1–6)

Between transects 1 and 6 in Figure 6, the eastern part of the Santa Barbara shelf increases in width from ~7.5 km adjacent to Hueneme Canyon on the southeast), to ~17 km south of Summerland (transect 6). Most of the shelf is smooth and covered by sediment (Figs. 4, 6, 18, and 19). The gradient of the shelf (~0.2°–0.4°) is relatively uniform and increases slightly as the shelf narrows; however, it steepens to as much as 1.5° on the outer shelf in the southeast, creating a notable convex-upward bathymetric profile (transects 1–4).

At Rincon Point, the relatively flat inner shelf is modified by a lobate boulder delta at the mouth of Rincon Creek (Fig. 20). The 750-m-wide, finger-like lobe extends 1600 m to water depths of ~20 m (Fig. 20A). The lobe consists of coarse-grained pebbly to bouldery sediment (Fig. 20B) and has as much as 8 m and 4 m of vertical relief above the adjacent shelf on its west and east flanks, respectively.

This section of inner to mid-shelf is crossed by several active faults (Montalvo fault, Oak Ridge fault, Pitas Point fault, Red Mountain fault, Rincon Creek fault) and folds (Mid-Channel anticline, Montalvo anticline, Rincon anticline) that are covered by sediment and have minimal impact on shelf morphology. Where the Red Mountain fault crosses the late Holocene coarse-grained delta lobe of Rincon Creek, it forms a 300-m-long, ~30-cm-high, south-side-up seafloor scarp on the east lobe margin (Fig. 20C). Farther west, the Red Mountain fault bifurcates into two strands that bound a low-relief bedrock uplift a few kilometers west of Carpinteria (Figs. 2 and 20D).

The 32-km-long shelf break between transects 1 and 6 trends 294° (Fig. 6), is relatively sharp, and ranges in depth from ~100 to 116 m. This variation partly reflects an oblique intersection with the Mid-Channel anticline (Figs. 2, 4A, and 8A), which underlies the shelf break on profile 5 and is located progressively down the slope and farther offshore on profiles 6, 7, and 8. On the east flank of Hueneme Canyon, the outer shelf and shelf break are character-
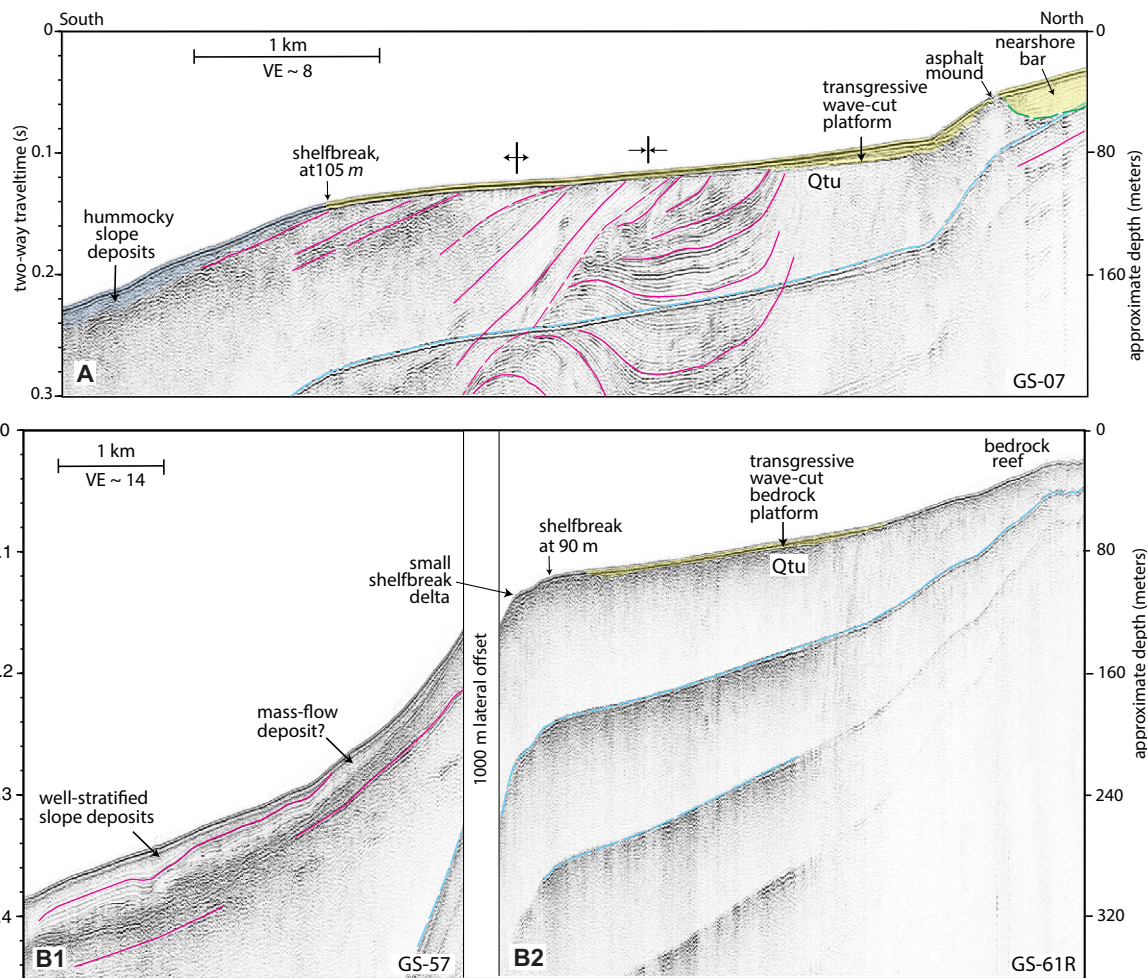
Figure 16. U.S. Geological Survey mini-sparker seismic reflection profiles. (A1, A2) GS-07. (B) Northern and combined GS-61R and GS-57. Locations are shown in Figure 3. VE—vertical exaggeration. Yellow shading shows latest Pleistocene to Holocene (post–Last Glacial Maximum) deposits. QTu is older Quaternary and Neogene strata. Thin magenta lines highlight prominent reflections and are intended to highlight dips; blue dashed line shows seafloor multiple.

ized by three well-developed sets of relatively flat platforms that are bounded (upslope) by inclined risers at depths of 77 m, 105 m, and 123 m (Figs. 18 and 19; Ritchie and Johnson, 2012).

West of Hueneme Canyon (transects 1–4 in Fig. 6), the upper slope dips ~2.5°–4.5°. There is a large (~4 km wide) radial debris fan that covers the upper slope ~4 km west of Hueneme Canyon (transect 1; Fig. 18). Farther northwest (transects 2–3), the upper slope between depths of 150 and 220 m is characterized by a 9-km-long, 1–2-km-wide, crenulated zone of slope-parallel ridges and swales. Ridges have 1–6 m of relief above adjacent swales and are spaced 80–200 m apart. The gradient of the slope increases to ~6° where the axis of the

Mid-Channel anticline crosses the shelf break (Figs. 4A and 6), but decreases farther west (to ~1.2°–1.4°) where the fold axis is in deeper water and there is a trough between the anticline and the shelf break (Fig. 8A).

Offshore Summerland to Montecito (Transects 7–8)

In the area of transects 7 and 8, shelf width progressively narrows from ~17 km southeast of Summerland to ~13 km between Montecito and Santa Barbara. The shelf gradient (~0.3°–0.4°) is relatively uniform and increases slightly as the shelf narrows. Significant post-LGM sediment is present only

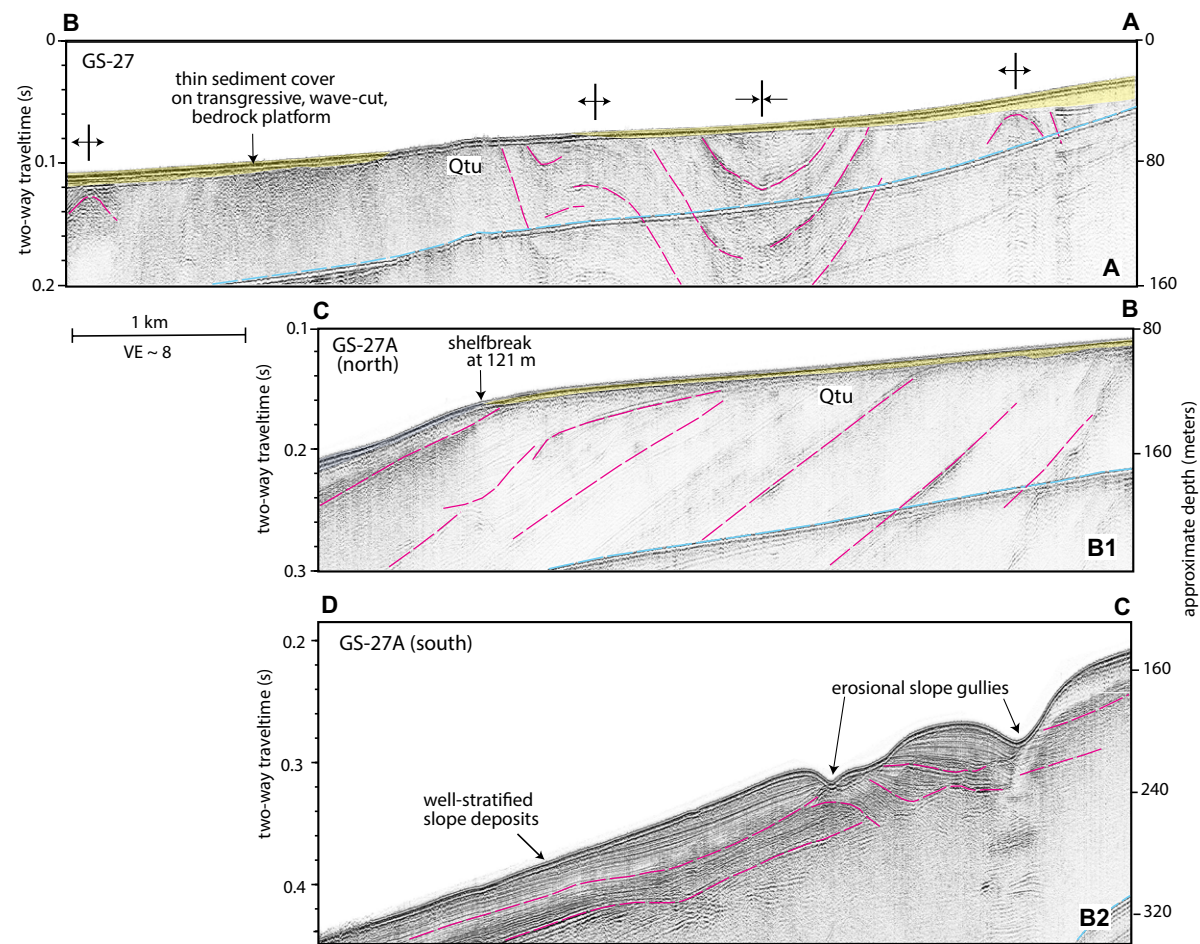Johnson et al. | Shelf evolution, Santa Barbara Channel

Figure 17. Combined U.S. Geological Survey minisparker seismic reflection profiles. (A) GS-27. (B1, B2) GS-27A. Locations are shown in Figure 3. VE—vertical exaggeration. The profile is segmented for display, but was collected continuously (location shown in Fig. 3) from A to B to C to D. Yellow shading shows latest Pleistocene to Holocene (post–Last Glacial Maximum) deposits. QTu is inferred Quaternary and Neogene strata. Thin magenta lines highlight prominent reflections and are intended to highlight dips; blue dashed line shows seafloor multiple.

on the inner shelf, and the mid- to outer shelf is largely sediment free (Fig. 5). There is a low-relief, convex-upward bedrock bulge in the mid-shelf on transects 8 and 9 that aligns with the Rincon anticline.

The shelf break in this area is curvilinear and bends to the north (mean trend of 310°), crossing the Ventura Basin where the buried tips of the Pitas Point and Oak Ridge faults are just 4–5 km apart. Shelf break depth decreases to the northwest from ~114 m in the Ventura Basin to 102 m on the basin margin above the Pitas Point fault.

Offshore Montecito to Gaviota (Transects 9–18)

The central part of the Santa Barbara shelf (between transects 9 and 18 in Fig. 6) ranges in width from ~4.7 to 7 km, and is notably narrower than to the southeast (see preceding). The gradient of the shelf decreases with increased depth, yielding concave-up bathymetric profiles. For example, the slope of the shelf on transect 9, which lacks significant sediment cover, is 2.0° between depths of 0 and 50 m, and 0.4° between depths of 50 and 90 m. The zone of
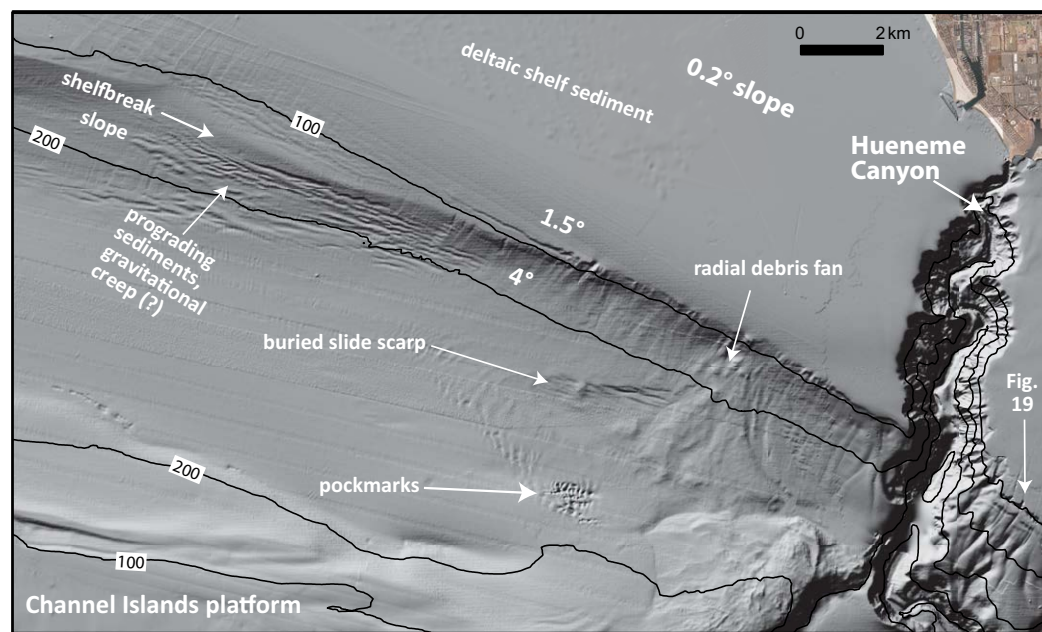
Figure 18. Hillshade digital elevation model showing the morphology of Hueneme Canyon and the southeast part of the eastern Santa Barbara shelf and slope. Note the notched outer shelf and shelf break on the east flank of Hueneme Canyon, highlighted in Figure 19.

decreased gradient aligns with the axis of the Rincon anticline, continuing the pattern noted to the east. West of El Capitan, the zone of decreased gradient on the mid- to outer shelf aligns with the axis of the Molino anticline.

The nearshore and inner shelf consists of interspersed bedrock platforms and depositional bars located at the mouths of a few larger coastal watersheds (Figs. 11, 12, and 21). Smaller mouth bars between Goleta and El Capitan (transects 11, 14, 15) have relatively flat (≤1°) top surfaces and gentle to steep (as much as 5°) bar fronts formed by prograding clinoforms; internal sediment thickness is as much as 17 m. These bars extend offshore for as much as 2 km to water depths of ~40 m (Johnson et al., 2014, 2015a).

The Gaviota bar (transect 18; Figs. 5, 6, 14, 15, and 21) occurs at the mouth of Gaviota Creek, the largest coastal watershed (~52 km²) between the Ventura River and Point Conception. This bar extends southwest for ~9 km to the shelf break, is as wide as 2 km, and has a relatively flat (~1.4°) top that extends to water depths of 60 m. The steep (as much as 5°) clinoforms on the bar front (Fig. 15B) are bounded by an apron of coalescing hummocky debris lobes (Figs. 14A, 15B, and 21B).

Bedrock outcrops on the inner shelf are typically smooth, beveled by erosion. Mid- to outer shelf seafloor bedrock is typically rougher, commonly yielding differentially eroded, low-relief, ribbed outcrops that facilitate mapping of faults and folds (e.g., Fig. 22), including the Rincon and Molino anticlines.

The 50-km-long shelf break between transects 9 and 18 is relatively straight, trends 276°–286°, and ranges in depth from 88 to 94 m. Between transects 9 and 11, the smooth upper slope dips 2.7°–4.0° and is underlain by prograding, well-stratified Quaternary sediments that thicken downslope into the Santa Barbara Basin. The upper slope along transects 12 and 13 is characterized by the west-northwest–trending (287°) headwall scarp of the large (130 km²) Goleta submarine landslide complex (Fig. 21; Eichhubl et al., 2002; Fisher et al., 2005c; Greene et al., 2006). The top of the landslide scarp ranges in depth from 85 to 200 m, the slope in the headwall scarp varies but is as steep as 40°–45° (Fisher et al., 2005c; Fig. 12C), and an extensive field of outer shelf to upper slope (~80–200 m depths) pockmarks (Fig. 22) extends west just above the headwall of the Goleta landslide for at least 8 km (Conrad et al., 2014). The landslide complex is ~14.5 km long and 11 km wide, and extends downslope to depths of ~570 m. Landsliding is inferred to have been initiated more than 200 k.y. ago and includes 3 recent failures that occurred ~6–10 k.y. ago and displaced ~1.75 km³ of landslide debris (Fisher et al., 2005c).

The smooth upper slope between transects 14 and 18 is locally as steep as 6°, but there is no evidence of significant landsliding. The relatively small (3.78 km²) Gaviota slide occurs on the mid-slope (depths of 400–500 m) ~8 km west of the Goleta landslide (Fig. 21A; Edwards et al., 1995; Fisher et al., 2005c; Greene et al., 2006; Lee et al., 2009), and may have failed as recently as 300 yr ago. Greene et al. (2006) described the Goleta bulge between the Goleta and Gaviota slides as an incipient slide in the mid-slope, bounded above by pockmarks and a 7-km-long slope-parallel crack.
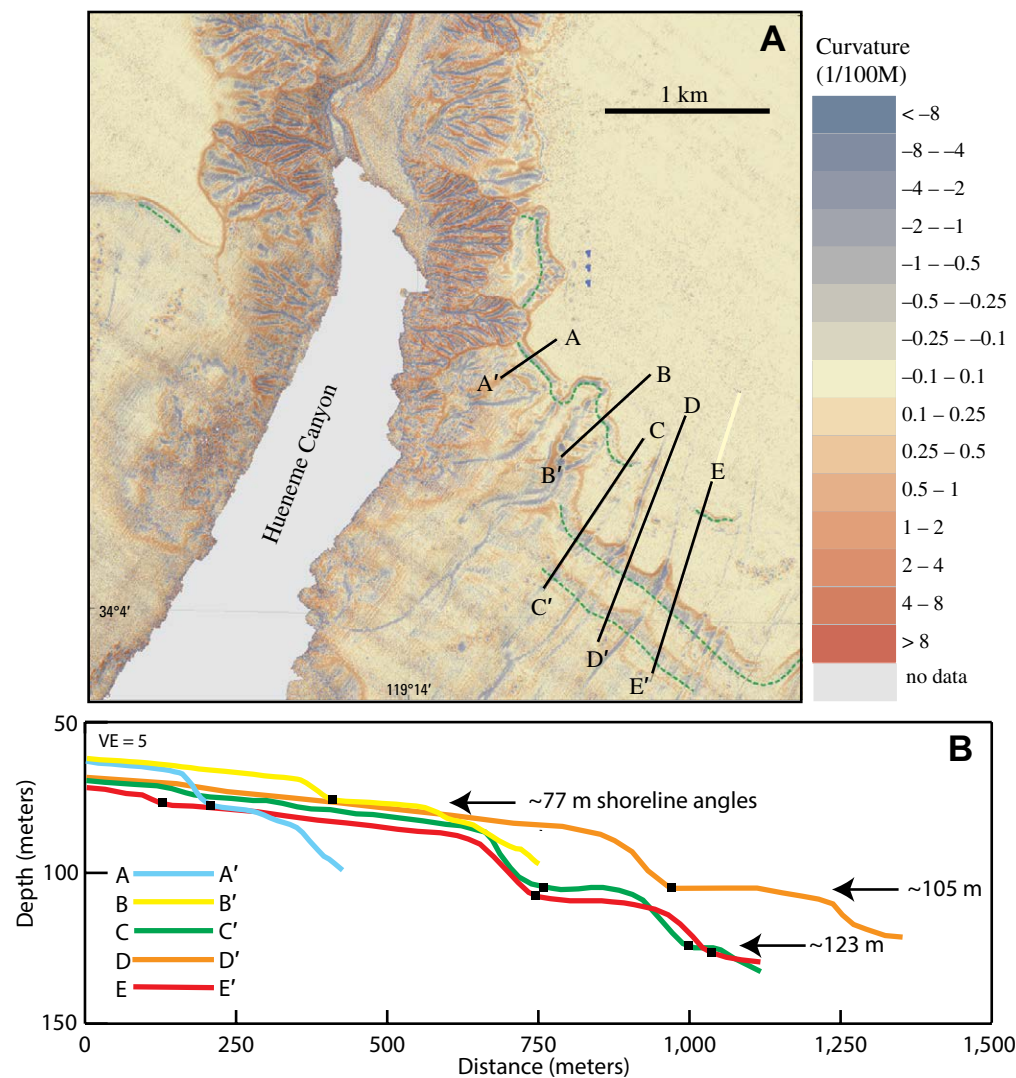
Figure 19. (A) Curvature map (from Ritchie and Johnson, 2012) showing submerged wave-cut platforms, shoreline angles (blue dashed lines), and risers along the shelf break on the east flank of Hueneme submarine canyon (Figs. 2 and 18). Curvature values (in 1/100 m) are second derivative values of elevation surface (i.e., slope of slope, calculated using methods of Zevenbergen and Thorne, 1987): positive (red) values are convex; zero (yellow) values are flat; negative (blue) values are concave. Note that ranges of curvature values represented by each color decrease as values (positive or negative) approach zero. (B) Bathymetric profiles showing wave-cut platforms, shoreline angles (black squares), and risers. Shoreline angles are at depths of ~77 m (A-A', B-B', E-E'), 105 m (C-C', D-D', E-E'), and 123 m (C-C', E-E'). VE—vertical exaggeration.

Offshore Gaviota to Point Conception (Transects 19–21)

Between the Gaviota bar and Point Conception (transects 19–21 in Fig. 6), the shelf extends southwest (~241°) for ~10 km. Shelf width varies from ~4.4 km on the east to ~7 km offshore of Point Conception, and shelf gradient decreases from ~1.0° to 0.7° as the shelf widens. The three bathymetric transects in this area (Fig. 6) have the same concave-up shape as central Santa Barbara shelf transects, caused by steeper gradients in the inner to mid-shelf relative to the mid- to outer shelf.

Slightly west of transect 19, the shelf break passes through a significant bend (from 270° in the east to 246° in the west) that coincides with marked shelf narrowing (to just 4.4 km). The shelf break is at a depth of 87–90 m east of the bend, shallows abruptly to 60 m at the bend, then progressively drops to 90 m to the west between transects 20 and 21. The shallower shelf break

Figure 20. (A) Perspective view showing the bouldery delta at the mouth of Rincon Creek. (B) Video strip of Rincon Creek lobe showing pebble-boulder composition. Location is shown in A by pink rectangle on yellow track line. (C) Color bathymetry hillshade showing surface roughness and scarp (white arrow) along the Red Mountain fault. Diagonal linear features are trackline artifacts. (D) Hillshade view west of Rincon Point showing trace of Rincon anticline (RA), Red Mountain fault bifurcating into northern (RMF-N) and southern (RMF-S) splays on the flanks of an offshore bedrock uplift, and Rincon Creek fault (RCF) on the north flank of uplifted bedrock west of Carpinteria (C). (E) The world-class Rincon surfing break, highlighting well-shaped waves refracting around the submerged Rincon Creek lobate delta.
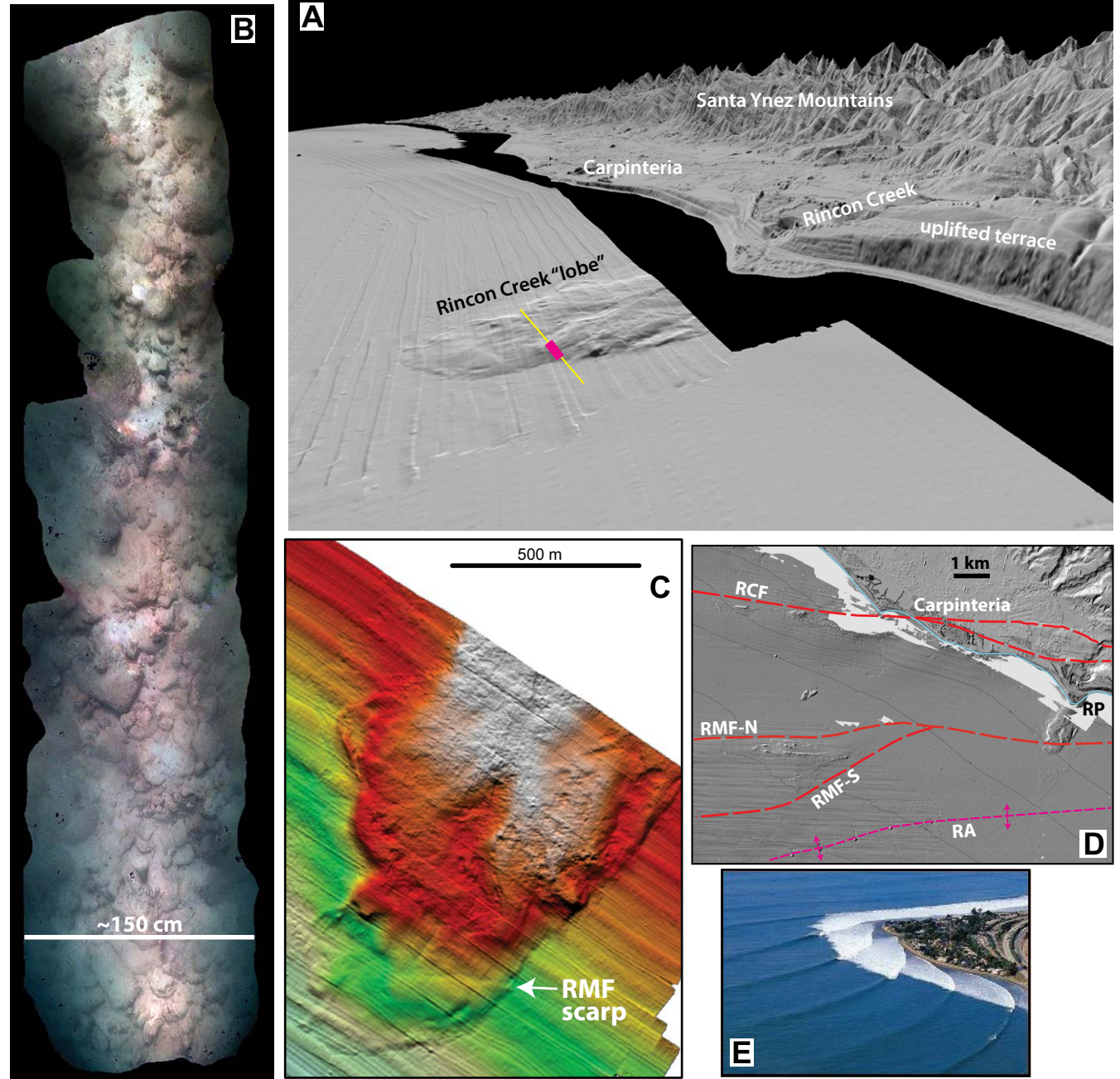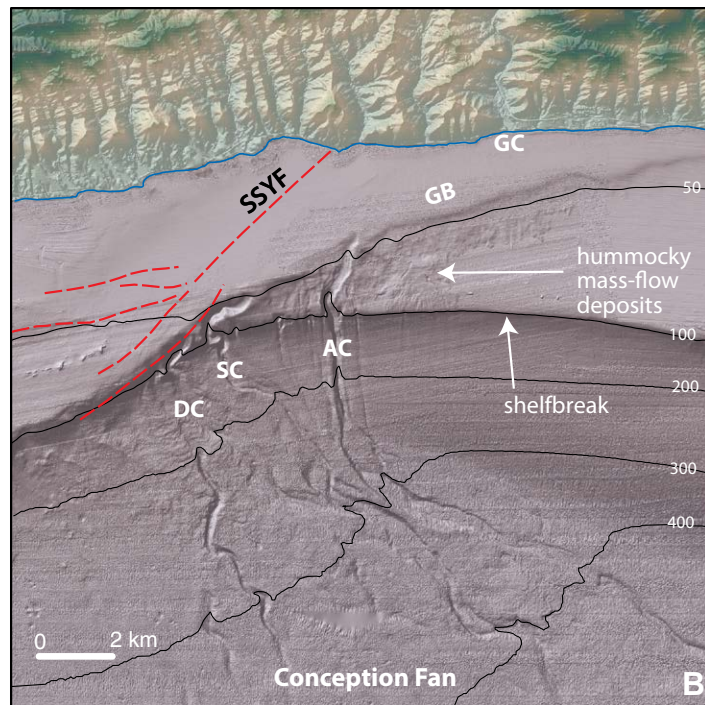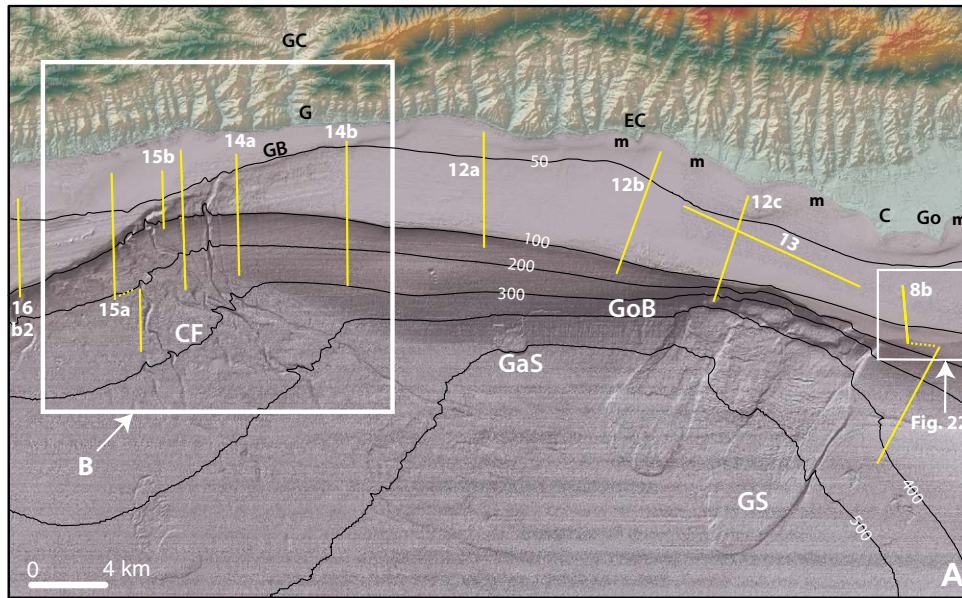
Figure 21. (A) Hillshade digital elevation model (DEM) of the west-central Santa Barbara shelf and slope. Yellow lines show tracks of seismic reflection profiles included herein (with figure numbers). (B) Smaller scale hillshade DEM of box shown in A. Red lines show strands of south Branch of Santa Ynez fault (SSYF). Abbreviations: AC—Alegria Canyon; C—Coal Oil Point; CF—Conception fan; DC—Drake Canyon; EC—El Capitan; G—Gaviota; GaS—Gaviota slide; GB—Gaviota bar; GC—Gaviota Creek; Go—Goleta; GoB—Goleta bulge; GS—Goleta slide; m—inner-shelf mouth bars; SC—Sacate Canyon.

west of the bend is underlain by bedrock and thin sediment cover, whereas the deeper shelf break east of the bend is underlain by sediment, including distal parts of the Gaviota bar. The shelf break and the distal portion of the Gaviota bar are incised by three large (150–300 m wide) channels (Fig. 21B) that have been referred to as the Gaviota Canyons (Fischer and Cherven, 1998) or as Drake Canyon, Sacate Canyon, and Alegria Canyon (Eichhubl et al., 2002).

The upper slope below this section of the shelf break consists of a hummocky incised debris apron referred to as the Conception fan (Figs. 15 and 21B) (Fischer and Cherven, 1998; Eichhubl et al., 2002). The three channels that incise the shelf break bend and traverse the southeast-sloping surface form a braided channel network comprising both continuous and discontinuous isolated channel segments. Seismic reflection profiles crossing the hummocky upper slope reveal massive zones and chaotic reflections (Fig. 15), in marked contrast to the smooth slope and continuous reflections to the east between transects 14 and 18 (Fig. 14).

Offshore and West of Point Conception (Transects 22–25)

Following the coastline, the Point Conception shelf (transects 22–25 in Fig. 6) bends to the northwest around Point Conception, and the shelf break trend changes from ~241° to 298°. Shelf width increases from ~7 km south of Point
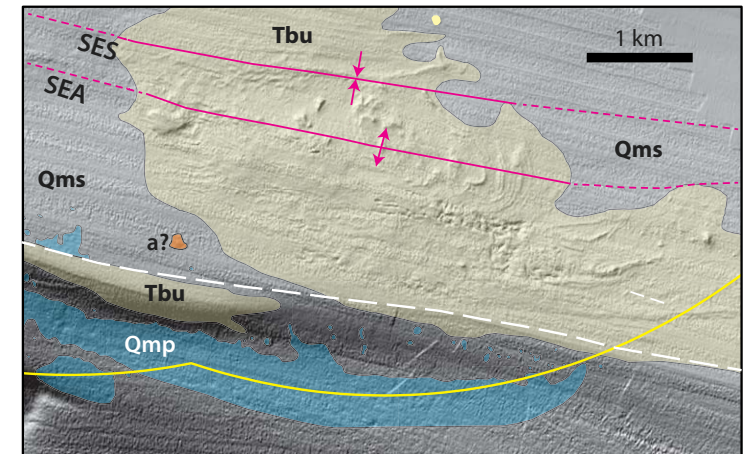
Figure 22. Colored hillshade showing the outer shelf and upper slope, crossed by the Rincon (South Ellwood) anticline (SEA) and South Ellwood syncline (SES) (Figs. 2, 11, and 20). White dashed line shows shelf break at depth of ~90 m. The rough surface texture on unit Tbu (light brown shading, undivided Miocene–Pliocene Monterey, Siquoc, and Pico Formations) results from differentially eroded sediment layers and from hydrocarbon-induced topography that can include seeps, asphalt mounds ("a?"), carbonate mats, mud volcanoes, pockmarks, mounds, and other features (Keller et al., 2007). Unit Qmp (blue shading) represents individual or large groupings of dense pockmarks, including the large occurrence on the upper slope. Qms is Quaternary marine sediment. Mapping is from Conrad et al. (2014). Location of western part of map is shown in Figure 21, and map area is crossed by seismic profile shown in Figure 8B.

Conception to ~11 km to the northwest on transect 25. The average shelf gradient varies from ~0.7° to 0.6°, decreasing to the west-northwest as the shelf widens. Shelf gradient is relatively uniform: the noted concave-upward profile of transects 9–22 is no longer apparent. The depth of the shelf break increases steadily from ~90 m southeast of Point Conception (transect 20) to ~121 m west of Point Conception on (transect 25; Figs. 16 and 17).

Five large (as much as 600–1000 m wide and 60–90 m deep) gullies incise the outer shelf and shelf break and extend more than 25 km downslope (Fig. 2). During the LGM sea-level lowstand, the three larger western gullies may have been directly connected (at different times) to Jalama Creek, the largest coastal watershed (63.5 km^2) between Point Conception and Point Arguello. Seismic reflection profiles reveal that upper slope deposits are predominantly characterized by continuous subparallel reflections, but locally include thin massive to chaotic intervals (Figs. 16 and 17).

■ DISCUSSION: POST-LGM SEA-LEVEL RISE, CHRONOLOGY, AND DEFORMATION RATES

Post-LGM Sea-Level History

The Santa Barbara shelf is here regarded as a wave-cut platform, progressively formed during the LGM (ca. 21 ka) and post-LGM transgression. The outermost shelf represents the deepest wave erosion during the LGM and, if local LGM sea level is known, the depth of the LGM shelf break can provide a vertical datum for developing a local sea-level history, for estimating post-LGM deformation rates, and for evaluating the role of accommodation space in shelf sedimentation.

We propose that an LGM sea level of ~123 m below present provides a reasonable upper estimate for the Santa Barbara Channel. This inference is based in part on the outer shelf and shelf break morphology on the east flank of Hueneme Canyon (Figs. 18 and 19), where we interpret coupled platforms and risers as indicators of former shorelines. This location is only a few kilometers north of (on the upthrown side) the active, north-dipping Malibu Coast fault system (Fig. 1; Fisher et al., 2005a; Sorlien et al., 2006), on strike with Anacapa Island and the Channel Islands platform to the west (uplift rates of 0.1–0.4 mm/yr; Pinter et al., 2003; Muhs et al., 2014) and the Santa Monica Mountains (uplift rates of 0.5 mm/yr; Meigs et al., 1999) to the east (Fig. 1). Given that post-LGM uplift is likely in this structural position, we consider the lowest shoreline angle (–123 m) an upper depth limit for the local LGM sea level. Global reconstructions put LGM sea level at ~121 m below present (e.g., Stanford et al., 2011).

Sites to the north along the central California coast also support a local LGM sea level of 121 m below present or slightly lower. On the flanks of the Monterey submarine canyon, ~300 km north of the Santa Barbara Channel, Maier et al. (2016) mapped well-developed wave-cut platforms and risers with intersecting shoreline angles at depths of 98, 108, and 122 m. This marine setting is adjacent to Aptos and Santa Cruz, where estimated uplift rates

based on emergent marine terraces range from ~0.2 mm/yr (e.g., Bradley and Griggs, 1976; Lajoie et al., 1991) to as much as 1.1 mm/yr (Perg et al., 2001). The absence of significant faulting or folding between the onshore terraces and the offshore platforms and risers (Johnson et al., 2015b, 2015c) indicates that the lowest submerged shoreline angle approximates LGM sea level at this location. Approximately 100 km north of Santa Barbara Channel near Point Buchon, most of the shelf break measured on a dense network (800 m line spacing) of seismic reflection profiles (Sliter et al., 2009; Johnson and Watt, 2012; Watt et al., 2015) is at a depth of 120–130 m, and we consider this the likely range of local LGM sea level along this section of California coast.

Previous work on estimating LGM sea level for the Santa Barbara Channel region has generated debate. Chaytor et al. (2008) used the shelf break as a datum to estimate uplift on the south flank of the Channel Islands platform (Fig. 2), which overlies the blind north-dipping Channel Islands thrust (Shaw and Suppe, 1994; Seeber and Sorlien, 2000). Chaytor et al. (2008) noted that the depth of the shelf break ranges from 90 to 100 m and 90 to 125 m on the south and north flanks, respectively, of Santa Cruz Island and Anacapa Island, assumed an LGM sea level of –140 m, and calculated an uplift rate of 1.50 ± 0.59 mm/yr for the south flank of the platform, significantly higher than nearby uplift rates reported by Pinter et al. (2003) and Muhs et al. (2014). Muhs et al. (2014) stated that the discrepancy between the on-land uplift rates and the proposed higher offshore rates would disappear with a large LGM glacial-isostatic adjustment (GIA); they proposed a local GIA model that put the Channel Islands on the peripheral forebulge of the Cordilleran LGM ice sheet and yielded an LGM sea level of 95 m below present. Clark et al. (2014) and Reeder-Myers et al. (2015) subsequently presented GIA models that proposed that LGM sea level was 100 m to 111 m lower than present for the Channel Islands. These GIA models do not incorporate information on LGM shorelines and instead rely at least in part on inferences derived from analysis of uplifted marine isotope stage (MIS) 5 terraces (e.g., Simms et al., 2016b). Only significant post-LGM subsidence (≥12–28 m, 0.6–1.4 mm/yr) could reconcile the observed depth of what we interpret as a shoreline angle on the outer shelf east of Hueneme Canyon (Fig. 19) with these GIA models.
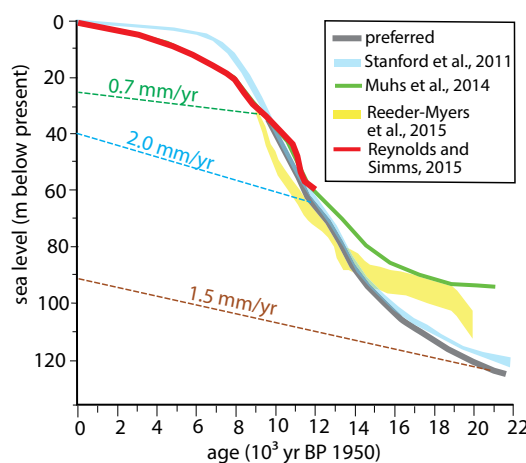
Application of the proposed GIA models to the Santa Barbara shelf and adjacent on-land terraces is also problematic. For example, the Muhs et al. (2014) GIA model would yield minimal uplift (0–0.2 mm/yr) for the central and western Santa Barbara outer shelf and shelf break (depths of 88–94 m), despite their location in the proximal hanging wall of the active North Channel–Pitas Point fault system (Figs. 2 and 7), where models of deformation above blind thrusts (e.g., Ellis and Densmore, their figure 5) suggest uplift should be maximized. In addition, because onshore mainland uplift rates range to 6–8 mm/yr (Lajoie et al., 1982, 1991; Rockwell et al., 1988, 2016; Gurrola et al., 2014), a much lower uplift rate on the shelf than on land inverts the conditions in the Channel Islands that at least in part prompted development of the Muhs et al. (2014) GIA model.

Both Chaytor et al. (2008) and Muhs et al. (2014) considered their uplift rates applicable to the large Channel Island platform without fully considering

the importance of local tectonics in creating steep, across-strike, deformation gradients. The south flank of the Channel Islands is above the active Channel Islands blind thrust fault (Shaw and Suppe, 1994; Seeber and Sorlien, 2000), a structurally complex setting characterized by upper plate folding and faulting (Dibblee et al., 1998; Pinter et al., 1998; Dibblee and Minch, 2001a, 2001b; Chaytor et al., 2008). This structural setting is somewhat similar to that of the complexly deformed Santa Barbara shelf and adjacent mainland above the North Channel–Pitas Point fault system. For the mainland, Gurrola et al. (2014) provided local uplift rates that change rapidly and range from <0 (i.e., subsidence) in synclines to as much as 2.0 mm/yr along anticlines and in fault blocks. For example, an MIS 3 (ca. 45 ka) terrace emerges above present sea level west of Carpinteria and rises to an elevation of ~200 m a few kilometers to the east near Punta Gorda (Figs. 2, 20A; Lajoie et al., 1982; Trecker et al., 1998; Frederickson, 2016).

Figure 23 shows a range of proposed sea-level curves for the Santa Barbara Channel region. Our preferred curve uses the relative sea-level curve between 12 ka and the present developed by Reynolds and Simms (2015) for southern California from analysis of coastal deposits. From 21 to 12 ka, our preferred curve slightly adjusts the global curve of Stanford et al. (2011) so that LGM sea level is 123 m below present. We acknowledge that there must have been an LGM GIA influence in this region (however slight), but suggest that this influence more likely yielded an LGM sea level that is lower than the global sea-level curve, rather than significantly higher (Muhs et al., 2014; Reeder-Myers et al., 2015). Using Figure 23, the age of the transgressive surface of erosion can be approximated based on depth. For example, the transgressive surface of erosion at water depths of 20 m and 60 m formed ~8 k.y. and 11–12 k.y. ago, respectively. In a tectonically active area such as the Santa Barbara Channel, however, such estimates need to be adjusted to incorporate ongoing uplift or subsidence.

Post-LGM Deformation Rates

The combination of high-resolution bathymetric and seismic reflection data and the proposed sea-level curve (Fig. 23) provide the basis for constraining post-LGM deformation rates on the major active structures cutting the Santa Barbara Channel shelf.

Oak Ridge Fault

The amount of relief on tilted seismic reflections in the post-LGM, 140–220-m-wide panel above the blind Oak Ridge fault shown in Figure 4 ranges from ~6.7 to 10.5 m (calculated at 1600 m/s). The discrepancy in relief results from the variable (shoreward decreasing) ages of folded post-LGM strata. When the age of strata overlying the post-LGM transgressive surface of erosion is correlated by depth with the post-LGM sea-level curve of Figure 23, the lower folded reflections for three different datums (estimated ages of ca. 18.9, 11.4, and 10.5 ka ±1 k.y.) in the narrow folds have structural-relief growth rates of ~0.6–0.7 mm/yr. Dips of post-LGM strata on the fault-tip fold range from ~2.5° to 7° (Fig. 4), notably less than forelimb dips at depth (e.g., Fisher et al., 2005b, their figure 3A; Shaw and Suppe, 1994); thus, neither constant-dip fault-propagation-fold nor fault-bend-fold models (e.g., Suppe and Medwedeff, 1990; Suppe et al., 1992) are applicable to the late Quaternary fold history. Following the method of Schneider et al. (1996) for analyzing fault-propagation folds with progressive limb rotation (Fig. 24), measurements of shortening and growth for the 3 folds in Figure 4 yielded a dip-slip rate on the underlying blind fault (dip of 63°–81°) of 0.7 ± 0.1 mm/yr. Significant left-

Figure 23. Range of post–Last Glacial Maximum sea-level curves. Our preferred model uses that of Reynolds and Simms (2015) from 12 to 0 ka (red line) and a curve very close to global sea level (Stanford et al., 2011) from 21 to 12 ka. See text for discussion. Dashed lines connect present depths (on vertical axis) of uplifted features on shelf and at shelf break with the sea-level curve at inferred uplift rates. Dashed green and blue lines show uplift on folds above Oak Ridge fault and Pitas Point fault on shelf; dashed brown line shows uplift of shelf break along central and western Santa Barbara shelf.

Figure 24. Calculation of the vertical (growth) and shortening (old bed length minus young bed length) components of folding above a blind thrust (from Schneider et al., 1996, their figure 10). Fault dip = tan⁻¹ (growth and/or shortening). For the Oak Ridge fault and Pitas Point fault examples shown in Figures 4 and 9, growth is measured on the post–Last Glacial Maximum (LGM) transgressive surface of erosion. For the outer shelf in the central and western Santa Barbara Channel, the amount of growth is determined by the depth and uplift of the LGM wave-cut platform. See text for discussion.

lateral slip on the Oak Ridge fault system was suggested (in Sorlien et al., 2000) that cannot be accounted for with our data set. Therefore, the fault slip rate presented here should be considered a minimum.

North Channel–Pitas Point Fault System

There is significant along-strike variation in the shallow local fold that formed above the tip of the Pitas Point fault, and the largest structural relief occurs in the easternmost nearshore region. Three profiles (Figs. 9A–9C) that obliquely cross the inner shelf reveal that local relief on the folded base-of-LGM reflections ranges from 21 to 25 m over a lateral distance of 200–300 m. Correlating the depth of the base of the deformed post-LGM unit to the post-LGM sea-level curve (Fig. 23) provides datum ages ranging from ca. 11.9 to 10.3 ka (±1 k.y.), indicating that subsequent structural relief was generated at growth rates of ~1.8–2.1 mm/yr. As with the Oak Ridge fault, increasing fore-limb dips with depth indicate progressive limb rotation. Following Schneider et al. (1996; Fig. 24), measurements of shortening and growth for the near-shore folds in Figures 9A–9C yielded a dip slip rate of 2.3 ± 0.3 mm/yr on the underlying steep (~68°–83°) blind fault.

This nearshore structural growth rate is consistent with the nearby on-land paleoseismologic history from Ventura outlined by McAuliffe et al. (2015), who reported 2 events with minimum uplifts of ~6 m and ~5.2 m above the fault tip occurring between 805 and 235 yr ago and 4665–4065 yr ago, respectively. Two additional onshore events with a 3800 yr recurrence interval would yield a minimum of 22.4 m of uplift in ~12 k.y., virtually the same as our reported offshore structural growth for that time interval.

Comparable analysis of deformation above the Pitas Point fault tip on seismic profiles 5 and 10 km west of the shoreline (Figs. 9D, 9E) yields much lower fault slip rates of 1.0 ± 0.1 and 0.3 ± 0. 1 mm/yr, respectively, for datums with inferred ages of 13.2 and 14.0 ka (±1 k.y.). This significant westward decrease in the amplitude of shallow folding is associated with increasing depth of the fault tip (e.g., Fig. 7) and possibly significant decreases in fault slip (see following).

In this eastern Santa Barbara Channel area, surface deformation appears to be partitioned between the local fault-tip fold and the hanging-wall Rincon anticline (Fig. 2). On the inner to mid-shelf, shore-parallel seismic reflection profiles (Fig. 3) image the post-LGM transgressive surface of erosion rising 20–25 m between the fault tip and the axis of the Rincon fold, an amount that we attribute to anticlinal growth. Combining this growth (20–25 m) with the amount developed at the fault tip (21–25 m) yields ~41–50 m of structural relief above the Pitas Point fault in the inner to mid-shelf over the past ~12 k.y., maximized on the crest of the Rincon anticline. Approximately half (~10–13 m) of the Rincon anticline component of structural relief would be manifested at Pitas Point (based on its location; Fig. 2), where Rockwell et al. (2016) documented 38 m of Holocene uplift based on elevations of 4 marine terraces with ages of 0.95, 2.09, 4.4, and 6.7 ka. Thus, the amount of Holocene uplift predicted for Pitas Point solely from offshore structural relief (30–38 m) and the observed on-land uplift (38 m) are similar, but the offshore record spans a longer time period (12 k.y. versus 6700 yr). The discrepancy could reflect the lack of chronological precision in the offshore record, or the contribution of slip on other faults (e.g., Padre Juan fault) to local Holocene uplift at Pitas Point (Nicholson et al., 2016).

Because of the partitioning between the local fault-tip fold and the regional hanging-wall anticline, the fault-slip rate that we report based solely on analysis of the local fault-tip fold (2.3 ± 0.3 mm/yr) represents a minimum estimate for the Pitas Point fault in the eastern Santa Barbara Channel. For comparison, Hubbard et al. (2014) derived much higher slip rates of ~4.4–6.9 mm/yr for the Ventura (i.e., Pitas Point) fault based on analysis and modeling of seismic reflection profiles and well data crossing the Ventura fault and Ventura Avenue (i.e., Rincon) anticline. Marshall et al. (2017) reported a forward mechanical model based on geodetic data that predicts a slip rate of 3.5 ± 0.3 mm/yr for the Ventura–Pitas Point fault.

The North Channel–Pitas Point fault system moves farther offshore in the central and western Santa Barbara shelf region, where surface deformation is manifested by warping and uplift of the mid-shelf to the east (e.g., transects 8 and 9 in Fig. 6) and outer shelf and shelf break to the west (e.g., transects 10–22 in Fig. 6). West of Goleta (Figs. 2 and 6), the maximum depth of the wave-cut platform at the shelf break provides the best indication of post-LGM uplift. Because of rapid post-LGM sea-level rise, there has been no erosion of this wave-cut platform and changes in its elevation can be considered uplift of rocks relative to the geoid (England and Molnar, 1990). Given that (1) we assume that LGM sea level in this region was ~123 m below present (Fig. 23), and (2) the shelf break in the central and western Santa Barbara channel (Santa Barbara to Point Conception) now has a mean depth of ~91 m, we infer a relatively consistent uplift rate for the shelf break in this area of ~1.5 mm/yr (~32 m in 21 k.y.).

Use of the shelf break as a datum for estimating uplift is consistent with models of ground surface displacement (e.g., Ellis and Densmore, 2006, their figure 5) above blind thrust faults with depths and dips similar to the North Channel–Pitas Point fault system. These models predict maximum uplift at the shelf break (1–4 km north of the fault tip), and rapidly decreasing uplift to the north across the shelf to the shoreline and on land. Such a northward decrease in uplift and relief can also be viewed on shelf transects (Fig. 6) and seismic reflection profiles (Figs. 16 and 17) around Point Conception that document progressive shelf flattening and shelf break deepening (from 91 to 121 m).

Dip-slip rate estimates on the fault system beneath the central and western Santa Barbara shelf are 2.0 ± 0.2 mm/yr, using the methods of Figure 24 for folds with progressive limb rotation (see preceding) and 45°–55° dips on the underlying North Channel–Pitas Point fault system (Sorlien and Nicholson, 2015). Both the estimated fault-slip and structural growth rates in the central and western Santa Barbara shelf region depend on a local LGM sea level of 123 m below present (Fig. 23; see preceding discussion). An alternative LGM sea level of –111 m (Reeder-Myers et al., 2015) would yield uplift and fault-slip rates of 1 mm/yr and 1.2 ± 0.2 mm/yr, respectively; an LGM sea level of –95 m (Muhs et al., 2014) would yield uplift and fault-slip rates of 0.2 mm/yr and 0.2 ± 0.1 mm/yr, respectively.

The inferred similarity in uplift and fault slip across the central and western Santa Barbara shelf region does not coincide with the decrease in modeled geodetic shortening rates (from 6 mm/yr to 2.5 mm/yr; Fig. 2). We think the decrease in shortening is instead accommodated by a significant westward decrease in hanging-wall deformation, consistent with our seismic reflection profiles (Figs. 3, 8–12, and 14–17) and regional north-south cross sections (Redin et al., 2005). Compared to the region west of Goleta, cross sections between Ventura and Goleta notably reveal denser sets of thrust and reverse faults with much larger stratigraphic offsets, tighter folding, and steeper dips.

In summary, our interpretation is that the North Channel–Pitas Point fault system has a minimum slip rate of 2.3 ± 0.3 mm/yr near Pitas Point in the easternmost Santa Barbara Channel, and this slip rate decreases to ~2.0 ± 0.2 mm/yr in the central and western Santa Barbara Channel.

■ POST-LGM SHELF AND UPPER SLOPE EVOLUTION

Active tectonics over the past few million years shaped the heterogeneous Western Transverse Range province (e.g., Atwater, 1998). In the Santa Barbara Channel region, uplift of the Santa Ynez Mountains created a significant drainage divide and sediment source, and subsidence of the Ventura Basin created a trough that focused the course and mouth of the Santa Clara River. Sediment from the Santa Clara River and much smaller watersheds entered a coastal environment modulated by eustatic fluctuations between continental shelf and alluvial plain. Erosion during transgressions beveled soft Neogene rocks and Quaternary sediments into a wave-cut platform, forming and reforming the continental shelf. Active tectonics (faulting and folding) modified the shelf and upper slope, creating local domains of uplift and subsidence. Sedimentation further modified the shelf, variably filling accommodation space.

Eustasy, tectonics, and sediment supply continued to be primary controls on the much shorter, post-LGM evolution of the Santa Barbara shelf and upper slope. The specific and variable influence of these different controls are described here for four discrete geographic domains, delineated on the basis of morphologic, stratigraphic, and structural data (Fig. 2): (1) the eastern Santa Barbara shelf, located south of the south-dipping Oak Ridge fault; (2) the asymmetric Ventura Basin, located in the footwall of both the Oak Ridge fault (to the south) and the Pitas Point fault (to the north); (3) the central and western shelf Santa Barbara shelf, located north of the north-dipping North Channel–Pitas Point fault system, extending from Pitas Point to Point Conception; and (4) the shelf west and northwest of Point Conception.

Eastern Santa Barbara Shelf

The eastern Santa Barbara shelf (Figs. 2, 5, and 6) is offshore of the mouth of the Santa Clara River and is characterized by a broad, gently dipping, shelf and thick post-LGM sediment cover (mean thickness = 24.7 m, sediment volume = 7.5 km³; Table 1). In the southeast where the shelf is narrower and has a distinct convex-up profile (Fig. 6), thick sediment cover (Fig. 5) is prograding

over the shelf break onto an upper slope characterized by a laterally extensive zone of swales and ridges (Fig. 18). Similar features on other prograding slopes (e.g., Gardner et al., 1999; Lee et al., 2007) have been attributed to migrating sand waves and/or slope failure. Sediment cover on the outer shelf thins to the northwest where the shelf is widest (~16 km).

Active tectonics influenced this supply-dominated shelf (Swift and Thorne, 1991; Sommerfield et al., 2009) primarily by determining the location of the mouth of the Santa Clara River, source of the thick sediment cover. Because of high sediment supply, active tectonic features (Montalvo fault and anticline, Mid-Channel fault and anticline) that trend across the shelf are draped and have no seafloor relief. Along the northwest part of the shelf, uplift of the Mid-Channel anticline may be resulting in slight ponding of shelf sediment and oversteepening of the upper slope (Fig. 4A).

Ventura Basin

The west-trending ~5–8-km-wide Ventura Basin obliquely crosses the shelf offshore of the mouths of the Santa Clara and Ventura Rivers (Fig. 2). The shelf is flat (active faults and folds have no relief), but the basin is markedly asymmetric (e.g., Figs. 4A and 5) and the thickest sediment fill is adjacent to the Oak Ridge fault. Mean post-LGM shelf sediment thickness, maximum thickness, and sediment volume are 30.4 m, 57 m, and 6.4 km³ (Fig. 5; Table 1), respectively. Sea-level rise and subsidence, forced in part by basin-margin loading, provided post-LGM sediment accommodation space.

Together the eastern Santa Barbara shelf and Ventura Basin shelf contain ~13.8 km³ of post-LGM sediment, significantly more than previous estimates (e.g., Sommerfield et al., 2009). At modern sediment supply rates (Warrick and Farnsworth, 2009), the Ventura Basin and eastern Santa Barbara shelf have retained ~5750 yr of the post-LGM sediment yield of the Santa Clara and Ventura Rivers. Most of the remaining post-LGM sediment has presumably been transported off the shelf to Santa Monica basin via Hueneme Canyon (Normark et al., 2009).

Central and Western Santa Barbara Shelf

Eastern Subarea

We divided the Santa Barbara shelf north of the North Channel–Pitas Point fault system into two areas at the approximate longitude (119°34′W) of Summerland (Fig. 5). The much smaller eastern area is offshore of very steep, unstable, rapidly uplifting (Rockwell et al., 2016), landslide-prone coastal watersheds (e.g., Fig. 2; Johnson et al., 2013a, their sheet 10) that yield large sediment loads (~220,000 m³/yr; J. Warrick, 2016, written commun.). Mean sediment thickness and total sediment volume for this eastern subarea are 14.8 m and 1.8 km³ (Table 1), respectively. This subarea only includes portions of the inner and midshelf (Figs. 2, 5, and 20), including the Rincon Point delta lobe, and is crossed by the Rincon anticline and two strands of the Red Mountain fault (Fig. 8).

Western Subarea—Shelf

The western subarea between Summerland and Point Conception composes the bulk of the central and western Santa Barbara shelf. This shelf area is south of the uplifting, laterally continuous Santa Ynez Mountains (Fig. 2). Although these mountains have significant relief, they provide relatively limited sediment because watersheds are small and restricted to a narrow (~3–6 km wide) coastal zone between the drainage divide and the shoreline. Notably, just one watershed (Gaviota Creek) breaches the drainage divide over a lateral distance of ~100 km.

Most shelf sediment has been deposited in nearshore to inner shelf bars (Figs. 5, 11, 12, 14, and 15) at or near the mouths of coastal watersheds. These include the Gaviota bar, Goleta bar, and discontinuous bars between Coal Oil Point and El Capitan (Fig. 5). Mean sediment thickness and total sediment volume for this western part of the shelf (Fig. 5) are 3.8 m and 1.9 km³, respectively (Table 1). However, the mean thickness is misleading because the Gaviota bar (Fig. 5) covers only 8.3% of the shelf area but contains 42% of its post-LGM shelf sediment (Table 2). When the Gaviota bar is excluded from the analysis, the mean sediment thickness decreases to 2.6 m. Table 2 highlights depth dependency of sediment distribution; steeper inner shelf zones at depths of 10–40 m occupy ~23.5% of the shelf but contain ~54.4% of shelf sediment. In contrast, the flatter mid- to outer shelf at water depths of 60–90 m occupies ~46% of the shelf but contains only 19.5% of shelf sediment. The south branch of the Santa Ynez fault coincides with the northwest margin of the Gaviota bar on the mid- to outer shelf (Figs. 5A and 21B), a relationship that suggests faulting was at least a partial control on its location.

Warrick and Farnsworth (2009) estimated sediment flux from coastal watersheds between the Ventura River and Point Arguello (Fig. 2) as 448,000 m³/yr, and J. Warrick (2016, written commun.) estimated the sediment supplied by watersheds to the region between Point Conception and Summerland as 141,000–283,000 m³/yr. At these modern rates, the western shelf area has retained between ~6900–13,800 yr of sediment supply. The shelf therefore seems capable of storing sediment (largely in nearshore bars), but that capability is clearly limited by sediment supply as most of the shelf lacks significant sediment. We agree with Slater et al. (2002) and Sommerfield et al. (2009), who considered the central and western Santa Barbara shelf "sediment starved" or "accommodation dominated," and attributed this condition to lack of sediment supply.

Western Subarea—Upper Slope

The upper slope between Santa Barbara and Point Conception (Figs. 12, 14, 15, 21, and 22) are underlain by the south-dipping forelimb of the large growth fold forming above the North Channel–Pitas Point fault system (see preceding). Modification of the upper slope has occurred by both landsliding and progradation, resulting in three distinct slope morphologies. From east to west

(Fig. 21A), these include: (1) the Goleta slide complex, underlain by steep landslide headwalls (Fig. 12C) and landslide deposits; (2) smooth, steep (as much as 6°) slope underlain by prograding, well-stratified Quaternary sediments that thicken downward into the Santa Barbara Basin (Fig. 14); and (3) the Conception fan (transects 19–21 on Fig. 6; Fig. 15), underlain by a mix of massive landslide and stratified sedimentary deposits.

Why did the slope beneath the Goleta landslide complex fail when the adjacent, geologically similar slope did not fail? Fisher et al. (2005c) and Greene et al. (2006) listed several factors that may have contributed to the development of the Goleta complex: (1) strong ground motions generated by local earthquakes; (2) rock and sediment layers weakened by active hydrocarbon seepage; (3) high sediment supply to the shelf edge during sea-level lowstands, forming unstable, shelf-edge deltas; (4) south-dipping slopes in the bedrock along the shelf edge, facilitating slope failure along bedding planes; and (5) location along a shallow structural discontinuity on the shelf aligned with tear faults that would decrease slope integrity. Although important, factors 1–3 are not specific to the Goleta slide failure zone in comparison to unfailed adjacent slopes, and thus cannot explain the differences in slope behavior.

Regarding factor 4, although the entire outer shelf from offshore Carpinteria to Point Conception (Fig. 2) is underlain by south-dipping bedrock, the steepest upper slope coincides with the Goleta slide (Figs. 6, 12, and 14). This steeper zone results from a location directly above the tip of the Pitas Point fault; to the west and east, the tip is mapped farther downslope (Fig. 2; Sorlien and Nicholson, 2015). Alignment with a shallow structural discontinuity (factor 5) is unique to the location of the Goleta landslide and may also be a contributing factor to slope instability, but the presence of crosscutting shallow tear faults and related structures needs further investigation (see preceding).

Fischer and Cherven (1998) suggested that, along the westernmost slope, the Conception fan was mainly fed by streams during sea-level lowstands and that continuous and partly buried fan channels form a distributary slope apron that progressively migrated from west to east. The work of Fischer and Cherven (1998) was conducted prior to the collection of high-resolution bathymetry and seismic reflection data (see preceding), and the new data sets support a modified paleographic model (Fig. 25) that accounts for these observations: (1) the elevation of the shelf break at the head of the fan is as shallow as 60 m; (2) bathymetric and seismic reflection data suggest significant landsliding; (3) sediment supply from Gaviota Creek to the outer shelf and upper slope is greater than in adjacent slope environments; and (4) fan channels and the locus of fan deposition have migrated eastward. In Figure 25, submarine landsliding in all frames is attributed to coseismic ground motions and/or depositional oversteepening on an uplifting outer shelf. The four phases of this model are as follows.

1. Pre-LGM, ca. 25 ka (Fig. 25A), sea level was ~125 m below present. The Gaviota Creek flowed southwest across an alluvial plain (the emergent continental shelf), captured by an erosional trough adjacent to the south branch of the Santa Ynez fault. Deltaic deposition occurred along the present shelf break and sediment density flows incised the marine slope at and near Drake Canyon
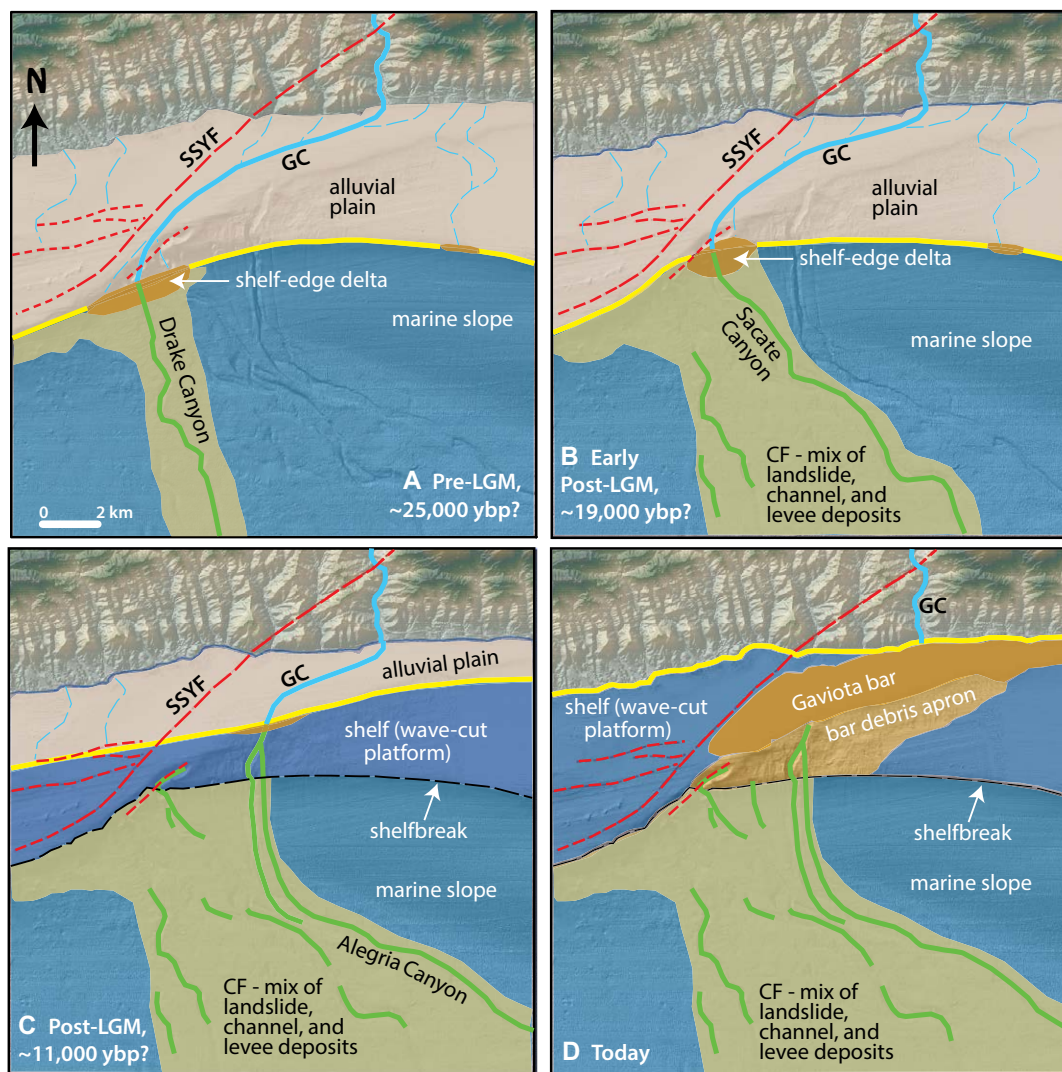
Figure 25. Proposed latest Pleistocene paleogeographic reconstruction for the Conception fan (CF). GC—Gaviota Creek (blue line), SSYF—south strand of Santa Ynez fault and associated faults (red lines); ypb—years before present (A.D. 1950); LGM—Last Glacial Maximum. Yellow line shows shoreline. Green lines show submarine canyons on Conception fan. See text for discussion.

(Fig. 21B). Deposition on the Conception fan occurred by landsliding on the upper slope and in Drake Channel and flanking levees.

2. Early post-LGM, ca. 19 ka (Fig. 25B), sea level was ~115 m below present. Landslides occurred on the upper slope on the northwest margin of the Conception fan, covering upper Drake Canyon with landslide deposits and creating an embayment in the coast at the landslide headwall. In response, the mouth of Gaviota Creek (still aligned with the Santa Ynez fault) moved eastward and

Sacate Canyon became the focus of upper slope marine incision. Gaviota Creek provided abundant sediment to Sacate Canyon and its adjacent levees.

3. Post-LGM, ca. 11 ka (Fig. 25C), sea level was ~50 m below present. More collapse of the shelf break occurred during the early and middle stages of post-LGM sea-level rise. Landslide deposits covered upper Sacate Canyon. Gaviota Creek moved farther east to align with Alegria Canyon. Transgressive erosion created and expanded a wave-cut platform over the outer shelf. Abundant

sediment from Gaviota Creek was mostly trapped close to shore because of new accommodation space created by rapid sea-level rise.

4. Today (Fig. 25D), the shoreline has been in approximately the same location for 7 k.y., since the rate of sea-level rise slowed dramatically (Fig. 23). With minimal new accommodation space being created, the Gaviota bar progrades over the transgressive surface of erosion, almost to the collapsed section of the shelf break near Drake and Sacate Canyons. The outer edge of the Gaviota bar periodically collapses (from oversteepening or earthquake-induced ground motions), creating small debris lobes.

Point Conception Shelf

West of Point Conception, the shelf widens and has a notably planar profile that contrasts with the concave-up profile of the central and western Santa Barbara shelf (Fig. 6). The transition in the shape of the shelf occurs over a distance of ~15 km as the outer shelf flattens and the shelf break drops to the northwest from ~90 m to 121 m below present sea level (Figs. 2, 16, and 17). This change is inferred to result from progressive upwarping of the shelf above the blind North Channel–Pitas Point fault system.

Sediment distribution on the shelf west of Point Conception is also notably different (Table 2). The area between water depths of 60 and 80 m occupies ~22% of the shelf but contains ~43% of shelf sediment. On the central and western Santa Barbara shelf, the same depth zone occupies 40% of the shelf but contains only 18% of shelf sediment (Table 2). Mean sediment thickness and total sediment volume for the Point Conception shelf (Fig. 5) are 3.6 m and 0.5 km³, respectively (Table 1).

■ SIGNIFICANCE FOR HAZARDS ASSESSMENT

Earthquake Hazards Assessment

Recorded and historical seismicity in the Santa Barbara Channel region is characterized by earthquake swarms, relatively frequent minor earthquakes, and infrequent large earthquakes (Lee and Vedder, 1973; Sylvester, 2001; Southern California Earthquake Data Center, 2016). The two most recent large earthquakes thought to be located in the region occurred on 21 December 1812 (assigned M7.1) and 29 June 1925 (assigned M6.8). After seismic networks became operational in 1932, notable events include a 30 June 1941 M5.5 earthquake with an offshore epicenter 8–24 km southeast of Santa Barbara; a swarm of 62 earthquakes (M2.5–5.2) between 26 June and 3 August 1968, located 10–15 km south (offshore) of Santa Barbara (Sylvester et al., 1970); a 13 August 1978 M5.1 event ~1 km southeast of Santa Barbara (Corbett and Johnson, 1982); and a 29 May 2013 M4.8 event ~6 km west of Goleta. The latter two events occurred within the North Channel–Pitas Point fault system and had focal mechanisms indicating compression on west-northwest–striking nodal planes. Relevant information for hazard assessment from our investigation is summarized in the following.

Oak Ridge Fault

The Oak Ridge fault is considered a significant earthquake hazard because it extends inland from Santa Barbara Channel for ~130 km, and has been interpreted as the westward continuation of the fault responsible for the 1994 M6.7 Northridge earthquake (Yeats and Huftile, 1995). Our work confirms previous mapping that shows the Oak Ridge fault extending for 33 km across the shelf, and others have extended the structure an additional 25 km or more into the Santa Barbara Basin (e.g., Heck, 1998; Sorlien et al., 2000; Redin et al., 2005). For hazard assessment, Field et al. (2013) and Southern California Earthquake Data Center (2016) used slip rates of 3.5–4.5 mm/yr and 3.5–6 mm/yr, respectively, for onshore areas, but did not provide offshore rates.

Our data (e.g., Fig. 4) image the Oak Ridge fault as a blind structure overlain by a narrow zone of folded reflections in post-LGM strata. Fold parameters indicate a minimum fault slip rate (not accounting for lateral offset) of 0.7 ± 0.1 mm/yr. Given the much higher onshore rates, the Oak Ridge fault must lose significant slip westward into the offshore. Nevertheless, empirical relationships between fault length and earthquake magnitude (Wells and Coppersmith, 1994) suggest that, on its own, the >58-km-long offshore section of the fault could generate an earthquake with moment magnitude, M_w, of 7.1 or higher.

North Channel–Pitas Point Fault System

As described here, the North Channel–Pitas Point fault system is continuous with the onshore Ventura fault and extends in the offshore for more than 105 km from Ventura to Point Conception (Fig. 2; Redin et al., 2005; Sorlien and Nicholson, 2015). The offshore fault is a blind north-dipping thrust and the overlying shelf is underlain by a hanging-wall fold beveled by marine erosion. A few kilometers offshore of Pitas Point, we used local folding of post-LGM strata above the fault tip to estimate a minimum fault slip rate of 2.3 ± 0.3 mm/yr (see preceding). Farther west, where the fault tip is deeper and fault-related deformation is distributed more broadly, we used the elevation of the shelf break and buried shelf wave-cut platforms as uplift indicators to estimate fault slip rates of 2.0 ± 0.2 mm/yr. Westward-decreasing slip is consistent with westward-decreasing shortening based on geodesy (Marshall et al., 2013).

If the entire offshore fault is continuous and ruptured in a single event, empirical relationships between fault length and earthquake magnitude (Wells and Coppersmith, 1994) indicate that an earthquake with M_w of 7.5 or higher is possible. However, our work suggests that one possible segment boundary is located a few kilometers west of Goleta and it is conceivable that the south strand of the Santa Ynez fault represents another such boundary. If the fault system is divided into multiple segments (e.g., 63, 32, and 10 km long) that do not rupture together, then possible magnitudes for offshore-only ruptures drop to M_w 7.2 and lower. As discussed herein, further work is needed to clarify the likely rupture length on this fault system.

Hubbard et al. (2014) and McAuliffe et al. (2015) suggested that larger events (M_w 7.7–8.1) had occurred on the Ventura–North Channel–Pitas Point system, based in part on uplifted coastal terraces at Pitas Point (Rockwell et al., 2016); they also suggested that hazard would be increased by likely multisegment ruptures through deep (below 7.5 km) linkages with the Red Mountain, San Cayetano, and other faults. Because our focus is on shallow offshore data, we don't consider the impacts of these possible deep linkages and associated increases in rupture area, but acknowledge that, given such circumstances, earthquakes larger than the ones outlined above are possible.

Tsunami Hazard Assessment

There are records of a few historical tsunamis in the Santa Barbara Channel (e.g., Toppozada et al., 1981; Borrero et al., 2002). Most notably, runup from the 1812 earthquake (see preceding) is thought to have reached as high as 4 m at Refugio Beach and 2 m in Santa Barbara (Fig. 2). Models in Greene et al. (2006) suggest that tsunamis generated by the Holocene Goleta slide (Figs. 2 and 21A) could have achieved local runups of 10 m. Ryan et al. (2015) developed a tsunami model for an M_w 7.7 earthquake on the Pitas Point fault, characterized by a 40-km-long rupture and more than 7 m of abrupt seafloor relief, generating a local tsunami height of 7–8 m. This model locates the Pitas Point fault ~2–3 km north of the fault tip that we map (Fig. 2), and also incorrectly inputs the Pitas Point fault as a seafloor-rupturing structure, not a blind fault that progressively deepens to the west. The seismic profiles of Figure 9 indicate that large uplift events generating several meters of relief could have created fold scarps on the seafloor, but only in shallow water within ~3 km west of the shoreline. For almost the entire length of the offshore Pitas Point fault system, earthquake-induced seafloor displacement should be modeled as a broad fold rather than as an abrupt seafloor uplift.

Submarine landslides, activated through failure and collapse of the upper slope, are a second potential tsunami source. In the central and western Santa Barbara Channel, significant late Quaternary slope failure has occurred on both the Goleta slide (Figs. 21 and 25; Eichhubl et al., 2002; Fisher et al., 2005c; Greene et al., 2006) and the Conception fan (Figs. 21 and 25). Given a common geomorphologic and seismotectonic setting, it is surprising that the ~24-km-long section of upper slope between these two zones of mass movement has not similarly failed. This intermediate zone is here considered a potential site of future slope failure and deserves further investigation.

■ CONCLUSIONS

The Santa Barbara Channel provides an important case history for continental shelf and upper slope evolution along a transpressional continental margin, highlighting the role of crustal faults in creating a dynamic and heterogeneous landscape and seascape. The mainland shelf in Santa Barbara Chan-

nel extends for ~120 km from Point Conception to the Hueneme submarine canyon and ranges significantly in both width (5–19 km), gradient (0.2°–0.8°), and sediment cover. Stratigraphic, structural, and morphologic data support division of the shelf in this region into three domains.

1. The eastern Santa Barbara shelf is south of and in the hanging wall of the blind, south-dipping Oak Ridge fault. The broad, gently dipping shelf has a convex-upward shape resulting from thick, post-LGM sediment (mean = 24.7 m) derived from the Santa Clara River. Sediment locally progrades on to the upper slope, and the shelf break and upper slope are impinged on and deformed by the Mid-Channel anticline.

2. The ~5–8-km-wide Ventura Basin obliquely crosses the shelf and forms an asymmetric trough that is between and in the footwalls of the blind, south-dipping Oak Ridge fault to the south and the blind, north-dipping North Channel–Pitas Point fault system to the north. Thick post-LGM sediment fill (mean = 30.4 m), derived from the Santa Clara and Ventura Rivers, thins markedly on the outer shelf.

3. The central and western Santa Barbara shelf is located north of and in the hanging wall of the blind, north-dipping North Channel–Pitas Point fault system. The concave-up shape of the shelf results from active folding of a transgressive wave-cut platform. Thin post-LGM sediment cover (mean = 3.8 m) is mainly derived from small, steep coastal watersheds and largely stored in the Gaviota bar and other nearshore mouth bars. Three distinct upper slope morphologies result from a mix of progradation and both large- and small-scale submarine landsliding.

A local sea-level curve constrains ages and rates of deformation. Post-LGM slip rates on the offshore Oak Ridge fault are a minimum of 0.7 ± 0.1 mm/yr. Slip rates on the North Channel–Pitas Point fault system are a minimum of 2.3 ± 0.3 mm/yr and decrease to the west. A decrease in regional east to west shortening is largely accommodated by diminished faulting and folding in the hanging wall above the North Channel–Pitas Point fault system. Based on their mapped offshore lengths and slip rates, both the Pitas Point and Oak Ridge faults are capable of large (M_w > 7.1) earthquakes that, in the offshore, will largely result in broad folding of the seafloor. Both earthquakes and submarine landslides along the steep shelf break are potential tsunami sources.

REFERENCES CITED

Argus, D.F., and Gordon, R.G., 2001, Present tectonic motion across the Coast Ranges and San Andreas fault system in central California: Geological Society of America Bulletin, v. 113, p. 1580–1592, doi:10.1130/0016-7606(2001)113<1580:PTMATC>2.0.CO;2.

Atwater, T., 1998, Plate tectonic history of southern California with emphasis on the Western Transverse Ranges and Santa Rosa Island, in Weigand, P.W., ed., Contributions to the Geology of the Northern Channel Islands, Southern California: Pacific Section, American Association of Petroleum Geologists Miscellaneous Publication 45, p. 1–8.

Barnard, P.L., et al., 2009, Coastal processes study of Santa Barbara and Ventura Counties, California: U.S. Geological Survey Open-File Report 2009-1029, 926 p., http://pubs.usgs.gov/of/2009/1029/.

Borrero, J.C., Dolan, J.F., and Synolakis, C.E., 2002, Tsunamis within the eastern Santa Barbara Channel: Geophysical Research Letters, v. 28, p. 643–646, doi:10.1029/2000GL011980.

Bradley, W.C., and Griggs, G.B., 1976, Form, genesis, and deformation of central California wave-cut platforms: Geological Society of America Bulletin, v. 87, p. 433–449, doi:10.1130/0016-7606(1976)87<433:FGADOC>2.0.CO;2.

Burdick, D.J., and Richmond, W.C., 1982, A Summary of Geologic Hazards for Proposed OCS Oil and Gas Lease Sale 68, Southern California: U.S. Geological Survey Open-File Report 82-33, 41 p.

California State University at Monterey Bay Seafloor Mapping Lab, 2016, Data Library: http://.otterlabs.org/SFMLwebDATA.htm (accessed June 2016).

Chaytor, J.D., Goldfinger, C., Meinter, M.A., Huftile, G.J., Rosmos, C.G., and Legg, M.R., 2008, Measuring vertical tectonic motion at the intersection of the Santa Cruz–Santa Catalina Ridge and Northern Channel Islands platform, California Continental Borderland, using submerged paleoshorelines: Geological Society of America Bulletin, v. 120, p. 1053–1071, doi:10.1130/B26316.1.

Christie-Blick, N., and Biddle, K.T., 1985, Deformation and basin formation along strike-slip faults, in Biddle, K.T., and Christie-Blick, N., eds., Strike-Slip Deformation, Basin Formation, and Sedimentation: Society of Economic Paleontologists and Mineralogists Special Publication 37, p. 1–34, doi:10.2110/pec.85.37.0001.

Clark, J., Mitrovica, J.X., and Alder, J., 2014, Coastal paleogeography of the California-Oregon-Washington and Bering Sea continental shelves during the latest Pleistocene and Holocene—Implications for the archaeological record: Journal of Archaeological Science, v. 52, p. 12–23, doi:10.1016/j.jas.2014.07.030.

Conrad, J.E., Ritchie, A.C., Johnson, S.Y., Greene, H.G., Dartnell, P., Seitz, G.G., and Gutierrez, C.I., 2014, Offshore and onshore geology and geomorphology, offshore of Coal Oil Point map area, California, sheet 10, in Johnson, S.Y., et al., California State Waters Map Series—Offshore of Coal Oil Point, California: U.S. Geological Survey Scientific Investigations Map 3302, 57 p., 12 sheets, scale 1:24,000, http://dx.doi.org/10.3133/sim3302.

Conrad, J.E., Ritchie, A.C., Johnson, S.Y., Seitz, G.G., and Gutierrez, C.I., 2015, Offshore and onshore geology and geomorphology, offshore of Refugio Beach map area, California, sheet 10, in Johnson, S.Y., et al., California State Waters Map Series—Offshore of Refugio Beach, California: U.S. Geological Survey Scientific Investigations Map 3319, 42 p., 11 sheets, scale 1:24,000, doi:10.3133/sim3319.

Corbett, E.J., and Johnson, C.E., 1982, The Santa Barbara, California, earthquake of 13 August, 1978: Bulletin of the Seismological Society of America, v. 72, p. 2201–2226.

Dahlen, M.Z., 1992, Sequence stratigraphy, depositional history, and middle to late Quaternary sea levels of the Ventura shelf, California: Quaternary Research, v. 38, p. 234–245, doi:10.1016/0033-5894(92)90059-R.

Dahlen, M.Z., Osborne, R.H., and Gorsline, D.S., 1990, Late Quaternary history of the Ventura mainland shelf: Marine Geology, v. 94, p. 317–340, doi:10.1016/0025-3227(90)90062-O.

Dartnell, P., Finlayson, D.P., Ritchie, A.C., Cochrane, G.R., and Erdey, M.D., 2012, Bathymetry and Acoustic Backscatter—Outer Mainland Shelf, Eastern Santa Barbara Channel, California: U.S. Geological Survey Data Series 702, http://pubs.usgs.gov/ds/702/.

Dibblee, T.W., Jr., 1950, Geology of Southwestern Santa Barbara County, California, Point Arguello, Lompoc, Point Conception, Los Olivos, and Gaviota quadrangles: California Division of Mines and Geology Bulletin 150, 95 p., scale 1:62,500.

Dibblee, T.W., Jr., 1981a, Geologic map of the Tajiguas quadrangle, California: U.S. Geological Survey Open-File Report 81-371, scale 1:24,000.

Dibblee, T.W., Jr., 1981b, Geologic map of the Gaviota quadrangle, California: U.S. Geological Survey Open-File Report 81-374, scale 1:24,000.

Dibblee, T.W., and Minch, J.A., 2001a, Geologic Map of Eastern Santa Cruz Island, Santa Barbara, California: Santa Barbara, California, Dibblee Geological Foundation Map DF-77, scale 1:24,000.

Dibblee, T.W., and Minch, J.A., 2001b, Geologic Map of Western Santa Cruz Island, Santa Barbara, California: Santa Barbara, California, Dibblee Geological Foundation Map DF-77, scale 1:24,000.

Dibblee, T.W., Woolley, J.J., and Ehrenspeck, H.E., 1998, Geologic Map of Santa Rosa Island: Santa Barbara, California, Dibblee Geological Foundation Map DF-68, scale 1:24,000.

Draut, A.E., Hart, P.E., Lorenson, T.D., Ryan, H.F., Wong, F.L., Sliter, R.W., and Conrad, J.E., 2009, Late Pleistocene to Holocene sedimentation and hydrocarbon seeps on the continental shelf of a steep, tectonically active margin, southern California, USA: Marine Geophysical Researches, v. 30, p. 193–206, doi:10.1007/s11001-009-9076-y.

Duvall, A., Kirby, E., and Burbank, D., 2004, Tectonic and lithologic controls on bedrock channel profiles and processes in coastal California: Journal of Geophysical Research, v. 109, F03002, doi:10.1029/2003JF000086,2004.

Edwards, B.D., Lee, H.J., and Field, M.E., 1995, Mudflow generated by retrogressive slope failure, Santa Barbara basin, California continental borderland: Journal of Sedimentary Research, v. A65, p. 57–68, doi:10.1306/D4268022-2B26-11D7-8648000102C1865D.

Eichhubl, P., Greene, H.G., and Maher, N., 2002, Physiography of an active transpressive margin basin—High-resolution bathymetry of the Santa Barbara basin, southern California continental borderland: Marine Geology, v. 184, p. 95–120, doi:10.1016/S0025-3227(01)00280-8.

Ellis, M.A., and Densmore, A.L., 2006, First-order topography over blind thrusts, in Willett, S.D., et al., eds., Tectonics, Climate, and Landscape Evolution: Geological Society of America Special Paper 398, p. 251–266, doi:10.1130/2006.2398(15).

England, P., and Molnar, P., 1990, Surface uplift, uplift of rocks, and exhumation of rocks: Geology, v. 18, p. 1173–1177, doi:10.1130/0091-7613(1990)018<1173:SUUORA>2.3.CO;2.

Fader, G.B.J., 1997, Effects of shallow gas on seismic-reflection profiles, in Davies, T.A., et al., eds., Glaciated Continental Margins—An Atlas of Acoustic Images: London, Chapman & Hall, p. 29–30, doi:10.1007/978-94-011-5820-6_4.

Field, E.H., et al., 2013, Uniform California Earthquake Rupture Forecast, Version 3 (UCERF3)—The Time Independent Model: U.S. Geological Survey Open-File Report 2013-1165, California Geological Survey Special Report 228, Southern California Earthquake Center Publication 1792, 97 p.

Fischer, P.J., 1998, Structure and tectonics of northwestern Santa Barbara basin, in Kunitomi, D.S., et al., eds., Structure and Petroleum Geology, Santa Barbara Channel, California: Pacific Section, American Association of Petroleum Geologists Miscellaneous Publication 46, p. 79–96.

Fischer, P.J., and Cherven, B.B., 1998, The Conception Fan, Santa Barbara Basin, California, in Kunitomi, D.S., et al., eds., Structure and Petroleum Geology, Santa Barbara Channel, California: Pacific Section, American Association of Petroleum Geologists Miscellaneous Publication 46, p. 155–181.

Fisher, M.A., Langenheim, V.E., Sorlien, C.C., Dartnell, P., Sliter, R.W., Cochrane, G.R., and Wong, F.L., 2005a, Recent deformation along the offshore Malibu Coast, Dume, and related faults west of Point Dume, California: Bulletin of the Seismological Society of America, v. 95, p. 2486–2500, doi:10.1785/0120050042.

Fisher, M.A., Greene, H.G., Normark, W.R., and Sliter, R.W., 2005b, Neotectonics of the offshore Oak Ridge fault near Ventura, southern California: Bulletin of the Seismological Society of America, v. 95, p. 739–744, doi:10.1785/0120040126.

Fisher, M.A., Normark, W.R., Greene, H.G., Lee, H.J., and Sliter, R.W., 2005c, Geology and tsunami-genic potential of submarine landslides in Santa Barbara Channel, southern California: Marine Geology, v. 224, p. 1–22, doi:10.1016/j.margeo.2005.07.012.

Fisher, M.A., Langenheim, V.E., Nicholson, C., Ryan, H.F., and Sliter, R.W., 2009a, Recent developments in understanding the tectonic evolution of the southern California offshore area—Implications for earthquake hazard assessment, in Lee, H.J., and Normark, W.R., eds., Earth Science in the Urban Ocean—The Southern California Continental Borderland: Geological Society of America Special Paper 454, p. 229–250, doi:10.1130/2009.2454(4.2).

Fisher, M.A., Sorlien, C.C., and Sliter, R.W., 2009b, Potential earthquake faults offshore southern California from the eastern Santa Barbara channel to Dana Point, in Lee, H.J., and Normark, W.R., eds., Earth Science in the Urban Ocean—The Southern California Continental Borderland: Geological Society of America Special Paper 454, p. 271–290, doi:10.1130/2009.2454(4.4).

Frederickson, S.M., 2016, The geomorphic transition between the Santa Barbara and Ventura fold belts near Rincon Point, California [M.S. thesis]: Santa Barbara, University of California, 114 p.

Gardner, J.V., Prior, D.B., and Field, M.E., 1999, Humboldt slide—A large shear-dominated retrogressive slope failure: Marine Geology, v. 154, p. 323–338, doi:10.1016/S0025-3227(98)00121-2.

Green, A.N., Cooper, J.A.G., and Salzmann, L., 2014, Geomorphic and stratigraphic signals of postglacial meltwater pulses on continental shelves: Geology, v. 42, p. 151–154, doi:10.1130/G35052.1.

Greene, H.G., Wolf, S.C., and Blom, K.G., 1978, The marine geology of the eastern Santa Barbara Channel with particular emphasis on the ground water basins offshore from the Oxnard Plain, southern California: U.S. Geological Survey Open-File Report 78-305, 104 p.

Greene, H.G., Murai, L.Y., Watts, P., Maher, N.A., Fisher, M.A., and Eichhubl, P., 2006, Submarine landslides in the Santa Barbara channel as potential tsunami sources: Natural Hazards and Earth System Sciences, v. 6, p. 63–88, doi:10.5194/nhess-6-63-2006.

Gurrola, L.D., Keller, E.A., Chen, J.H., Owen, L.A., and Spencer, J.Q., 2014, Tectonic geomorphology of marine terraces—Santa Barbara fold belt, California: Geological Society of America Bulletin, v. 126, p. 219–233, doi:10.1130/B30211.1.

Hapke, C.J., Reid, D., Richmond, B.B., Ruggiero, P., and List, J., 2006, National assessment of shoreline change part 3—Historical shoreline change and associated coastal land loss along sandy shorelines of the California coast: U.S. Geological Survey Open-File Report 2006-1219, 72 p., http://pubs.usgs.gov/of/2006/1219/.

Heck, R.G., 1998, Santa Barbara Channel regional formline map, top Monterey Formation, in Kunitomi, D.S., et al., eds., Structure and Petroleum Geology, Santa Barbara Channel, California: Pacific Section, American Association of Petroleum Geologists Miscellaneous Publication 46, 1 plate, p. 183–184.

Hopkins, S.E., 2006, Geometry and Quaternary evolution of the Oak Ridge fault system, Santa Barbara Channel, California [M.S. thesis]: Santa Barbara, University of California, 55 p.

Hornafius, J.S., Luyendyk, B.P., Terres, R.R., and Kamerling, M.J., 1986, Timing and extent of Neogene rotation in the western Transverse Ranges, California: Geological Society of America Bulletin, v. 97, p. 1476–1487, doi:10.1130/0016-7606(1986)97<1476:TAEONT>2.0.CO;2.

Hovland, M., and Judd, A.G., 1988, Seabed Pockmarks and Seepages: Impact on Geology, Biology and the Marine Environment: London, Graham and Trotman, Inc., 293 p.

Hubbard, J., Shaw, J.H., Dolan, J., Pratt, T.L., McAuliffe, L., and Rockwell, T.R., 2014, Structure and seismic hazard of the Ventura anticline and Ventura fault, California—Prospect for large multisegment ruptures in the Western Transverse Ranges: Bulletin of the Seismological Society of America, v. 104, p. 1070–1087, doi:10.1785/0120130125.

Huftile, G.J., and Yeats, R.S., 1995, Convergence rates across a displacement transfer zone in the western Transverse Ranges, Ventura basin, California: Journal of Geophysical Research, v. 100, p. 2043–2067, doi:10.1029/94JB02473.

Jackson, P.A., and Yeats, R.S., 1982, Structural evolution of Carpinteria basin, western Transverse Ranges, California: American Association of Petroleum Geologists Bulletin, v. 66, p. 805–829.

Jennings, C.W., and Bryant, W.A., 2010, Fault activity map of California: Sacramento, California Geological Survey, 94 p., scale 1:750,000.

Johnson, S.Y., and Watt, J.T., 2012, Influence of fault trend, bends, and convergence on shallow structure and geomorphology of the Hosgri strike-slip fault, offshore Central California: Geosphere, v. 8, p. 1632–1656, doi:10.1130/GES00830.1.

Johnson, S.Y., et al., 2012, California State Waters Map Series—Hueneme Canyon and Vicinity, California: U.S. Geological Survey Scientific Investigations Map 3225, 41 p., 12 sheets, scale 1:24,000, http://pubs.usgs.gov/sim/3225/.

Johnson, S.Y., et al., 2013a, California State Waters Map Series—Offshore of Santa Barbara, California: U.S. Geological Survey Scientific Investigations Map 3281, 45 p., 11 sheets, scale 1:24,000, http://dx.doi.org/10.3133/sim3281.

Johnson, S.Y., et al., 2013b, California State Waters Map Series—Offshore of Ventura, California: U.S. Geological Survey Scientific Investigations Map 3254, 42 p., 11 sheets, scale 1:24,000, http://pubs.usgs.gov/sim/3254/.

Johnson, S.Y., et al., 2013c, California State Waters Map Series—Offshore of Carpinteria, California: U.S. Geological Survey Scientific Investigations Map 3261, 42 p., 11 sheets, scale 1:24,000, http://pubs.usgs.gov/sim/3261/.

Johnson, S.Y., et al., 2014, California State Waters Map Series—Offshore of Coal Oil Point, California: U.S. Geological Survey Scientific Investigations Map 3302, 57 p., 12 sheets, scale 1:24,000, http://dx.doi.org/10.3133/sim3302.

Johnson, S.Y., et al., 2015a, California State Waters Map Series—Offshore of Refugio Beach, California: U.S. Geological Survey Scientific Investigations Map 3319, pamphlet 42 p., 11 sheets, scale 1:24,000, http://dx.doi.org/10.3133/sim3319.

Johnson, S.Y., Hartwell, S.R., and Davenport, C.W., 2015b, Offshore and onshore geology and geomorphology, Offshore of Santa Cruz map area, California, in Cochrane, G.R., et al., California State Waters Map Series—Offshore of Santa Cruz, California: U.S. Geological Survey Open-File Report 2015-1024, 40 p., 10 sheets, scale 1:24,000, http://dx.doi.org/10.3133/ofr20151024.

Johnson, S.Y., Hartwell, S.R., Davenport, C.W., and Maier, K.L., 2015c, Offshore and onshore geology and geomorphology, Offshore of Aptos map area, California, sheet 10, in Cochrane, G.R., and Cochran, S.A., eds., California State Waters Map Series—Offshore of Aptos, California: U.S. Geological Survey Open-File Report 2015-1025, 43 p., 10 sheets, scale 1:24,000, http://dx.doi.org/10.3133/ofr20151025.

Johnson, S.Y., Cochrane, G.R., Golden, N.E., Dartnell, P., Hartwell, S.R., Cochran, S.A., and Watt, J.T., 2017a, The California Seafloor Mapping Program—Providing science and geospatial data for California's State Waters: Ocean and Coastal Management, v. 140, p. 88–104, doi:10.1016/j.ocecoaman.2017.02.004.

Johnson, S.Y., Dartnell, P., Hartwell, S.R., Cochrane, G.R., Golden, N.E., Kvitek, R.G., and Davenport, C.W., 2017b, California State Waters Map Series—Offshore of Point Conception, California: U.S. Geological Survey data release, https://doi.org/10.5066/F7QN64XQ.

Johnson, S.Y., Dartnell, P., Hartwell, S.R., Cochrane, G.R., Golden, N.E., Kvitek, R.G., and Davenport, C.W., 2017c, California State Waters Map Series—Offshore of Gaviota, California: U.S. Geological Survey data release, doi:10.5066/F7TH8JWJ.

Johnson, S.Y., Hartwell, S.R., and Beeson, J.W., 2016, Marine Geophysical Data, Point Sal to Gaviota: U.S. Geological Survey Data Release, https://www.sciencebase.gov/catalog/item/583dd91ee4b088b77f51be4f.

Kamerling, M.J., and Luyendyk, B.P., 1979, Tectonic rotations of the Santa Monica Mountains region, western Transverse Ranges, California, suggested by paleomagnetic vectors: Geological Society of America Bulletin, v. 90, p. 331–337, doi:10.1130/0016-7606(1979)90<331:TROTSM>2.0.CO;2.

Kamerling, M.J., and Luyendyk, B.P., 1985, Paleomagnetism and Neogene tectonics of the northern Channel Islands, California: Journal of Geophysical Research, v. 90, p. 12,485–12,502, doi:10.1029/JB090iB14p12485.

Keller, E.A., Duffy, M., Kennett, J.P., and Hill, T., 2007, Tectonic geomorphology and hydrocarbon-induced topography of the mid-Channel anticline, Santa Barbara basin, California: Geomorphology, v. 89, p. 274–286, doi:10.1016/j.geomorph.2006.12.006.

Lajoie, K.R., Sarna-Wojcicki, A.M., and Yerkes, R.F., 1982, Quaternary chronology and rates of crustal deformation in the Ventura area, California: Field Trip 3, in Cooper, J.D., compiler, Neotectonics in Southern California: Geological Society of America Cordilleran Section Annual Meeting Field Trip Guidebook, p. 43–52.

Lajoie, K.R., Ponti, D.J., Powell, C.L., II, Mathieson, S.A., and Sarna-Wojcicki, A.M., 1991, Emergent marine strandlines and associated sediments, coastal California—A record of Quaternary sea-level fluctuations, vertical tectonic movements, climatic changes, and coastal processes, in Morrison, R.B., ed., Quaternary Nonglacial Geology, Conterminous U.S.: Boulder, Colorado, Geological Society of America, Geology of North America, v. K-2, p. 190–214.

Lee, H.J., Locat, J., Desgagnes, P., Parsons, J.D., McAdoo, B.G., Orange, D.L., Puig, P., Wong, F.L., Dartnell, P., and Boulanger, E., 2007, Submarine mass movements on continental margins, in Nittrouer, C.A., et al., eds., Continental Margin Sedimentation: From Sediment Transport to Sequence Stratigraphy: International Association of Sedimentologists Special Publication 37, p. 213–274, doi:10.1002/9781444304398.ch5.

Lee, H.J., Greene, H.G., Edwards, B.D., Fisher, M.A., and Normark, W.R., 2009, Submarine landslides in the southern California borderland, in Lee, H.J., and Normark, W.R., eds., Earth Science in the Urban Ocean—The Southern California Continental Borderland: Geological Society of America Special Paper 454, p. 251–269, doi:10.1130/2009.2454(4.3).

Lee, W.H.K., and Vedder, J.G., 1973, Recent earthquake activity in the Santa Barbara Channel region: Bulletin of the Seismological Society of America, v. 63, p. 1757–1773.

Leifer, I., Kamerling, M., Luyendyk, B.P., and Wilson, D.S., 2010, Geologic control of natural marine hydrocarbon seep emissions, Coal Oil Point seep field, California: Geo-Marine Letters, v. 30, p. 331–338, doi:10.1007/s00367-010-0188-9.

Luyendyk, B.P., Kamerling, M.J., and Terres, R.R., 1980, Geometric model for Neogene crustal rotations in southern California: Geological Society of America Bulletin, v. 91, p. 211–217, doi:10.1130/0016-7606(1980)91<211:GMFNCR>2.0.CO;2.

Maier, K.L., Hartwell, S.R., Johnson, S.Y., Davenport, C.W., and Greene, H.G., 2016, Offshore and onshore geology and geomorphology, Monterey Canyon and Vicinity map area, California,

sheet 10, *in* Dartnell, P., et al., California State Waters Map Series—Monterey Canyon and Vicinity: U.S. Geological Survey Open-File Report 2016-1072, 48 p., 10 sheets, scale 1:24,000, http://dx.doi.org/10.3133/ofr20161072.

Mann, P., 2007, Global catalogue, classification, and tectonic origin of restraining and releasing bends on active and ancient strike-slip fault systems, *in* Cunningham, W.D., and Mann, P., eds., Tectonics of Strike-Slip Restraining and Releasing Bends: Geological Society of London Special Publication 290, p. 13–142, doi:10.1144/SP290.2.

Marshall, S.T., Funning, G.J., and Owen, S.E., 2013, Fault slip rates and interseismic deformation in the western Transverse Ranges, California: Journal of Geophysical Research, v. 118, p. 4511–4534, doi:10.1002/jgrb.50312.

Marshall, S.T., Funning, G.J., Krueger, H.E., Owen, S.E., and Loveless, J.P., 2017, Mechanical models favor a ramp geometry for the Ventura–Pitas Point fault, California: Geophysical Research Letters, v. 44, p. 1311–1319, doi:10.1002/2016GL072289.

McAuliffe, L.J., Dolan, J.F., Rhodes, E.J., Hubbard, J., Shaw, J.H., and Pratt, T.L., 2015, Paleoseismologic evidence for large magnitude (M_w 7.5–8.0) earthquakes on the Ventura blind thrust fault—Implications for multifault ruptures in the Transverse Ranges of southern California: Geosphere, v. 11, p. 1629–1650, doi:10.1130/GES01123.1.

McCaffrey, 2005, Block kinematics of the Pacific–North American plate boundary in the southwestern United States from inversion of GPS, seismological, and geologic data: Journal of Geophysical Research, v. 110, B07401, doi:10.1029/2004JB003307.

Meigs, A., Brozovic, N., and Johnson, M.L., 1999, Steady, balanced rates of uplift and erosion of the Santa Monica Mountains, California: Basin Research, v. 11, p. 59–73, doi:10.1046/j.1365-2117.1999.00083.x.

Minor, S.A., Kellogg, K.S., Stanley, R.G., Gurrola, L.D., Keller, E.A., and Brandt, T.R., 2009, Geologic Map of the Santa Barbara Coastal Plain Area, Santa Barbara County, California: U.S. Geological Survey Scientific Investigations Map 3001, scale 1:25,000, 38 p., available at http://pubs.usgs.gov/sim/3001/.

Mitchum, R.M., Jr., Vail, P.R., and Sangree, J.B., 1977, Seismic stratigraphy and global changes of sea level, part 6—Stratigraphic interpretation of seismic reflection patterns in depositional sequences, *in* Payton, C.E., ed., Seismic Stratigraphy—Applications to Hydrocarbon Exploration: American Association of Petroleum Geologists Memoir 26, p. 117–133, doi:10.1306/M26490C8.

Monterey Bay Aquarium Research Institute, 2002, Santa Barbara Multibeam Survey: Moss Landing, California, Monterey Bay Aquarium Research Institute Digital Data Series 4 (CD-ROM).

Muhs, D.R., Rockwell, T.K., and Kennedy, G.L., 1992, Late Quaternary uplift rates of marine terraces on the Pacific coast of North America, southern Oregon to Baja California Sur: Quaternary International, v. 15/16, p. 121–133, doi:10.1016/1040-6182(92)90041-Y.

Muhs, D.R., Simmons, K.R., Schumann, R.R., Groves, L.T., DeVogel, S.B., Minor, S.A., and Laurel, D., 2014, Coastal tectonics of the eastern Pacific rim—Late Quaternary sea-level history and uplift rates, Channel Islands National Park, California, USA: Quaternary Science Reviews, v. 105, p. 209–238, doi:10.1016/j.quascirev.2014.09.017.

Nicholson, C., Sorlien, C.C., Atwater, T., Crowell, J.C., and Luyendyk, B.P., 1994, Microplate capture, rotation of the western Transverse Ranges, and initiation of the San Andreas transform as a low-angle fault system: Geology, v. 22, p. 491–495, doi:10.1130/0091-7613(1994)022<0491:MCROTW>2.3.CO;2.

Nicholson, C., Sorlien, C.C., Hopps, T., and Kamerling, M., 2016, Anomalous uplift at Pitas Point: Localized phenomena or indicator of tsunamigenic M8 earthquake along coastal California: American Geophysical Union Fall General Assembly, abs. OS21A-1947.

National Oceanic and Atmospheric Administration National Centers for Environmental Information, 2014, 2013 NOAA Coastal California TopoBathy Merge Project: http://www.ngdc.noaa.gov/docucomp/page?xml=NOAA/NESDIS/NGDC/MGG/Lidar/iso/xml/2013_CA_TopoBathy_m2612.xml&view=getDataView&header=none. (accessed February 2016).

Normark, W.R., Fisher, M.A., Gutmacher, C.E., Sliter, R., Hibbeler, L., Feingold, B., and Reid, J.A., 2003, Cruise Report for A1–02-SC Southern California CABRILLO Project, Earthquake Hazards Task: U.S. Geological Survey Open-File Report 03-110, 68 p., http://pubs.usgs.gov/of/2003/0110/.

Normark, W.R., Piper, D.J.W., Romans, B.W., Covault, J.A., Dartnell, P., and Sliter, R.W., 2009, Submarine canyon and fan systems of the California Continental Borderland, *in* Lee, H.J., and Normark, W.R., eds., Earth Science in the Urban Ocean—The Southern California Continental Borderland: Geological Society of America Special Paper 454, p. 141–168, doi:10.1130/2009.2454(2.7).

Perg, L.A., Anderson, R.S., and Finkel, R.C., 2001, Use of a new ^{10}Be and ^{26}Al inventory to data marine terraces, Santa Cruz, California, USA: Geology, v. 29, p. 879–882, doi:10.1130/0091-7613(2001)029<0879:UOANBA>2.0.CO;2.

Pinter, N., Lueddecke, S.B., Keller, E.A., and Simmons, K.R., 1998, Late Quaternary slip on the Santa Cruz Island fault, California: Geological Society of America Bulletin, v. 110, p. 711–722, doi:10.1130/0016-7606(1998)110<0711:LQSOTS>2.3.CO;2.

Pinter, N., Sorlien, C.C., and Scott, A.T., 2003, Fault-related growth and isostatic subsidence, California Channel Islands: American Journal of Science, v. 303, p. 300–318, doi:10.2475/ajs.303.4.300.

Plesch, A., et al., 2007, Community Fault Model (CFM) for southern California: Bulletin of the Seismological Society of America, v. 97, p. 1793–1802, doi:10.1785/0120050211.

Pratson, L., et al., 2007, Seascape evolution on clastic continental shelves and slopes, *in* Nittrouer, C.A., et al., eds., Continental Margin Sedimentation—From Sediment Transport to Sequence Stratigraphy: International Association of Sedimentologists Special Publication 37, p. 339–380, doi:10.1002/9781444304398.ch7.

Redin, T., Forman, J., Kamerling, M., and Galloway, J., 2005, Santa Barbara Channel Structure and Correlation Sections—CS32 to CS42: Pacific Section, American Association of Petroleum Geologists Cross Section 36, 12 sheets.

Reeder-Myers, L., Erlandson, J.M., Muhs, D.R., and Rick, T.C., 2015, Sea level, paleogeography, and archeology on California's Northern Channel Islands: Quaternary Research, v. 83, p. 263–272, doi:10.1016/j.yqres.2015.01.002.

Reynolds, L.C., and Simms, A.R., 2015, Late Quaternary relative sea level in southern California and Monterey Bay: Quaternary Science Reviews, v. 126, p. 57–66, doi:10.1016/j.quascirev.2015.08.003.

Ritchie, A.C., and Johnson, S.Y., 2012, Detailed geology and geomorphology, Hueneme Canyon and vicinity, California, sheet 11, *in* Johnson, S.Y., et al., California State Waters Map Series—Hueneme Canyon and Vicinity, California: U.S. Geological Survey Scientific Investigations Map 3225, 41 p., 12 sheets, http://pubs.usgs.gov/sim/3225/.

Rockwell, T.K., Keller, E.A., and Dembroff, G.R., 1988, Quaternary rate of folding of the Ventura Avenue anticline, western Transverse Ranges, southern California: Geological Society of America Bulletin, v. 100, p. 850–858, doi:10.1130/0016-7606(1988)100<0850:QROFOT>2.3.CO;2.

Rockwell, T.K., Nolan, J., Johnson, D.L., and Patterson, R.H., 1992, Ages and deformation of marine terraces between Point Conception and Gaviota, Western Transverse Ranges, California, *in* Wehmiller, J.F, and Fletcher, C., eds., Quaternary Coasts of the United States—Marine and Lacustrine Systems: Society of Economic Paleontologists And Mineralogists Special Publication 48, p. 333–341, doi:10.2110/pec.92.48.0333.

Rockwell, T.K., Clark, K., Gamble, L., Oskin, M.E., Haaker, E.C., and Kennedy, G.L., 2016, Large Transverse Range earthquakes cause coastal upheaval near Ventura, southern California: Bulletin of the Seismological Society of America, v. 106, p. 2706–2720, doi:10.1785/0120150378.

Ryan, K.J., Geist, E.L., Barall, M., and Oglesby, D.D., 2015, Dynamic models of an earthquake and tsunami offshore Ventura, California: Geophysical Research Letters, v. 42, p. 6599–6606, doi:10.1002/2015GL064507.

Sarna-Wojcicki, A.M., Williams, K.M., and Yerkes, R.F, R.F., 1976, Geology of the Ventura Fault, Ventura County, California: U.S. Geological Survey Miscellaneous Field Studies Map MF-781, 3 sheets, scale 1:6,000.

Schindler, C.S., 2010, 3D Fault Geometry and Basin Evolution in the Northern Continental Borderland Offshore Southern California [M.S. thesis]: Bakersfield, California State University, 41 p.

Schneider, C.L., Hummon, C., Yeats, R.S., and Huftile, G.L., 1996, Structural evolution of the northern Los Angeles basin, California, based on growth strata: Tectonics, v. 15, p. 341–355, doi:10.1029/95TC02523.

Seeber, L., and Sorlien, C.C., 2000, Listric thrusts in the western Transverse Ranges, California: Geological Society of America Bulletin, v. 112, p. 1067–1079, doi:10.1130/0016-7606(2000)112<1067:LTITWT>2.0.CO;2.

Shaw, J.H., and Suppe, J., 1994, Active faulting and growth folding in the eastern Santa Barbara Channel, California: Geological Society of America Bulletin, v. 106, p. 607–626, doi:10.1130/0016-7606(1994)106<0607:AFAGFI>2.3.CO;2.

Sieh, K.E., and Jahns, R.H., 1984, Holocene activity of the San Andreas fault at Wallace Creek, California: Geological Society of America Bulletin, v. 95, p. 883–896, doi:10.1130/0016-7606(1984)95<883:HAOTSA>2.0.CO;2.

Simms, A., Reynolds, L.C., Bentz, M., Roman, A., Rockwell, T., and Peters, R., 2016a, Tectonic subsidence of California estuaries increases forecasts of relative sea-level rise: Estuaries and Coasts, v. 39, p. 1571–1581, doi:10.1007/s12237-016-0105-1.

Simms, A.R., Rouby, H., and Lambeck, K., 2016b, Marine terraces and rates of vertical tectonic motion: The importance of glacio-isostatic adjustment along the Pacific coast of central North America: Geological Society of America Bulletin, v. 128, p. 81–93, doi:10.1130/B31299.1.

Slater, R.A., Gorsline, D.S., Kolpack, R.L., and Shiller, G.I., 2002, Post-glacial sediments of the California shelf from Cape San Martin to the US-Mexico border: Quaternary International, v. 92, p. 45–61, doi:10.1016/S1040-6182(01)00114-8.

Sliter, R.W., Triezenberg, P.J., Hart, P.E., Draut, A.E., Normark, W.R., and Conrad, J.E., 2008, High-resolution chirp and mini-sparker seismic reflection data from the southern California continental shelf—Gaviota to Mugu Canyon: U.S. Geological Survey Open-File Report 2008-1246, http://pubs.usgs.gov/of/2008/1246/.

Sliter, R.W., Triezenberg, P.J., Hart, P.E., Watt, J.T., Johnson, S.Y., and Scheirer, D.S., 2009, High resolution seismic-reflection and marine magnetic data along the Hosgri Fault Zone, central California: U.S. Geological Survey Open-File Report 2009-1100, v. 1.1, http://pubs.usgs.gov/of/2009/1100/index.html.

Sommerfield, C.R., Lee, H.J., and Normark, W.R., 2009, Postglacial sedimentary record of the southern California continental shelf and slope, Point Conception to Dana Point, in Lee, H.J., and Normark, W.R., eds., Earth Science in the Urban Ocean—The Southern California Continental Borderland: Geological Society of America Special Paper 454, p. 89–115, doi:10.1130/2009.2454(2.5).

Sorlien, C.C., and Nicholson, C., 2015, Post 1-Ma deformation history of the Pitas Point–North Channel–Red Mountain fault system and associated folds in Santa Barbara channel, California: U.S. Geological Survey National Earthquake Hazards Reduction Program final report, award G14AP00012, 24 p.

Sorlien, C.C., Kamerling, M.J., and Mayerson, D., 1999, Block rotation and termination of the Hosgri strike-slip fault, California, from three-dimensional map restoration: Geology, v. 27, p. 1039–1042, doi:10.1130/0091-7613(1999)027<1039:BRATOT>2.3.CO;2.

Sorlien, C.C., Gratier, J.P., Luyendyk, B.P., Hornafius, J.S., and Hopps, T.E., 2000, Map restoration of folded and faulted late Cenozoic strata across the Oak Ridge fault, onshore and offshore Ventura basin, California: Geological Society of America Bulletin, v. 112, p. 1080–1090, doi:10.1130/0016-7606(2000)112<1080:MROFAF>2.0.CO;2.

Sorlien, C.C., Kamerling, M.J., Seeber, L., and Broderick, K.G., 2006, Restraining segments and reactivation of the Santa Monica–Dume–Malibu Coast fault system, offshore Los Angeles, California: Journal of Geophysical Research, v. 111, B11402, doi:10.1029/2005JB003632.

Southern California Earthquake Data Center, 2016, Southern California Earthquake Catalog: Southern California Earthquake Data Center database, accessed April 25, 2016, at http://www.data.scec.org/eq-catalogs/index.html.

Stanford, J.D., Hemingway, R., Rohling, E.J., Challenor, P.G., Medina-Elizalde, M., and Lester, A.J., 2011, Sea-level probability for the last deglaciation—A statistical analysis of far-field records: Global and Planetary Change, v. 79, p. 193–203, doi:10.1016/j.gloplacha.2010.11.002.

Stein, R.S., and Ekström, G., 1992, Seismicity and geometry of a 110-km-long blind thrust fault 2. Synthesis of the 1982–1985 California earthquake sequence: Journal of Geophysical Research, v. 97, p. 4865–4883, doi:10.1029/91JB02847.

Suppe, J., and Medwedeff, D.A., 1990, Geometry and kinematics of fault-propagation folding: Eclogae Geologicae Helvetiae, v. 83, p. 409–454.

Suppe, J., Chou, G.T., and Hook, S.C., 1992. Rates of folding and faulting determined from growth strata, in McClay, K.R., ed., Thrust Tectonics: New York, Chapman and Hall, p. 105–121, doi:10.1007/978-94-011-3066-0_9.

Swift, D.J.P., and Thorne, J.A., 1991, Sedimentation on continental margins, I: A general model for shelf sedimentation, in Swift, D.J.P., et al., eds., Shelf Sand and Sandstone Bodies—Geometry, Facies, and Sequence Stratigraphy: International Association of Sedimentologists Special Publication 14, p. 3–31, doi:10.1002/9781444303933.ch1.

Sylvester, A.G., 2001, Catalog of Santa Barbara Earthquakes—1800 to 1960: University of California, Santa Barbara, database: http://projects.crustal.ucsb.edu/sb_eqs/SBEQCatlog/SBEQCATINTRO.html (accessed March 2016).

Sylvester, A.G., Smith, S.S., and Scholz, C.H., 1970, Earthquake swarm in the Santa Barbara Channel, California, 1968: Bulletin of the Seismological Society of America, v. 60, p. 1047–1060.

Tennyson, M.E., and Kropp, A.P., 1998, Regional cross section across Santa Barbara channel from northwestern Santa Rosa Island to Canada de Molina, in Kunitomi, D.S., et al., eds., Structure and Petroleum Geology, Santa Barbara Channel, California: Pacific Section, American Association of Petroleum Geologists Miscellaneous Publication 46, 1 plate.

Titus, S.J., Dyson, M., DeMets, C., Tikoff, B., Rolandone, F., and Burgmann, R., 2011, Geologic versus geodetic deformation rates adjacent to the San Andreas fault, central California: Geological Society of America Bulletin, v. 123, p. 794–820, doi:10.1130/B30150.1.

Toppozada, T., Real, C., and Parke, D., 1981, Preparation of isoseismal maps and summaries of pre-1900 California earthquakes: California Division of Mines and Geology Open-File Report 81-11, 182 p.

Trecker, M.A., Gurrola, L.D., and Keller, E.A., 1998, Oxygen-isotope correlation of marine terraces and uplift of the Mesa Hills, Santa Barbara, California, USA, in Stewart, I.S., and Vita-Finzi, C., eds., Coastal Tectonics: Geological Society of London Special Publication 146, p. 57–69, doi:10.1144/GSL.SP.1999.146.01.04.

Triezenberg, P.J., Hart, P.E., and Childs, J.R., 2016, National Archive of Marine Seismic Surveys (NAMSS): A USGS Data Website of Marine Seismic Reflection Data Within the U.S. Exclusive Economic Zone (EEZ): U.S. Geological Survey Data Release, https://walrus.wr.usgs.gov/NAMSS/, doi:10.5066/F7930R7P (accessed May 2016).

U.S. Geological Survey, 2015, Quaternary Fault and Fold Database of the United States: U.S. Geological Survey website, http://earthquakes.usgs.gov/hazards/qfaults (accessed August 2015).

Vedder, J.G., 1975, Acoustic Reflection Profiles, R/V Kelez, May–June 1973, Leg 3, Offshore Southern California: U.S. Geological Survey Open-File Report 75-265, 85 p.

Warrick, J.A., and Farnsworth, K.L., 2009, Sources of sediment to the coastal waters of the Southern California Bight, in Lee, H.J., and Normark, W.R., eds., Earth Science in the Urban Ocean—The Southern California Continental Borderland: Geological Society of America Special Paper 454, p. 39–52, doi:10.1130/2009.2454(2.2).

Warrick, J.A., and Mertes, L.A.K., 2009, Sediment yield from the tectonically active semiarid Western Transverse Ranges of California: Geological Society of America Bulletin, v. 121, p. 1054–1070, doi:10.1130/B26452.1.

Watt, J.T., Johnson, S.Y., Hartwell, S.R., and Roberts, M., 2015, Offshore geology and geomorphology maps from Piedras Blancas to Pismo Beach, California, 2015: U.S. Geological Survey Scientific Investigations Map 3327, 6 sheets, scale 1:35,000, http://pubs.usgs.gov/sim/3327/.

Wells, D.L., and Coppersmith, K.J., 1994, New empirical relationship among magnitude, rupture length, rupture width, rupture area, and surface displacement: Bulletin of the Seismological Society of America, v. 84, p. 974–1002.

Wong, F.L., Phillips, E.L., Johnson, S.Y., and Sliter, R.W., 2012, Modeling of depth to base of Last Glacial Maximum and seafloor sediment thickness for the California State Waters Map Series, Eastern Santa Barbara Channel, California: U.S. Geological Survey Open-File Report 2012-1161, 16 p., http://pubs.usgs.gov/of/2012/1161/.

Yeats, R.S., 1983, Large-scale Quaternary detachments in Ventura basin, southern California: Journal of Geophysical Research, v. 88, p. 569–583, doi:10.1029/JB088iB01p00569.

Yeats, R.S., and Huftile, G.J., 1995, The Oak Ridge fault system and the 1994 Northridge earthquake: Nature, v. 373, p. 418–420, doi:10.1038/373418a0.

Yeats, R.S., Sieh, K.E., and Allen, C.R., 1997, The Geology of Earthquakes: New York, Oxford University Press, 568 p.

Yerkes, R.F., Sarna-Wojcicki, A.M., and Lajoie, K.R., 1987, Geology and Quaternary deformation of the Ventura area, in Recent Reverse Faulting in the Transverse Ranges: U.S. Geological Survey Professional Paper 1339, p. 169–178.

Zevenbergen, L.W., and Thorne, C.R., 1987, Quantitative analysis of land surface topography: Earth Surface Processes and Landforms, v. 12, p. 47–56, doi:10.1002/esp.3290120107.

Johnson et al. | Shelf evolution, Santa Barbara Channel